STUDIES OF STRUCTURES AND TEXTURES OF COLD-WORKED AND RECRYSTALLISED SAMPLES OF SOME Ni - Co ALLOYS
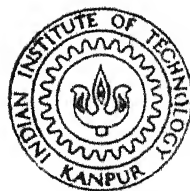
by

SWAPAN CHAKRABARTI

DEPARTMENT OF METALLURGICAL ENGINEERING
INDIAN INSTITUTE OF TECHNOLOGY KANPUR
APRIL, 1986

STUDIES OF STRUCTURES AND TEXTURES OF COLD-WORKED AND RECRYSTALLISED SAMPLES OF SOME Ni - Co ALLOYS

A Thesis Submitted

in Partial Fulfilment of the Requirements

for the Degree of

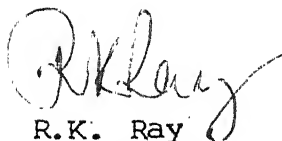MASTER OF TECHNOLOGY

by

SWAPAN CHAKRABARTI

to the

DEPARTMENT OF METALLURGICAL ENGINEERING

INDIAN INSTITUTE OF TECHNOLOGY KANPUR
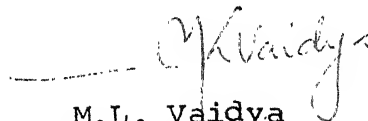
APRIL, 1986

ME-1986-M-CHA-STU

CERTIFICATE

This is to certify that the investigation on 'STUDIES ON STRUCTURES AND TEXTURES OF COLD-WORKED AND RECRYSTALLISED SAMPLES OF Ni-Co ALLOYS' has been carried out by SHRI SWAPAN CHAKRABARTI under our guidance and it has not been submitted elsewhere for a degree.

R.K. Ray
Professor
Department of Metallurgical
    Engineering
Indian Institute of Technology
Kanpur

M.L. Vaidya
Professor
Department of Metallurgical
    Engineering
Indian Institute of Technolo
Kanpur

APRIL, 1986

ACKNOWLEDGEMENTS

ABSTRACT

Widely differing deformation textures have been found in the present series of alloys. Deformation textures in alloys A, B and C have been found to be pure-metal type, that of alloy E is alloy-type. The deformation texture of alloy D has been found to lie somewhat in-between these two extremes. The recrystallisation textures of alloys A, B and C are rather similar showing mostly the cube-component. The recrystallisation texture of alloy E does not show any cube but a rather strong Goss component. The recrystallisation texture of alloy D has been found to be rather weak and more or less random. Addition of Co to Ni is found to decrease the average grain size of the recrystallised grains as well as their rate of growth.

CONTENTS

CHAPTER - 1

INTRODUCTION

In fcc metals and alloys it is usual to distinguish
between three different types of deformation textures:
(i) brass or alloy type texture in low stacking fault energy
materials, (ii) copper or pure metal type texture in medium
stacking fault energy materials and (iii) aluminium-type
texture in very high stacking fault energy materials. While
in the brass-type one has practically only the brass-component
{110} <112> and in the copper-type the Cu {112} <11̄1>,
S {123} <634> and brass components are nearly equally strong,
the S component predominates in the aluminium type.

Excepting Cu, Ag and Au extensive data on stacking
fault energy (SFE) are available for two other fcc metals,
e.g., aluminium and nickel. A reasonable value of the SFE
of Al, as estimated from its coherent twin energy is γ_{Al}
200 ergs/cm^2. Although the statement $\gamma_{Ni} \sim 250$ ergs/cm^2 is
probably reasonably accurate, it might be as well nearly to
say that the stacking fault energy of Ni is very high indeed.

Addition of cobalt to nickel has been known to
reduce the stacking fault energy of the latter drastically.
Thus it is possible to design a number of Ni-Co alloys with
widely varying stacking fault energies by simply changing
the cobalt content. Work in this system is expected to
throw much light on the whole phenomena of deformation and

recrystallisation texture formation as a function of stacking fault energy. Since hardly any systematic work has yet been carried out in this system of alloys, it was proposed to undertake work in this direction.

LITERATURE REVIEW

2.1 The Cold-worked State

Generally the cold-worked state may be taken as any strained or damaged condition of a crystalline material brought about by processes such as plastic deformation, particle bombardment, quenching from a high temperature or phase transformations.[1] The principal entities responsible for the cold-worked state are point defects such as vacancies and interstitials as well as linear and planar defects like dislocations and stacking faults, etc. In the present review only the cold-worked state produced by plastic deformation will be discussed, in general with reference to f.c.c. metals and alloys. Plastic deformation of a material involves a permanent shape change produced by stressing the material beyond its elastic limit. Any or all of the types of defects mentioned above may be produced in the solid during the course of plastic deformation. If the deformation occurs at a sufficiently low temperature, many of these defects will be retained. As a result of it, increased content of crystal defect, such a material is in a thermodynamically metastable state.

2.1.1. Microstructure of cold-worked metals

For more than two decades transmission electron microscopy techniques have been successfully applied to determine

the structure of cold-worked metals.

Bailey and Hirsch[2,3] made electron microscopic observations on polycrystalline silver, copper and nickel foils deformed in tension. They found that the dislocations introduced into these metals by plastic deformation are arranged in a cellular structure. The cell boundaries appear to consist of complex dislocation arrangements together with a large number of small loops. The misorientation across the cell walls were measured and found to be of the order of a degree. With increasing deformation the dislocation density and the misorientation across the cell-boundaries in the heavily deformed specimens (cold-rolled to 95% reduction) have been found to be quite large, even upto ~10°. Due to very high dislocation density ($>10^{11}$) present at this stage the individual dislocations are not easily resolved, and it is also very difficult to recognise the original grain boundaries. This is also confirmed by Bollmann's study[4] on nickel cold-rolled to 80% reduction.

Weissmann et.al.[5] have reported observations on the microstructure of high purity aluminium which was cold rolled to different amounts. Their result indicate that for a weakly deformed (5% cold-rolled) specimen the microstructure consists of long kinked dislocation lines which upon interaction with other dislocations, form dislocation tangles. Increased cold-working to 10% reduction by rolling, gives rise to a more pronounced dislocation entanglement and a distinct emergence of cell-structure. At about 30%

cold-reduction, the formation of cell-structure is well-advanced, with most of the dislocation tangles arranged in the cell-walls and relatively few dislocations within the cells. The cell walls become more sharply delineated with increasing deformation. It is rather interesting to note that in aluminium the cell interior remains relatively free of dislocations even for specimens cold worked as much as 90%, although there exists interspersed regions of high dislocation density in which cell structure is poorly developed. Frequently with external annealing, slip dislocations in heavily cold-rolled specimens are found to align themselves into distinct low-angle boundaries, and this is regarded as a manifestation of dynamical recovery.

Fine mechanical twins and stacking faults on closely-spaced planes have been observed by Hu et.al.[6] in thin foils parallel to the rolling plane section in Cu-4% Al crystals of the (110) $[1\bar{1}2]$ orientation when rolled 95% and 99% at room temperature. Such twins were only rarely found in similarly deformed copper single crystals of the same orientation. Heavy clusters of stacking faults and micro twins were also observed in thin foils prepared from the rolling plane section and the longitudinal section of Cu-4% Al crystals of the (112) $[11\bar{1}]$ orientation when rolled upto 50% reduction at 25°C. The occurence of micro-twins have been found to be more frequent in polycrystalline 70:30 brass than in copper[6] when rolled 50% at room temperature, although the cellular structure is almost the same in both metals, when rolled 95%

at room temperature. Clear sub-grain structure could be found in pure copper but no such dynamic recovery could be seen in the brass sample.

2.1.2. The stored energy produced by cold-rolling

A small percentage (usually from 1% to 10%) of the energy expended in plastically deforming a metal remains 'stored' in the metal causing an increase in internal energy. This increment in internal energy is associated with the defects generated during deformation and provides the energetic driving force for relaxation processes which occur when the cold-worked metal is subsequently annealed at a higher temperature. The magnitude of the stored energy produced by cold-working is affected by variables such as purity, method of deformation, temperature, grain size and composition.

Comparison of calorimetric and metallographic results have shown that the energy of plastic deformation can be stored by the following mechanism:

    a) Elastic strain energy

    b) Energy of dislocations

    c) Energy of point defects

    d) Energy associated with stacking faults and twins,

and   e) Energy associated with the destruction of ordered regions.

The elastic strain energy for filed 75% Au - 25% Ag alloy has been estimated at about 3% of the total stored energy by Averbach et.al.[7] Michell and Haig[8,9] have shown

that the elastic strain energy for ground nickel is about 12% of the stored energy. These datas show very convincingly that the elastic energy contribution is usually very small. This automatically leads to the conclusion that the major portion of the stored energy of cold-work, atleast for pure metals, is due to the lattice defects.

In order to arrive at an estimate of the fraction of the stored energy due to dislocations, information is needed on their density and distribution. Annealed metals normally have dislocation densities between 10^6 to 10^8 lines/cm^2, and severely cold-worked metals usually have between 10^{10} and 10^{12} lines/cm^2. The precise distribution of the dislocations depends strongly on the metal, its purity and history of deformation.

Both vacancies and interstitial atoms may be considered responsible for atleast some energy storage during plastic deformation. Although an estimate of the stored energy due to vacancies can be made from measured resistivity changes, no experiments have as yet established the effect of interstitial atoms. In many systems these point defects anneal out during or immediately after deformation.

Stacking faults which are formed during plastic deformation can account for an appreciable portion of the stored energy, γ, and on the temperature of the deformation.

Deformations twins on a fine scale comparable to stacking faults may also contribute significantly to the stored energy.

If originally there exists in a material, either short- or long-range order to some degree, then, during plastic deformation, the passage of dislocations through the order regions will disturb the degree of order leading to an increase of the internal energy of the system. Similarly, if, during cold-working, precipitates and clusters of solute atoms are sheared due to the passage of dislocations through them, the internal energy will again increase.

2.1.3. Release of stored energy during annealing

As has been mentioned previously, a plastically deformed material due to its increased content of physical defects is in a thermodynamically metastable state. On increasing the temperature the material can lower its free energy by the removal and rearrangement of lattice defects. Haessner[10] has made a systematic classification of the multitude of phenomena that may occur on annealing the cold-worked material (below the melting point) in terms of five fundamental structural processes. These are essentially the following:

a) Reaction of point defects and point defect agglomerates — their annihilation.

b) The annihilation of dislocations of opposite signs and the shrinking of dislocation loops,

c) The rearrangement of dislocations to form energetically more favourable configurations,

d) The absorption of point defects and dislocations by grain-boundary migrating through the metal,

and e) The reduction in total grain-boundary area.

Haessner[10] has termed processes (a) and (b) as
'recovery' and processes (d) and (e) as 'recrystallisation'.
In more general terms recovery is supposed to constitute all
these annealing phenomena before the appearence of new strain-
free recrystallised grains, regardless of how refined the
technique used to detect the new grains. Recrystallisation
is supposed to involve the nucleation and growth of these new
strain-free grains and the gradual consumption of the cold-
worked matrix by the movement of large-angle grain-boundaries.
It is worth mentioning here that it is often very difficult
to draw a distinction between recovery and recrystallisation,
and in practice the two processes are usually found to over-
lap one another.

As has been mentioned before, the stored energy of
cold-worked provides the driving force for both recovery and
recrystallisation. For a given set of materials and deforma-
tion conditions, the stored energy is fixed and finite in
magnitude. Hence, the apportionment of the stored energy
release between the two processes will depend on the relative
ease or difficulty of their occurrence.

Two different types of stored energy release during
recovery are usually observed. Sharp peaks of energy release
are found in case of pure metals and in a few impure metals.
In almost all impure materials, however, the energy is
released over an extended range of temperature and may be
either of a flat-plateau constant rate type or a gradually

increasing rate type. In contrast with recovery, the energy release during recrystallisation are always of the distinct peak-type. Illustrations of these processes are provided by Figures 1 and 2. Figure 1 which has been taken from the work of Clarebrough et.al.[11] clearly indicates that in the less pure metals both peaks due to recovery and recrystallisation appear to be superimposed on a plateau whereas two distinct energy releases can be observed in pure metals. Another point to be noted in this figure is that the second peak — that due to recrystallisation — occurs at a much lower temperature (450°C) in the pure metal than in the less pure material where it appears at a temperature of about 650°C.

A significant difference[12] in the behaviour of stored energy release for two grades of copper of 99.967 and 99.988% purity is shown in Figure 2. Both the materials were deformed to the same extent in torsion energy of the order of 21 calorie per gram-atom. For the purer material the fraction of the stored energy release during recovery was 5% whereas for the less pure material it was about 30%; the corresponding recrystallisation temperature were 170°C and 290°C respectively. It has been mentioned by these authors[12] that the main difference in chemical composition between two baths of copper used in their experiment was in the phosphorous content.

Alloying can significantly change the energy release characteristics of deformed material on heating. Figure 3 shows the power difference (ΔP) as a function of temperature

TORSION $\frac{nd}{l}$ = 201

(a)

NICKEL 99.6 %

TORSION $\frac{nd}{l}$ = 1.87

(b)

POWER DIFFERENCE ΔP mW

TEMP °C

B

A

POWER DIFFERENCE, ΔP (mW)

TEMPERATURE (°C)
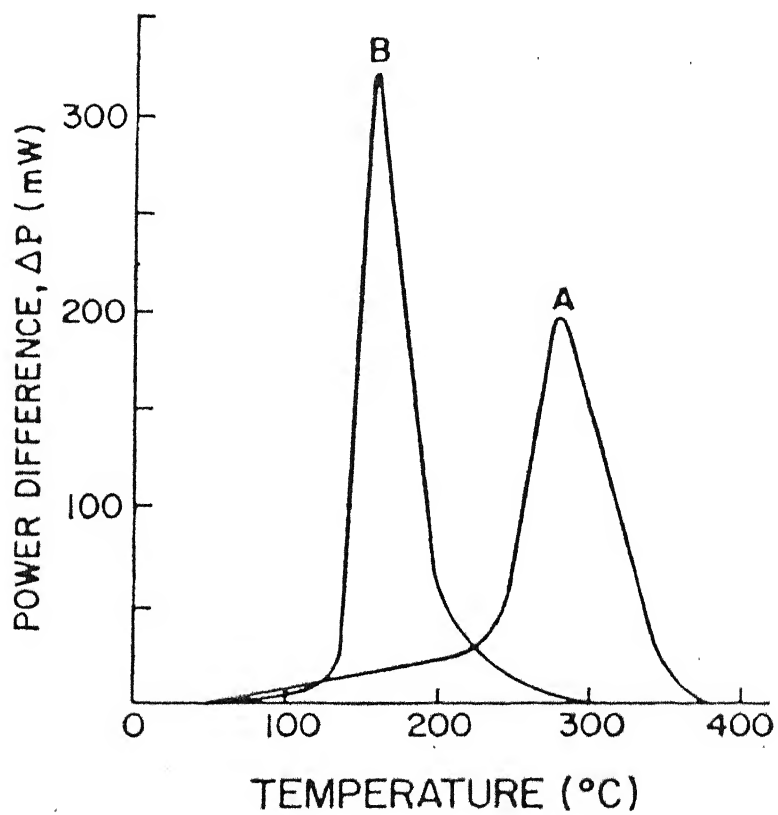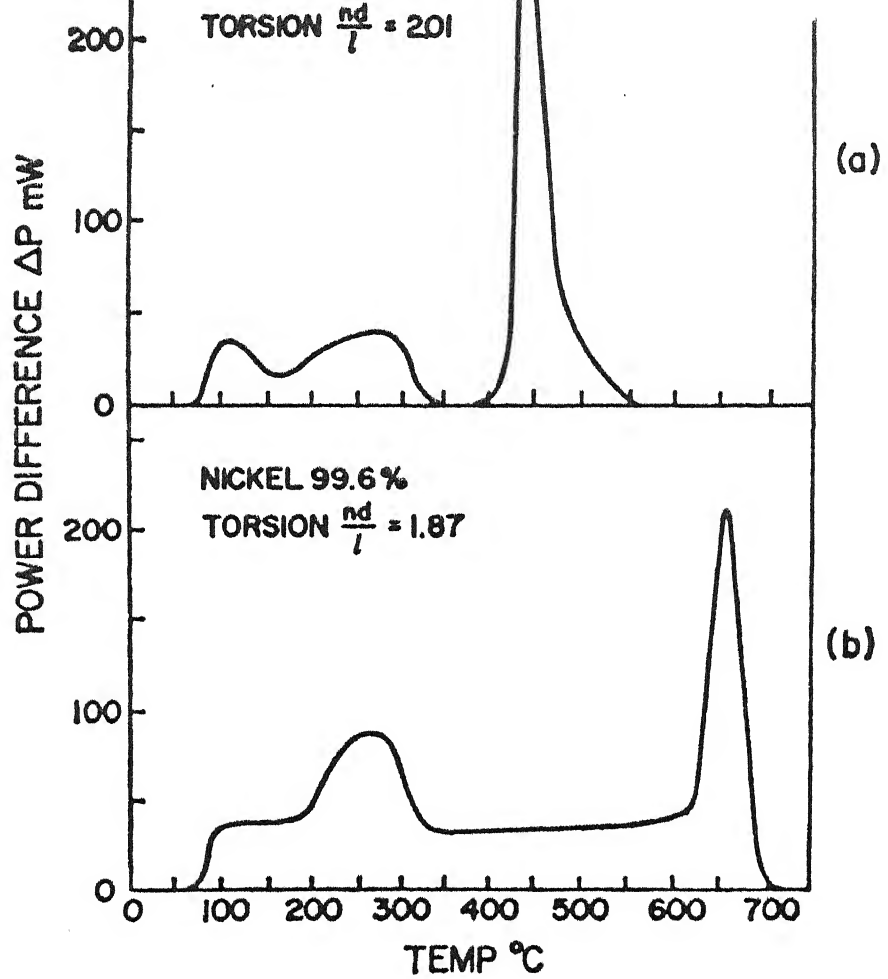
obtained at a heating rate of 6°C/min. for nominally 99.98%

copper deformed to 45% elongation and for arsenical copper

(0.35% As) deformed to 40% elongation.[13] It is clearly seen

here that for the pure copper one sharp (ΔP) peak occurs at

about 300°C; whereas for arsenical copper, a smaller (ΔP)

peak is found at about 440°C. This latter peak is superimpo-

sed on a low energy release plateau which begins to appear at

about 70°C.

Both the total stored energy and the manner in which

the stored energy is released depend on the grain size.

Clarebrough et.al.[11] who investigated specimens of 99.98%

pure copper deformed by compression found that for the fine-

grained material, the stored energy is released much more

rapidly than for the coarse-grained material. They also

noticed that for lower values of strain, more energy is

stored for the fine-grained material than in the coarse-

grained. For higher strains, however, the total energy stored

is the same for the both grain sizes but recrystallisation

temperature has been found to be lower in fine-grained material.

The manner in which the stored energy is released

from specimens deformed in fatigue is seen to be markedly

different from that obtained for unidirectional deformation

(Figure 4). Clarebrough et.al.[14] have shown it for 99.98%

pure copper.

The magnitude of stored energy released is also depen-

dent on temperature of plastic deformation. Henderson amd

Koehler[15] investigated the release of stored energy between
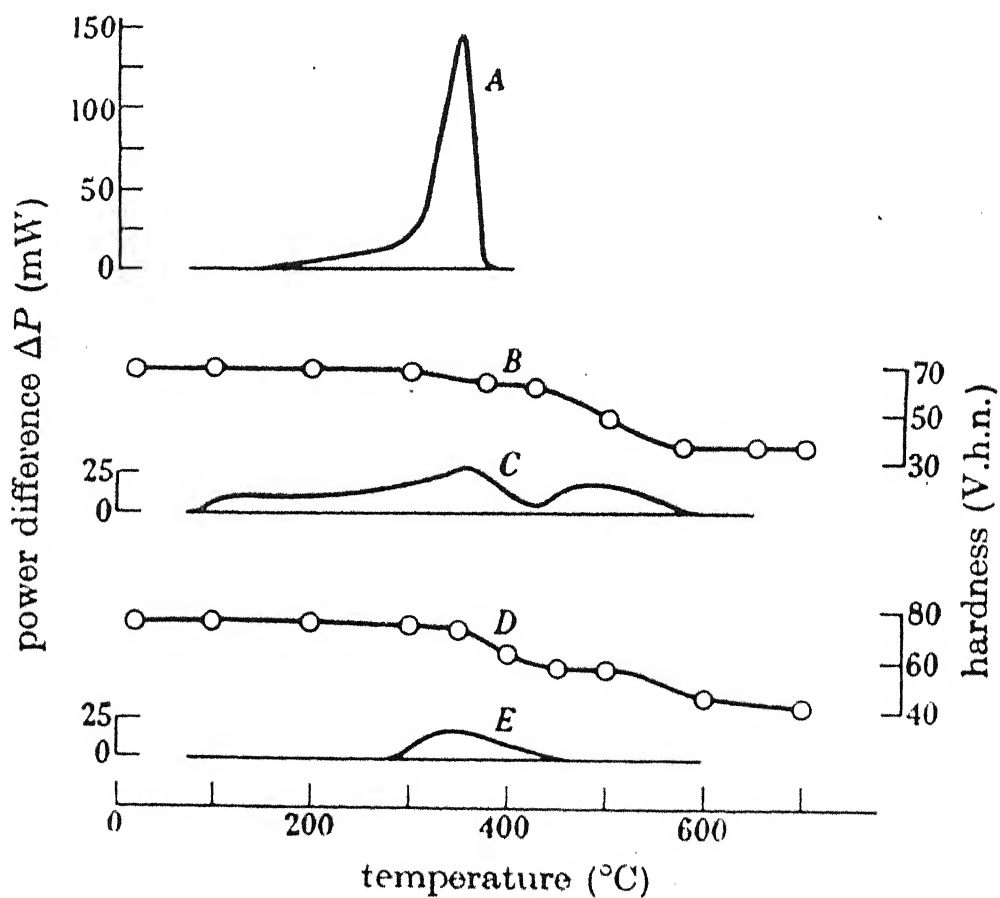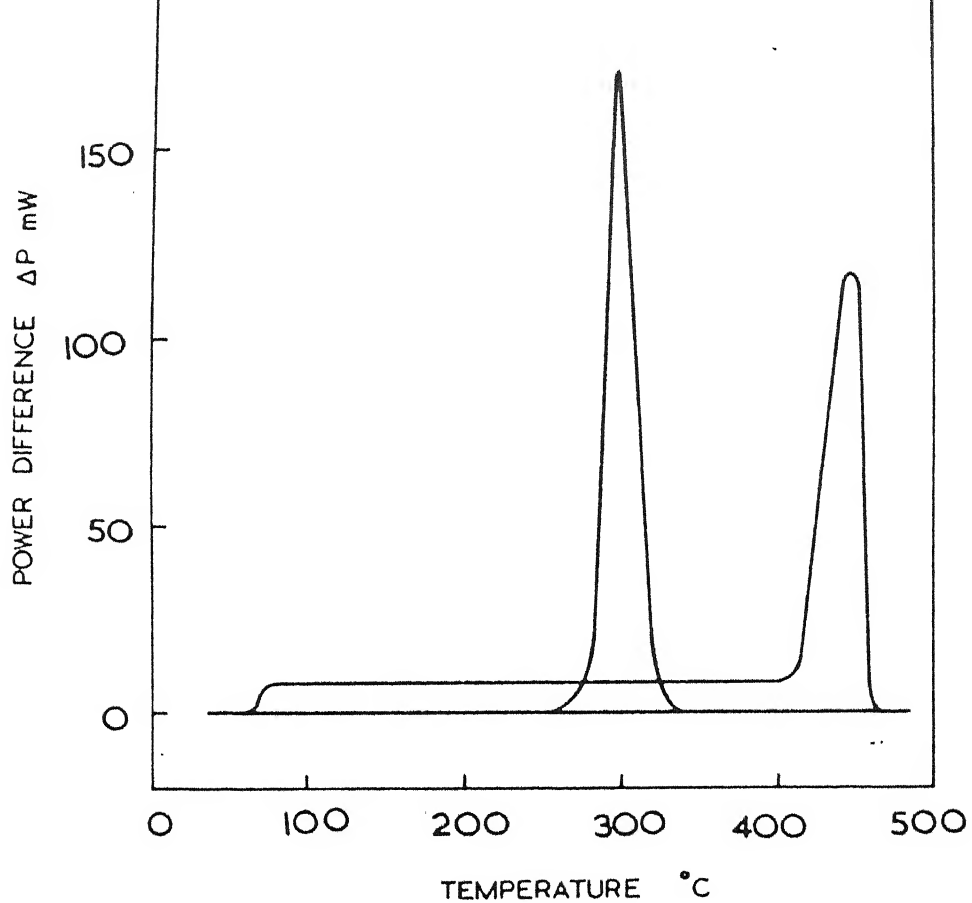
-185°C and 80°C for polycrystalline specimens of 99.999%
copper deformed in compression at -185°C.

2.2. Recovery

As mentioned earlier, recovery includes the migra-
tion of vacancies and of dislocations, leading to annihilation
or rearrangement of a certain portion of them. In more
general terms, however, recovery can be considered to be any
modification of properties during annealing, which occurs
before the appearence of new strain-free recrystallised grains,
regardless of how refined the experimental technique is used
to detect the new grains.[16]

2.2.1. Property changes during recovery

It is usual to find that during recovery both the
mechanical and the physical properties of materials show some
change from their values in the cold-worked state. Normally
the restoration of a mechanical property such as hardness or
yield strength to its fully annealed value is only about one
fifth completed during recovery.[16] Following the work of
Dronard et.al.[17.] a parameter R may be defined which gives
a measure of the fraction of the particular property recovered,

$$R = \frac{X_m - X}{X_m - X_o} \tag{1}$$

where, X_o is the hardness or flow stress of the fully annealed
material

X_m is the hardness or flow stress of the strain hardened material

and X is the hardness or flow stress of the strainhardened material.

Equation (1) may be rearranged to give,

$$1 - R = \frac{X - X_o}{X_m - X_o} \tag{2}$$

Physical properties like density and electrical resistivity are also found to undergo detectable change from their cold-worked values during subsequent annealing. The introduction of lattice defects like vacancies and dislocations produces a slight decrease in the density of a metal during cold working. During annealing when a gradual loss of these defects takes place, the density again approaches its annealed value during recovery and continues to do so during further annealing leading to recrystallisation.

Electrical resistivity changes from the cold worked value are frequently employed to follow the progress of both recovery and recrystallisation. It is usually found that the resistivity shows a slight decrease from its cold worked value during the recovery anneal and rather a sharper decrease as the annealing temperature is increased and recrystallisation starts.

The progress of the recovery process on annealing a cold worked metal can also be studied by following the changes of X-ray line broadening. Two factors, particle size and residual stress, determine the extent to which an

X-ray diffraction line is broadened, and the two contributions may be separated using the Fourier analysis technique developed by Warren and Averbach.[18] Using this analysis Hu[19] has shown that during the recovery of rolled single crystals of silicon iron, the particle size (which may be related to cell size) increases and the residual stresses decreases. To obtain really useful information from line broadening experiments, it is essential to analyse the diffraction line profile in detail which can only be done effectively with the help of a computer. Another simple method of analysis of the line broadening data which can be utilised to follow the recovery process has been suggested by Hu.[19] A line sharpening parameter $\underline{R}$ has been defined as,

$$\underline{R} = \frac{I_{min} - I_b}{I_{max} - I_b} \qquad (3)$$

where, I_{min} is the intensity minimum between K_{α_1} and K_{α_2} peaks

M_{max} is the intensity maximum of the K_{α_1} peak

and I_b is the background intensity.

Although the parameter $\underline{R}$ does not give any information regarding either the cell size or residual stresses, it does give some general indication of the progress of the recovery process.

2.2.2. The kinetics of recovery

In general it is observed that the rate of recovery of a property from the cold-worked value depends on the

activation energy for recovery. It is evident that Q can be obtained by plotting ln t vs. 1/T for various fraction of recovery and measuring the slope a/R of the straight line representing the amount of recovery in question.

2.2.3. Recovery mechanisms

The annealing of a plastically deformed material may be quite complicated in view of the fact that many types of point defects as well as dislocations and planar faults can be present simultaneously and interact in many ways during annealing.

Electron microscopic evidence indicates that, in general, a cold worked metal has a cell structure. The cell walls consists of dislocation tangles, and some additional dislocations are found to exist in the cell interiors. As annealing starts, the tangled dislocations in the cell walls are supposed to rearrange themselves while some of the dislocations from within the cells may be attracted to cell walls. During the whole process of recovery dislocation annihilation probably occurs since the dislocation density in the cell interiors is found to decrease gradually on continued annealing. The cell walls become more clearly defined and eventually form sub-grains of about the same size as the initial cells. The sub-grain size does not change much until quite late in the recovery process when it starts increasing slightly. Thus, it might be said that, in general, three processes — dislocation annihilation, subgrain formation and

Hu and Szirmae showed that at least some sub-grains in recovered silicon-iron satisfied the above condition.

Sub-grain growth by way of sub-grain boundary migration has been objected to on the grains that low angle boundaries are relatively immisible. Bainbridge et.al.[39] measured the rule of migration of simple tilt boundaries in zinc under a constant sheer stress. Figure 8 taken from their results indicates that although relatively high displacement rates are obtained at small misorientations, the rate falls to quite a low value when misorientation of $\sim 2°$ are approached.

The coalescence model of sub-grain growth proposed by Hu[37] overcomes the problem of boundary mobility to a large extent. According to this the increase in size of sub-grains during recovery is due to a coalescence process whereby adjoining sub-grains having slightly different orientation merge into the same orientation giving rise to a bigger sub-grain. Fujita[40] has also reported a similar process in aluminium. The entire process of coalescence is shown schematically in Figure 9. The boundary CH between two adjoining sub-grains in (a) is shown being eliminated by the physical rotation of the right hand side sub-grain in (b). Clearly if this has to be accomplished it is necessary to have some atom diffusion along boundaries from the shaded areas to the corresponding open areas (b). Finally a geometrical adjustment of the boundaries BC, CD, IH and HG is postulated to give the big sub-grain structure in (d) Thus

sub-grain growth — may take place during the recovery of most metals.

2.2.3.1. Dislocation annihilation

Keh[22] found direct experimental evidence that the dislocation density decreases during the initial stages of recovery (Figure 5). This presumably does not involve movements of dislocations over long distances. According to Li[23] dislocation annihilation takes place in the cell boundaries.

It has also been found that elongated dislocation loops, if formed during plastic deformation, will, during recovery, gradually becomes circular and finally vanish.[24]

Wagner[25] has shown that stacking faults, introduced by cold-work, can be annealed out during the recovery stage.

2.2.3.2. Polygonisation and subgrain formation

The process of polygonisation was originally proposed by Orowan[26] in 1947. It has been considered in detail by Cahn[27,28], Beck et.al.[29-31] and Hibbard and Dunn.[32] The first clear picture of polygonisation was proposed by Cahn[27] who reported the results of a study on the effects of annealing bent single crystals of aluminium, zinc, magnesium and sodium chloride. These crystals were bent about an axis parallel to their active slip planes. Cahn studied both the deformed and annealed states in these crystals by taking tansmission Laue patterns with the X-ray beam normal to the active slip planes. He observed that the continuous asterism of the Laue spots obtained from the bent crystals

became discontinuous after anneal. This has been explained as due to a process — polygonisation — which leads to a rearrangement of dislocations, with a resultant lowering of the lattice strain energy. The mechanism has been shown schematically in Figure 6. The random arrangement of excess parallel edge dislocations produced during deformation can clearly be seen, on heating, to align themselves, into walls to form small angle, polygonisation or sub-grain boundaries by a process of annihilation and rearrangement. That the dislocation walls so produced were normal to the main slip planes active during bending was verified by Cahn by producing etch pits after the anneal. The process of polygonisation is believed to start with the glide and climb of individual dislocations, thereby forming small segments of boundary perhaps five to ten dislocations high. By further glide and climb these short range boundary segments then combine to give larger boundaries, still of low angle, which may now be termed long range. At higher temperature the spacings between these boundaries are found to increase and this lies led to the suggestion by Dunn and Daniel[33] and later Gilman[34] that two neighbouring boundaries may coalesce. This is thought to take place by the so-called Y-junction mechanism[35] which produces a single boundary (Figure 7). Although misorientation across the single boundary will be the sum of both the original boundaries, the total energy of the system is lowered by this mechanism. The same suggestion was made by Bryshko et.al.[36] during their work on steady state creep at elevated temperatures.
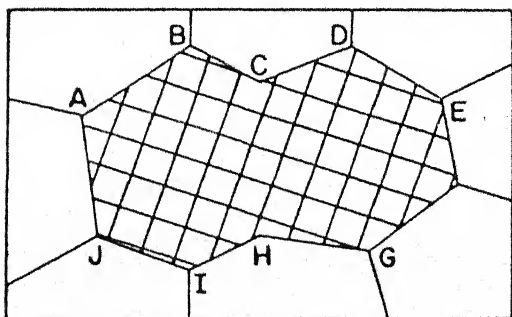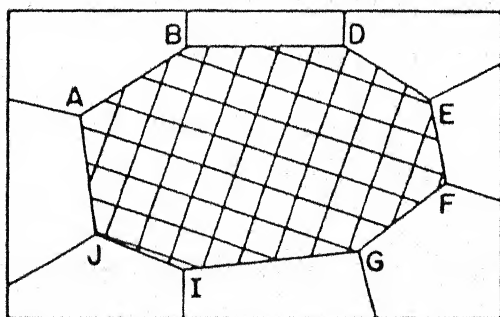
BOUNDARY ANGLE - DEGREES
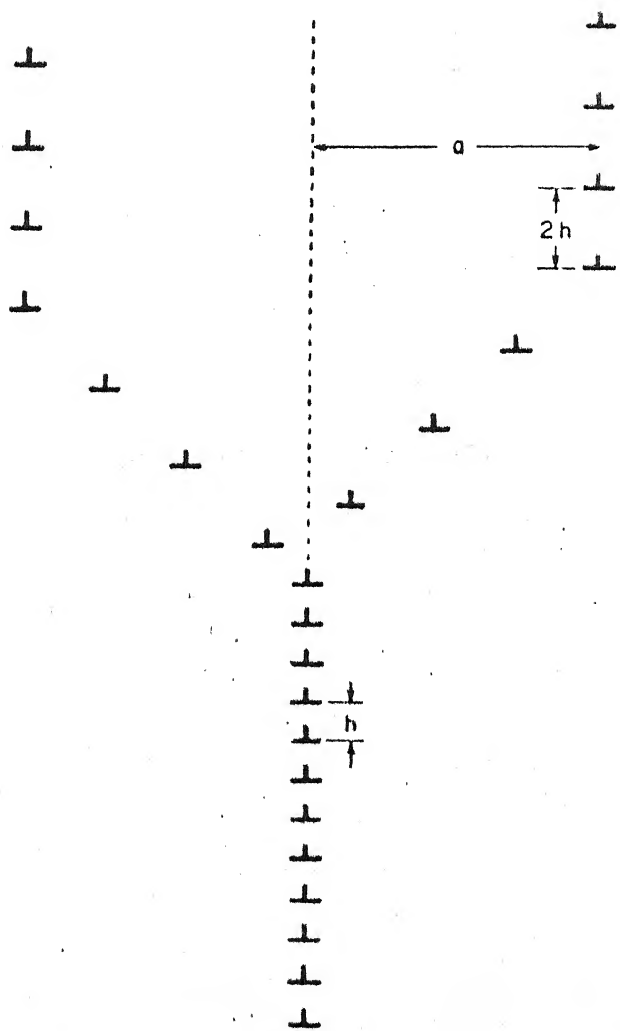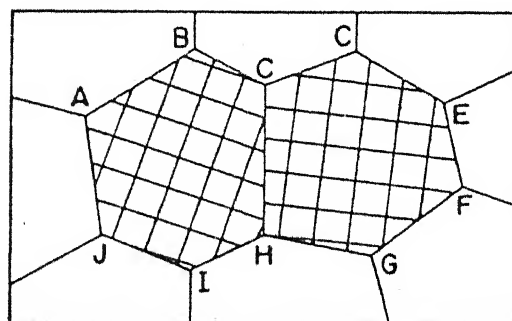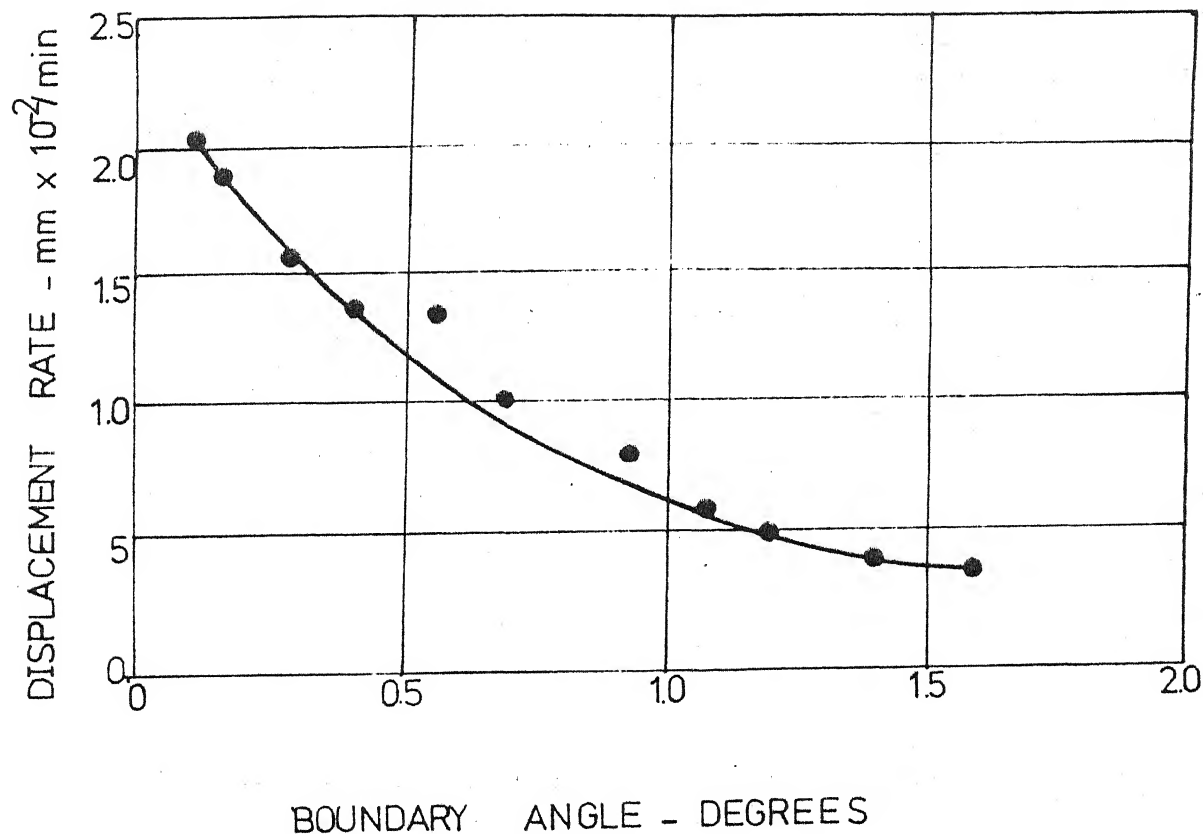
(a)
ORIGINAL SUBGRAIN STRUCTURE
BEFORE COALESCENCE
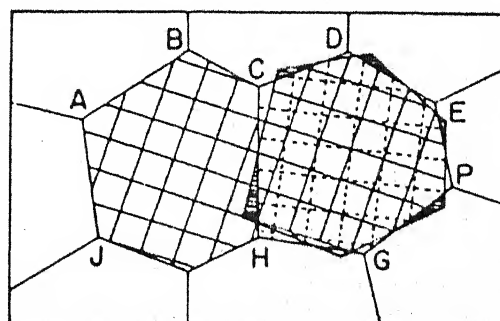
(b)
ONE SUBGRAIN IS UNDERGOING
A ROTATION

(c)
SUBGRAIN STRUCTURE JUST
AFTER COALESCENCE

(d)
FINAL SUBGRAIN STRUCTURE
AFTER SOME SUBBOUNDARY
MIGRATION

2.2.3.3. Sub-grain growth

Averbach et.al.[7] showed that a slight increase in average particle size occurs prior to the temperature at which a sharp hardness drop is produced by recrystallisation. Hu[37] has reported from electron microscopic evidences that sub-grains in a rolled 3% silicon-iron single crystal gradually increase in size prior to the appearance of recrystallisation. Two mechanisms — sub-boundary migration and sub-grain coalescence — have been proposed to explain the growth of sub-grains during recovery.

Growth by sub-grain boundary migration may be thought of in similar terms to primary grain growth where grains larger than a critical size are supposed to grow at the expense of those which are small than the critical size. The rate of growth of a particular sub-grain is given by Hu and Szirmae[38] as

$$\frac{dR}{dt} = M(\Delta G - \frac{2\sigma}{R}) \tag{8}$$

where R is the radius of the growing sub-grain

   M is the interface mobility

   ΔG is the free energy per unit volume for growth

and σ is the specific surface energy of the interface.

At equilibrium $\frac{dR}{dt} = 0$ so that

$$R = \frac{2\sigma}{\Delta G} \tag{9}$$

It follows that growth will occur if

$$R > \frac{2\sigma}{\Delta G} \tag{10}$$

the whole process probably requires some co-operative climb of dislocations along the disappearing sub-grain boundary and also some atom movements by vacancy diffusion around the sub-grains. The kinetics and thermodynamics of the coalescence process have been examined in detail by Li.[41]

The energy of a sub-grain boundary, E, is related to the misorientation across it, θ, by the Read-Shockley equation[42]

$$E = E_o\theta(A - \ln\theta) \qquad (11)$$

where, E_o and A are both constants. An E versus θ plot is shown in Figure 10. This curve reaches a maximum when $\theta = e^{A-1}$. Hence,

$$E_{max} = \theta_{max} E_o(A - \ln\theta_{max})$$

$$= \theta_{max} E_o \qquad (12)$$

So, the equation (11) can now be also written as,

$$\frac{E}{E_{max}} = \frac{\theta}{\theta_{max}} (1 - \ln\frac{\theta}{\theta_{max}}) \qquad (13)$$

Several checks have been made experimentally to test the validity of equation (13) and the combined results of Dunn et.al.[43,44] and Anst and Chalmers[45,46] are shown in Figure 11. It is seen that the four sets of data do seem to fit one theoretical curve quite well. Gjastein and Rhines[47] have pointed out that the equation (13) is misleading since it ensures a good fit even at very high values of θ. This is

the whole process probably requires some co-operative climb of dislocations along the disappearing sub-grain boundary and also some atom movements by vacancy diffusion around the sub-grains. The kinetics and thermodynamics of the coalescence process have been examined in detail by Li.[41]

The energy of a sub-grain boundary, E, is related to the misorientation across it, θ, by the Read-Shockley equation[42]
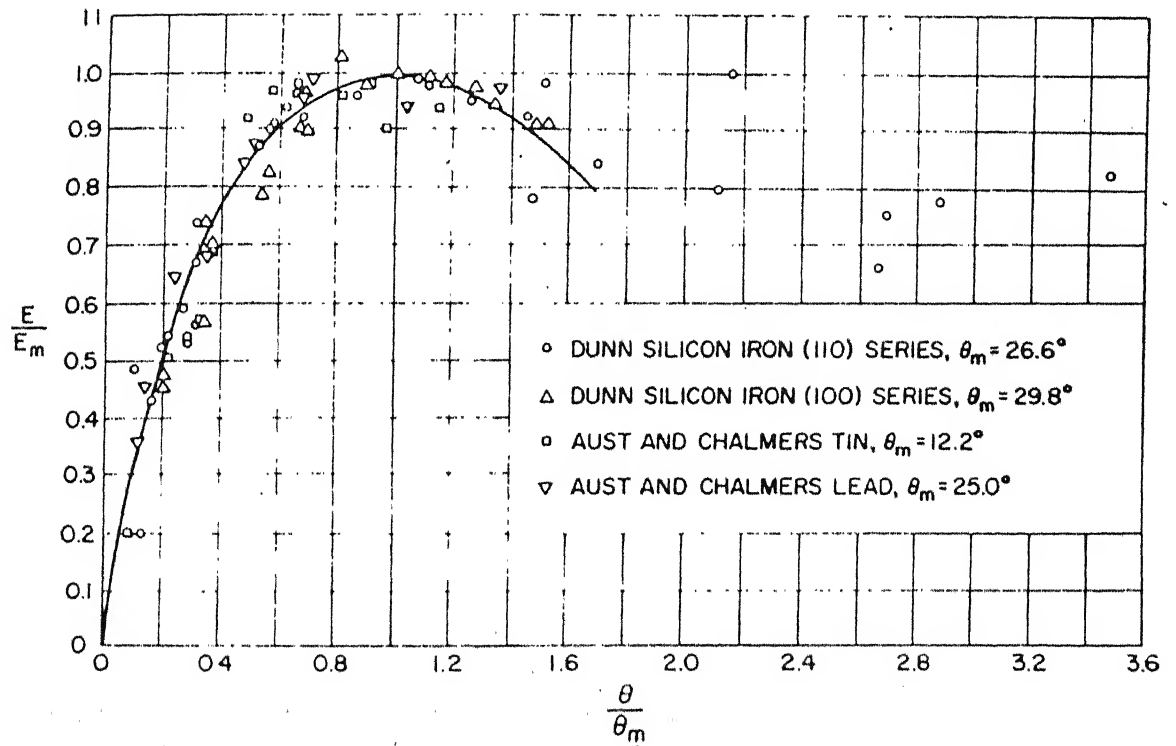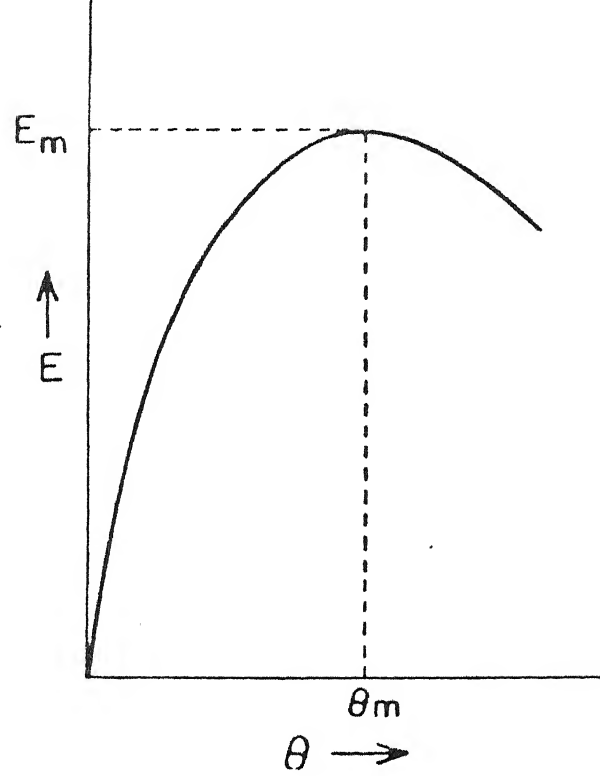
$$E = E_o \theta (A - \ln \theta) \tag{11}$$

where, E_o and A are both constants. An E versus θ plot is shown in Figure 10. This curve reaches a maximum when $\theta = e^{A-1}$. Hence,

$$E_{max} = \theta_{max} E_o (A - \ln \theta_{max})$$
$$= \theta_{max} E_o \tag{12}$$

So, the equation (11) can now be also written as,

$$\frac{E}{E_{max}} = \frac{\theta}{\theta_{max}} (1 - \ln \frac{\theta}{\theta_{max}}) \tag{13}$$

Several checks have been made experimentally to test the validity of equation (13) and the combined results of Dunn et.al.[43,44] and Anst and Chalmers[45,46] are shown in Figure 11. It is seen that the four sets of data do seem to fit one theoretical curve quite well. Gjastein and Rhines[47] have pointed out that the equation (13) is misleading since it ensures a good fit even at very high values of θ. This is

DUNN SILICON IRON (110) SERIES, $\theta_m = 26.6°$

DUNN SILICON IRON (100) SERIES, $\theta_m = 29.8°$

AUST AND CHALMERS TIN, $\theta_m = 12.2°$

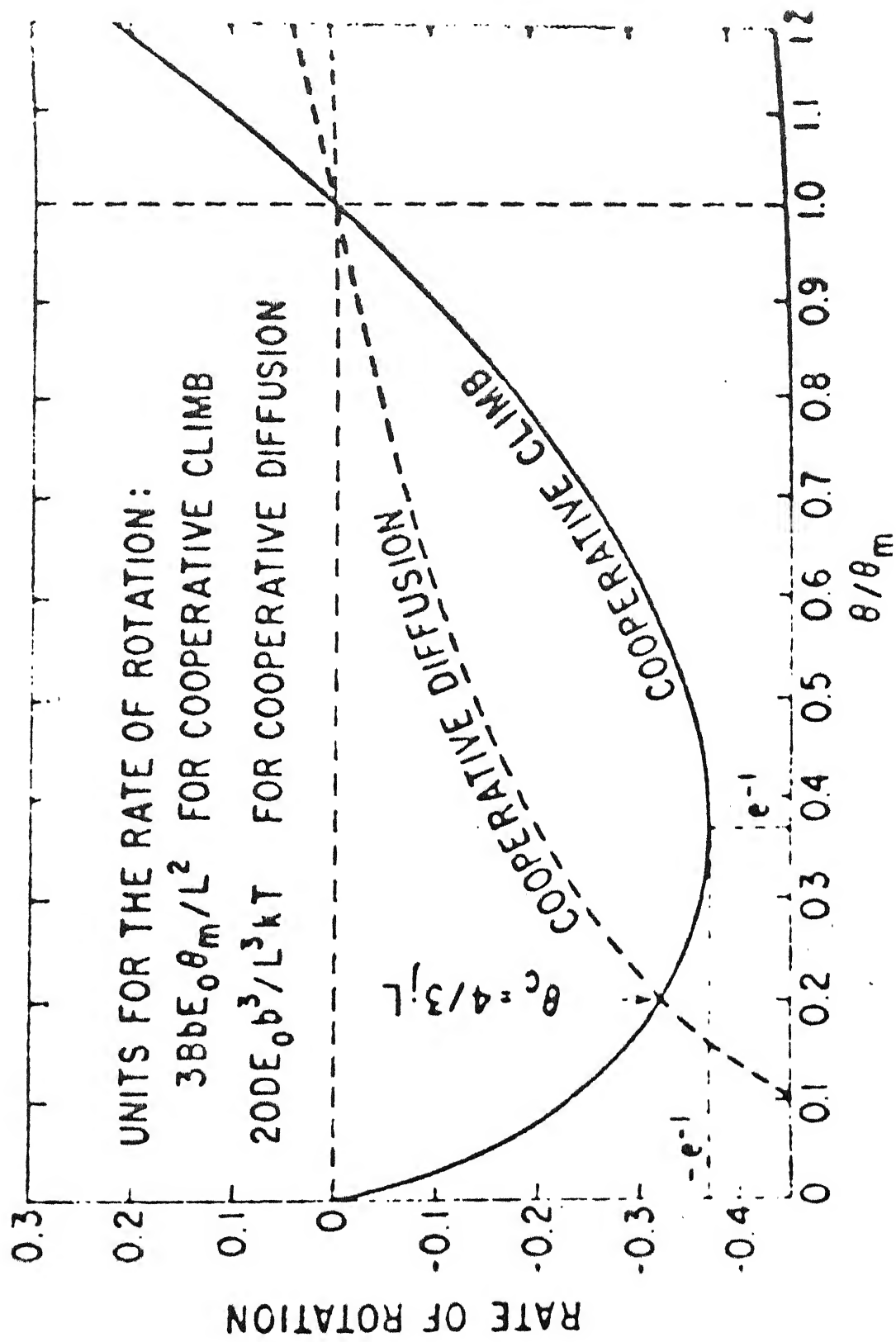AUST AND CHALMERS LEAD, $\theta_m = 25.0°$

far beyond the range of application of the original theory.
By measuring absolute values for the boundary energy in copper,
they were able to show that the Read-Shockley equation can be
applied to tilt and twist boundaries for angles upto 6° and
3° respectively.

In any case the equation (13) predicts that by
lowering the misorientation across a sub-boundary the overall
energy of the system is decreased. Li[41] considered the
case of two neighbouring sub-grains of small misfit, and showed
that a sub-grain could rotate naturally in a direction which
enables low angle boundaries to decrease their angles of
misfit. In fact, the mechanism of sub-grain growth on the
basis of the coalescence model can be treated either in terms
of co-operative vacancy diffusion or co-operative climb and
also the rate of rotation determined as a function of $\dfrac{\theta}{\theta_{max}}$
(Figure 12). Li has estimated that the time required to
eliminate the common boundary between two adjoining sub-
grains of slightly different orientation is given by

$$t = \frac{L^2 kT}{3DE_o b^3 j} \tag{14}$$

where L is the sub-grain size, D is the diffusion co-effi-
cient and j is the jog density. Using this equation he was
able to show that reasonable agreement exists between the
predicted and measured rates of sub-grain growth in aluminium.

The bulk of the evidence supporting sub-grain coal-
escence is due to Hu[37], who studied sub-grain growth direc-
tly by transmission electron microscopic technique. Studies

UNITS FOR THE RATE OF ROTATION:

$3BbE_0\theta_m/L^2$ FOR COOPERATIVE CLIMB

$20DE_0b^3/L^3kT$ FOR COOPERATIVE DIFFUSION

$\theta_c = 4/3\,jL$

made by Taneda[48] on pure iron, and Koo and Sell[49] on
zirconium, also favours coalescence mechanism. Walter[50] on
the other hand, put forward the alternative suggestion that
sub-grain growth may more readily secure by sub-boundary
migration. Smith and Dillamore[51] noticed that sub-grain
growth, on the annealing of cold-rolled iron sheet, occurred
too quickly for a sub-grain rotation process to be the cont-
rolling factor and required sub-boundary migration to account
for the kinetics.

2.3. Primary Recrystallisation

As mentioned earlier, recrystallisation of a deformed
metal involves the nucleation and growth of new strain-free
grains which may be widely different in orientation from the
surrounding matrix. The new grains grow at the expense of
the cold-worked matrix by high angle boundary migration.

2.3.1. The nucleation of recrystallised grains

Studies on the nucleation process in recrystallisa-
tion have, until now, yielded very little information about
the mechanism involved. This is quite understandable since
nuclei, by nature, are small and so it is extremely difficult
to observe a nucleas before it starts growing. Since the
advent of transmission electron microscopy, the structure
and orientation of very small regions can be examined in
more detail. Preciously for this reason this technique has,

for sometime, been considerably used in experiments designed
to study nucleation in recrystallisation.

2.3.2. Models of nucleation

In the course of time three principal models of
nucleation have been developed: a) classical nucleation,
b) sub-grain growth, and c) strain induced boundary migration.

2.3.2.1. Classical nucleation model

The classical Volmer-Becker theory of nucleation,
as ordinarily applied to the formation of solid nuclei in super-
cooled liquids, has been extended by Burke and Turnbull[52] to
the nucleation problem during primary recrystallisation. The
model is based on the assumption that the nucleas which is
stable and capable of growth is formed as a result of thermal
fluctuations in the sense of the classical nucleation theory
of phase transition. A critical nucleas size is determined
by the condition that for the nucleas to be just stable, the
free energy will not change due to an infinitesimal increase
in size, because the reduction in volume free energy will
just balance the increase in interfacial energy. In this
model the volume free energy change can be defined as the
difference in strain energy per unit volume between the cold-
worked state and the fully recrystallised condition. Simi-
larly, the interface between the recrystallisation nucleas and
the surrounding deformed matrix can be envisioned approxima-
tely as a small angle tilt boundary. New grains should want

to form only very small misfit angles with the matrix, since this would lead to lower values of the interfacial energy.

On the credit side this model can account for existence of an incubation period. It also predicts the preferential nucleation of recrystallised grains in the most severely deformed regions. On the other hand, this theory predicts that new grains should always be close in orientation with respect to the adjacent cold-worked matrix. Another drawback of this theory is that no effect of purity is allowed for, yet purity very often seems to be of paramount importance in recrystallisation.

2.3.2.2. Sub-grain growth model

Originally this model[53,54] was based on the idea that the cells produced in the cold-worked materials gradually become strain free during annealing by classical polygonisation. Further growth or coarsening of these polygonised cells or sub-grains was supposed to lead to the formation of a recrystallised grain.

It is now believed that by a process dislocation climb and rearrangement of small strain-free cells are formed in a deformed matrix from regions of high dislocation density. Once a sufficiently large dislocation free cell or sub-grain has formed it can grow into its neighbourhood. According to Cottrell[55] the misorientation of a sub-grain relative to its immediate surrounding is more important than its size in controlling its growth.

Cahn[56] has suggested that when a sub-grain starts growing its boundaries sweep up most of the dislocations which they come in contact with. Thus, the periphery of a growing sub-grain acquires an even higher dislocation density. As the sub-boundary angle increases there varies a point at which the individual dislocations on a boundary begin to loose their identity and it is at this stage that the boundary changes its character from a sweeper up of dislocations to a destroyer of dislocations. With such a state of affairs the growth of the enlarging subgrain (which can now be termed the of a recrystallising grain) may be expected to accelerate. However, early work on recrystallisation[57] has fairly established that larger new grains do not readily grow into matrix regions of orientations only a few degrees different from their own. Thus, the growth of the enlarged subgrains can be ensured only if long range lattice curvatures exist in cold-worked metal. The whole exercise points to a fact which is difficult to rationalise, namely, this small angle boundaries consisting of separate identifiable dislocations migrate freely while boundaries of rather larger angles do not, unless the misorientations across them exceeds about 10-15°. Cahn[56] used the terms 'sub-boundary' and 'boundary' to distinguish between the two categories. However, it has not been analysed preciously at what stage the transition from sub-boundary boundary takes place. A situation similar to this has been described by Walter and Koch[58] in their studies on recrystallisation in cold-rolled Si-Fe. Figure 13

shows schematically what has been observed to happen within a sharply misoriented deformation band in cold-rolled Si-Fe. Here relatively large subgrains have been found to act as preformed nuclei which grow into neighbouring subgrains having sharply different orientations. When this nuclei become large enough to reach the highly misoriented matrix region, they attain large angle boundaries and are then favoured for further growth. Evidences of subgrain growth by boundary migration, ultimately giving rise to recrystallised grains, have been found by Micheals and Ricketts[59], Granzer and Haase[60] and also by Marsden.[61]

The stored energy in cold-worked metal is inefficient for homogeneous nucleation of new grains in recrystallisation. Several models for inhomogeneous nucleation were examined; consideration of the geometry of the nucleation of the new grains at old grain boundaries shows that these sites to be undesirable due to the large contact angle. Others have considered the possibility of a low angle boundary between the deformed grain and the nucleas, but in this case the lack of mobility of the low angle boundary results in polygonisation rather than recrystallisation. Only boundaries that have misorientations $> \sim 20°$ are potential nuclei. Further, a subgrain of the same size as its neighbour would be unstable, that the sub-grain must have a size advantage over its neighbour and at least one high angle boundary to function as a nucleas.[62]

A variant of the subgrain growth model of nucleation based on boundary migration has been proposed by Hu.[63]

This has been termed 'subgrain coalescence' — the mechanism of which has already been described. On the basis of observations on Si-Fe single crystal, he suggested that a recrystallisation nucleas results from a sequence of subgrain coalescence process (Figure 14). Recently, Hu[64] observed a similar process during recrystallisation of heavily rolled copper.
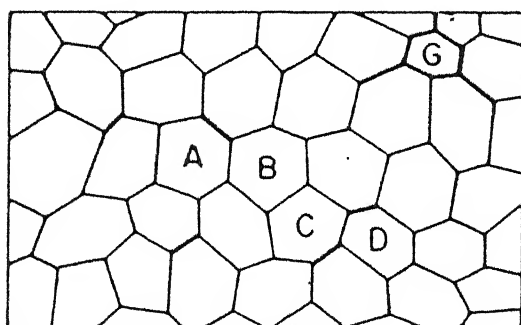
2.3.2.3. Strain-induced boundary migration

This is basically a model of growth since it assumes that the unstable cold-worked state already has large-angle boundaries of macroscopic or microscopic dimensions and that during recrystallisation these boundaries simply bow out leaving strain-free material behind. Observations made with light microscopy by Beck and Sperry[65] showed that sometimes recrystallisation does not involve any nucleation but only growth of strain-free regions brought about by grain-boundary migration. This process which has been termed as strain-induced boundary migration, consists of the irregular movement of an existing boundary with an irregular jagged front, shown schematically in Figure 15. According to this model there is no incubation period, since no nucleus of new orientation has to be formed. Frequently it is observed that the victim grain is the one which is more severely work-hardened, the stored energy of this grain provides the driving force for the entire process. The grain with the larger cell-size will have the lower energy, so that recrystallisation occurs by the movement of a portion of the boundary into the high energy

Fig. 13   Nucleation by subgrain growth in a deformation band
           in rolled Fe-Si alloy (Ref. 58)

Fig. 14   Schematic representation of the formation of a
           recrystallised grain by the coalescence of sub-
           grains (Ref. 63)

"PREFORMED NUCLEUS"

"PREFORMED NUCLEUS"
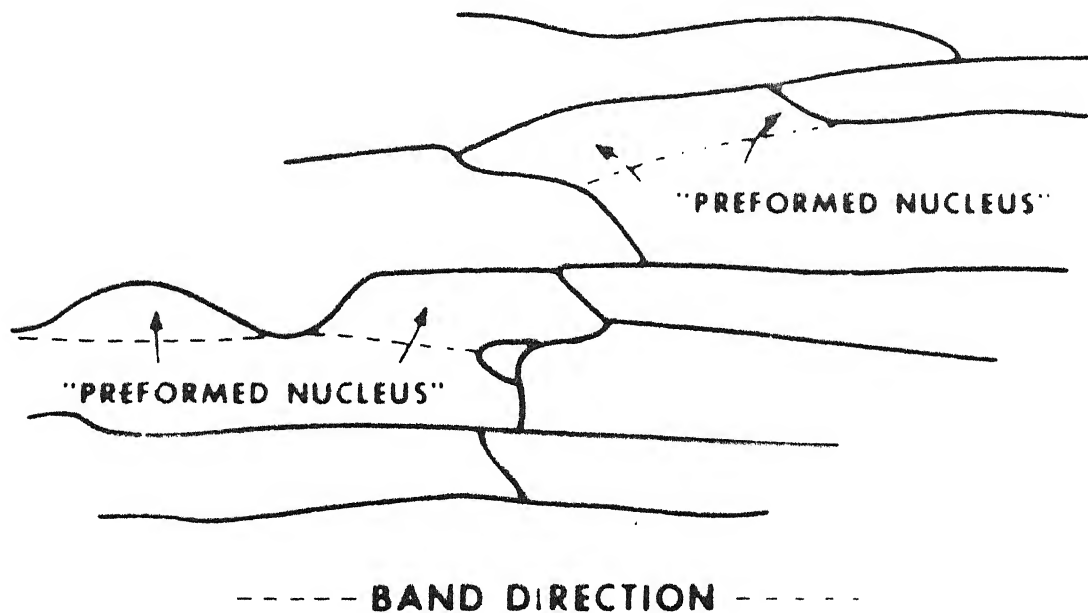
- - - - - BAND DIRECTION - - - - -

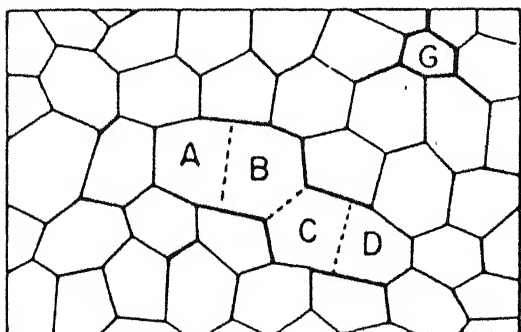(All boundaries parallel to this direction are tilt boundaries

(a)

SUBGRAIN STRUCTURE BEFORE
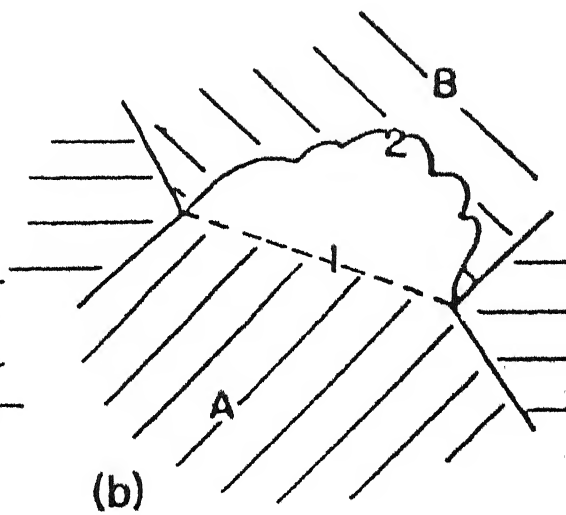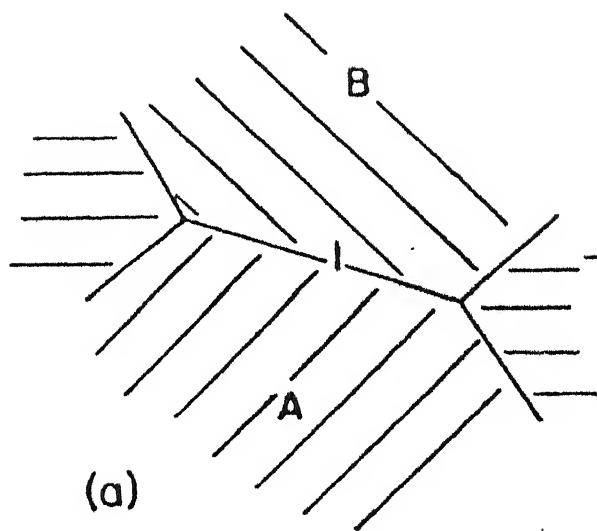NUCLEATION.
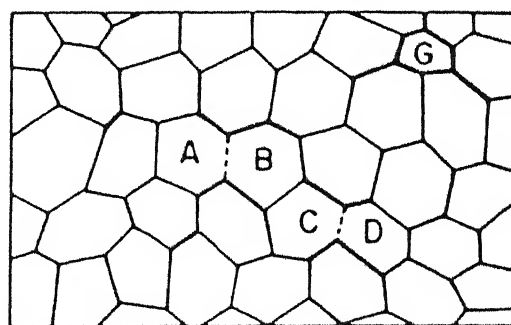
(b)

COALESCENCE OF SUBGRAIN A
AND B, AND C AND D.

(c)

FURTHER COALESCENCE OF
SUBGRAINS B AND C.
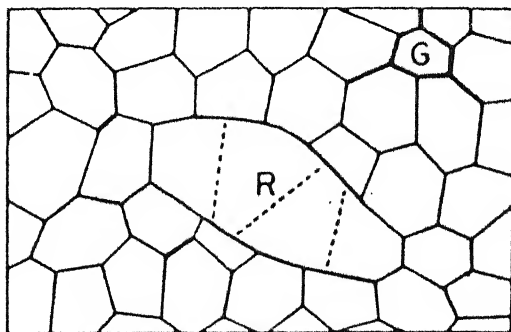
(d)

FORMATION OF A NUCLEUS WITH
HIGH ANGLE BOUNDARIES.

Fig. 15   Schematic representation of strain-induced boundary
            migration at a magnification of 100X.   a) Configura-
            tion before annealing.   b) The boundary between the
            two cold-worked grains A and B has migrated from
            position 1 to position 2 (Ref. J.G. Byrne, 'Recovery
            Recrystallisation and Grain Growth', p. 71 (1965),
            The Macmillan Co., N.Y.)

(a)   (b)

grain having a smaller cell-size. According to Dohertey[62]

nucleation at a grain boundary by strain-induced boundary

migration requires a heterogeneity of subgrain size which wa

achieved (in Al) by subgrain coalescence, but this coalescen

only occurs where a deformation band was present. In iron

reduced 40%, the heterogeneous strain allowed nucleation by

strain-induced boundary migration without the need of free

coalescence. Nucleation occurs steadily as shear bands but

the exact mechanism has not been developed.

Bailey[2] and Bailey and Hirsch[3] developed a simpl

model to analyse the energetics of this process. According

their model local regions of an original grain boundary

migrate by bowing out into the shape of a spherical cap.

Figure 16 shows how a length 2L of a grain boundary graduall

bulges out to successively larger sizes. Bailey and Hirsch[

have shown that growth rate of the recrystallising grain car

be written as,

$$\frac{dv}{dt} = Abf \left[E - \gamma(\frac{dA}{dv}) \right] \tag{15}$$

where, v = volume of the recrystallising grain

A = area of the recrystallising grain

E = difference in stored energy per unit volume

across the migrating boundary

γ = specific grain boundary energy

b^3 = volume occupied by one atom

and

$$f = (\frac{\nu K}{RT}) \exp(- \frac{\Delta F_a}{RT}) \tag{16}$$

Fig. 16   Model for high-angle grain boundary migration proces.
          in recrystallisation (Ref. 3)

where, ΔF_a = free energy difference per gram-atom between an
an atom in the initial state and the new acti-
vated state

R = gas constant

T = absolute temperature

K = atomic weight/density

and ν = atomic jump frequency.

It has been shown that the condition for growth to occur can
be given by the expression

$$L > \frac{2\gamma}{E} \qquad (17)$$

Bailey and Hirsch[3] found this criterion to be approximately
satisfied in their own work on cold-rolled deformed silver.
However, no attempt has been made to check if for the coarser
scale of strain-induced boundary migration claimed by Beck
and Sperry[55] in lightly deformed Al.

2.3.3. Grain boundary migration

Grain boundary migration is known to play an essential
role in recrystallisation and subsequent grain growth. A
grain boundary may be defined as a layer of distorted material
which is the result of atomic mismatch between two adjoining
crystals of different orientations.

2.3.3.1. Orientation dependence of boundary migration

Numerous experiments have been performed to study
the migration of grain boundaries in f.c.c. metals. Studies

where, ΔF_a = free energy difference per gram-atom between an an atom in the initial state and the new acti-vated state

   R = gas constant

   T = absolute temperature

   K = atomic weight/density

and ν = atomic jump frequency.

It has been shown that the condition for growth to occur can be given by the expression

$$L \; > \; \frac{2\gamma}{E} \qquad\qquad (17)$$

Bailey and Hirsch[3] found this criterion to be approximately satisfied in their own work on cold-rolled deformed silver. However, no attempt has been made to check if for the coarser scale of strain-induced boundary migration claimed by Beck and Sperry[55] in lightly deformed Al.

2.3.3. Grain boundary migration

   Grain boundary migration is known to play an essential role in recrystallisation and subsequent grain growth. A grain boundary may be defined as a layer of distorted material which is the result of atomic mismatch between two adjoining crystals of different orientations.

2.3.3.1. Orientation dependence of boundary migration

   Numerous experiments have been performed to study the migration of grain boundaries in f.c.c. metals. Studies

on the growth of new grains in strained single crystals have convincingly demonstrated that growth can be orientation dependent. This points to the fact that there is a marked orientation dependence of grain boundary migration. By careful experiments an anisotropy of the migration rate has been confirmed. The highest migration rate in f.c.c. metals has been obtained when the growing grain is crystallographically related to the matrix by a 30-40° rotation about a common <111> axis.[66,67]

More recently work done on lead[68-70], aluminium[71] and copper[72] has shown that for very high purity zone-refined metals there is practically no preferred orientation relationship for high mobility, at least at high temperature.

In principle, the anisotropy of the boundary migration rate can be interpreted as due to the orientation dependence of either the driving force or the boundary mobility. In highly deformed materials which show a complex dislocation structure, the anisotropy of driving force can be ruled out as a possibility and hence an orientation dependence of boundary mobility is quite expected. The first attempt to rationalise the orientation dependence of the grain boundary mobility arose from the work of Kronberg and Wilson[73] who proposed a grain boundary model based on lattice coincidences. A more recent model based on the concept of boundary coincidence has been proposed by Bishop and Chalmers[74] in order to characterise the special orientations which show high grain boundary mobility. The structure of a symmetric

tilt boundary with a rotation of 28.1° about a <100> axis based on this model is shown in Figure 17.

Theoretical treatments of the effect of impurities on grain boundary mobility have been presented by Cahn[75]. The theory is based on a common assumption that there is an interaction between the impurity atoms and the grain boundary and that during migration the solute atoms have to travel along with the boundary. If the driving force is large enough to overcome the dragging effect of the impurities then the boundary might breakaway from the impurity atmosphere and this according to all theories will increase the mobility considerably.

According to Ray[76], recrystallisation was found to be easier in foils made from the transverse and longitudinal sections than from ones parallel to the rolling plane. This is due to the fact that the cells produced by deformation are pancaked shaped with the cell boundaries lying nearly parallel to the rolling plane. Foils which were taken parallel to this plane may not contain a sufficient number of cells through the thickness to allow formation of a recrystallisation nucleus with a high-angle boundary. In such foils growth may also be inhibited.

During the initial stages of annealing of pure Cu, in the rolling plane section, the small grains having the orientation (110) $[1\bar{1}2]$ were found to nucleate in situ. In the later stages, however, cube-oriented grains appear to engulf small grains of other orientations. In contrast to

Fig. 17 Geometrical model of a symmetric <100> tilt boundary with ideal boundary coincidence in an f.c.c. lattice

a) formation of the boundary by two adjoining lattice with a misorientation angle θ;

b) visualisation of atomic steps in a partition surface between the two lattice regions;

c) arrangement of atoms in the grain boundary (as seen along the common <100>-direction) showing exact coincidence of the atoms lying in the boundary plane;

d) arrangement of atoms after having removed one of the 'overlapping' atoms adjoining the coincidence atoms in (c) (Ref. 74)

a.

b).

c)

d)

$[011\bar{1}]_1$

28,1°

$[01\bar{1}\bar{1}]_2$

$[010]_1$

$[010]_2$

$[001]_1$

$[001]_2$

$[001]$

$<110>$

$<111>$

$(0\bar{k}l)$

$<111>$

$<111>$

$(0kl)$

2ϑ

$[100]$

$<110>$
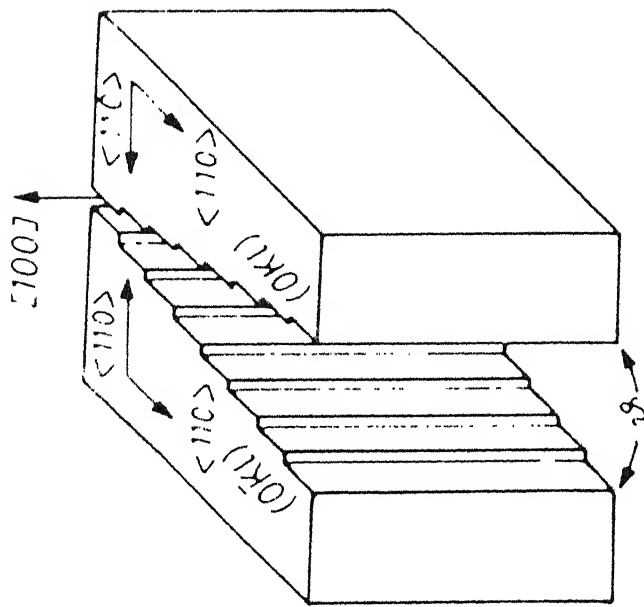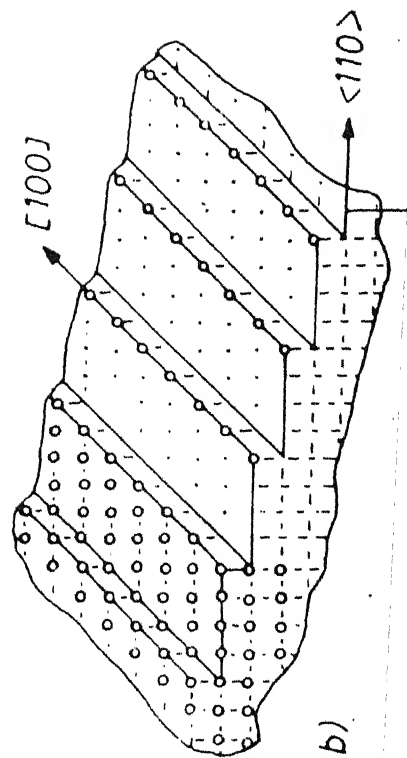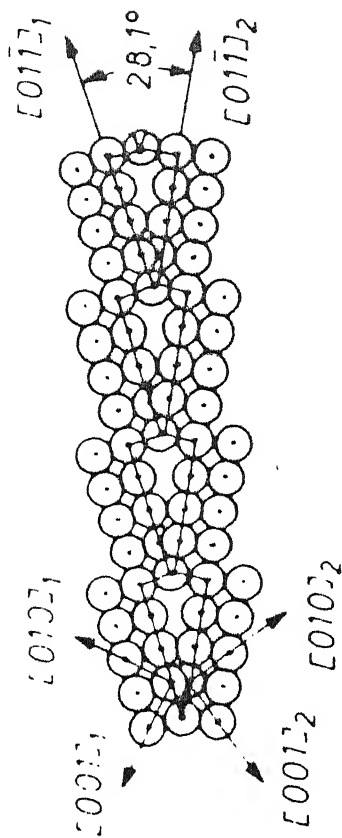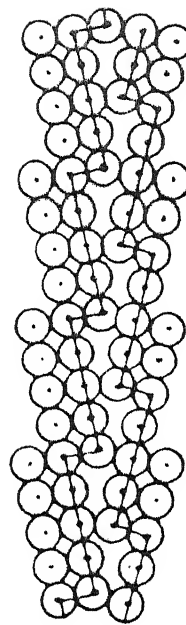
rolling plane sections in transverse section foils of pure Cu (110) [1$\bar{1}$2] oriented grains are found to grow to large sizes.[76]

According to Novikov[77], the kinetics of secondary recrystallisation is affected by 1) the value and the behaviour of pinning force and 2) the magnitude of the driving force for grain growth. The former depends on the volume fraction, the dispersion and the nature of the fine precipitates. The later is influenced by initial grain size distribution and the curvature of the moving boundaries.

The two dimensional growth slows down the secondary recrystallisation when the initial average grain size exceeds 1/10th of the sheet thickness.[77]

2.4. Preferred Orientation or Texture

2.4.1. Introduction

When a polycrystalline material is plastically deformed the lattice orientations in individual grains are found to rotate and the material, thereby, assumes a preferred orientation. The nature of the preferred orientation or the 'texture' which the material acquires is characteristics of the material itself and also depends on the variables connected with the deformation process. When the deformed material is recrystallised, grain rotation again takes place giving rise to a new preferred orientation.

2.4.2. Description of textures

The most complete description of textures in a poly-
crystalline material can be given by stating the crystallo-
graphic orientation of each and every crystallite belonging to
it. This is virtually impossible for fine-grained polycrys-
talline metals and alloys where the number of crystallites is
very high and therefore, it is customary to use a statistical
description instead. X-ray diffraction methods are now widely
used to yield a collective determination of orientation over
a large number of crystals through scanning and integrating
mechanisms. The diffracted intensity data obtained from the
X-ray techniques are corrected for background intensity and
absorption and then normalised relative to intensity level of
a random specimen. These data are then represented by the
use of either conventional or inverse pole figures or by means
of mathematical functions. There are two variations in the
conventional methods: the first one, called the transmission
technique, was originally described by Decker, Asp and
Harker[78] and the second one, known as the reflection tech-
nique, was first described by Schultz[79]. The basic geometry
of the two methods are shown schematically in Figure 18.
Conventional pole figures represent the special distribution
of the poles of a specific form as a function of angles, α
and δ, as defined in Figure 19. The entire pole figure cannot
be determined through the use of either of the above two
techniques, since the transmission method is limited to
approximately the outer 60° of the pole figure by the specimen

counter

2θ

$+\delta$ $-\alpha$

reflecting-
plane
normal

R.D.

T.D.

$-\delta$ $+\alpha$

δ

diffractometer
axis

α

sheet
normal

a

$\alpha = -90°$
$\delta = +90°$

diffractometer
axis

$-\alpha$ B

R.D.

$+\alpha$

δ

counter

$+\delta$

A

T.D.

C

α

$-\delta$

A'

N

B'

D

b

source
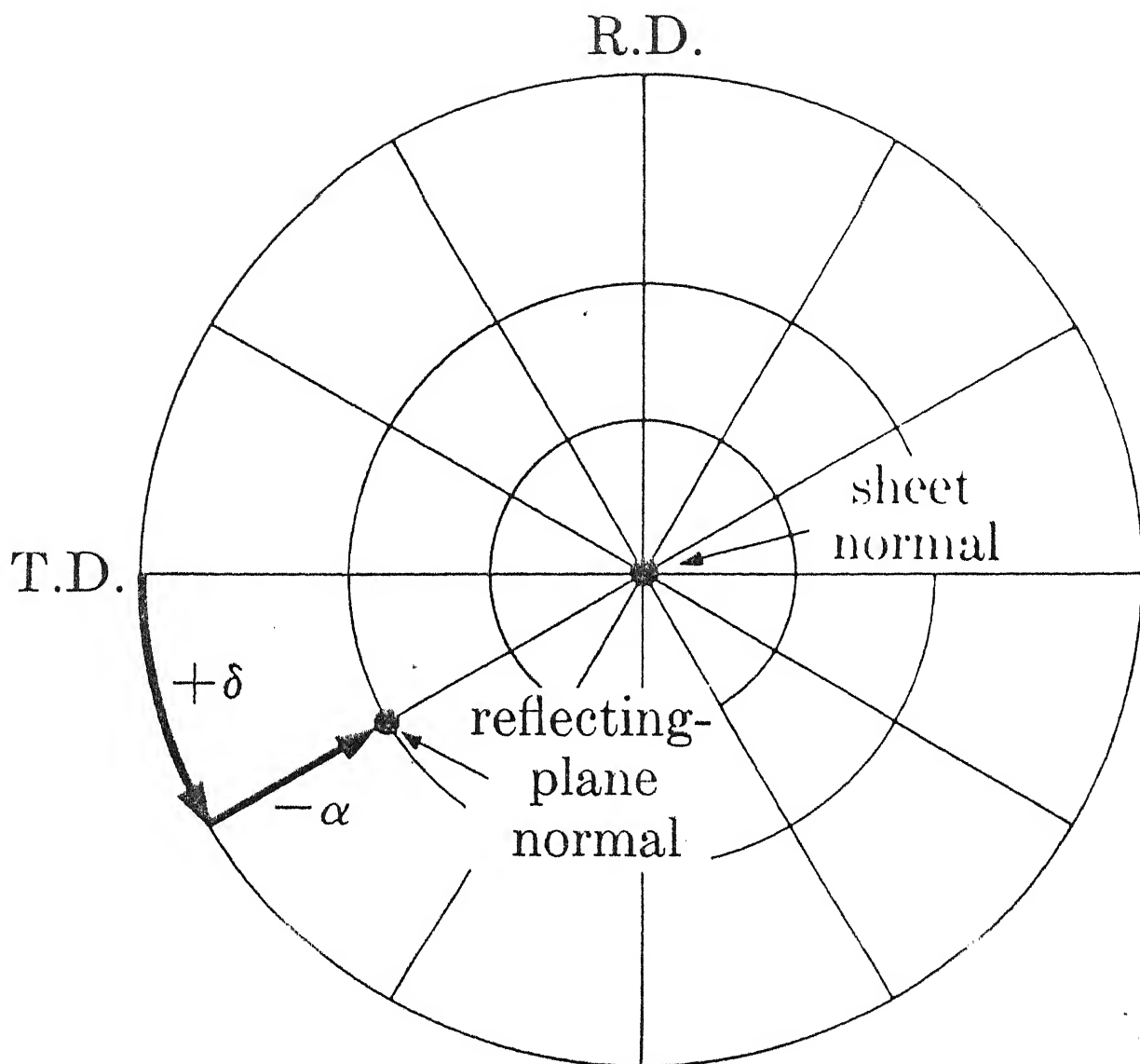
thickness and its linear absorption co-efficient, while the reflection method is restricted to the inner 70° of the pole figure due to defocussing of the Bragg reflection. The information given by a conventional pole figure is conveniently expressed in terms of 'ideal orientations' of the form {hkl} <uvw> where {hkl} denotes the indices of the plane in the plane of the sheet and <uvw>, the direction parallel to the rolling direction.

An alternative description of the texture involves showing the frequency with which a specific specimen direction, e.g. the wire axis of a fibre texture, coincides with crystallographic direction in the unit triangle of a stereographic projection. The axis distribution charts so obtained are commonly known as 'inverse pole figures'. Although many workers including Barrett[80], Harris[81] have used this technique for fibre textures, its application to the description of sheet textures using 3-axis distribution charts for the rolling, transverse and normal directions is a subject of controversy. Bunge[82] has shown mathematically that the 3-axis distribution charts contain less information than the pole figures from which they were deduced. To overcome this difficulty, the concept of biaxial pole figures, which completely represents sheet texture, was introduced by Williams[83,84]. Such a representation essentially consists in giving a continuous range of orientations which expresses the X-ray diffraction intensity data in an optimal fashion. In this method the crystallographic rotation of one of the

within a standard unit triangle by angle ρ and α (Figure
20a). A second direction, B (the rolling direction) is loca-
ted by means of the angle β measured counter-clockwise, from
the equator around A. The angular volume over which sheet
textures are defined is shown in Figure 20b. The orientation
of one grain would correspond to a single point in this volume.
As the number of grains increases, a density function, T, can
be so defined over the volume as to represent the collective
orientations. The density at a particular point in the
biaxial volume will then be proportional to the probability
that a given sample will show the orientation represented by
that point. The density function is related to the experi-
mental X-ray diffraction intensities.

Mathematical techniques for the representation of
preferred orientation have also been proposed, principally by
Bunge[85] and Roe[86]. Essentially the mathematical process
involves the formation of a distribution function of orienta-
tion from a set of suitably processed data of several indivi-
dual pole figures. Though it is apparent that the distribution
functions provide the most complete representation of a
texture, owing to inherent complexity of their derivation,
however, more use is normally made of the graphical methods
of pole figures which, for many purposes, appear to be a
reasonable method of texture representation.

The potential of neutron diffraction texture measu-
rement as a tool for accurate investigations of recrystalli-
sation kinetics is demonstrated by Hansen et.al.[87] by the

(a)

CRYSTALLOGRAPHIC
COORDINATES

BIAXIAL VOLUME

(b)
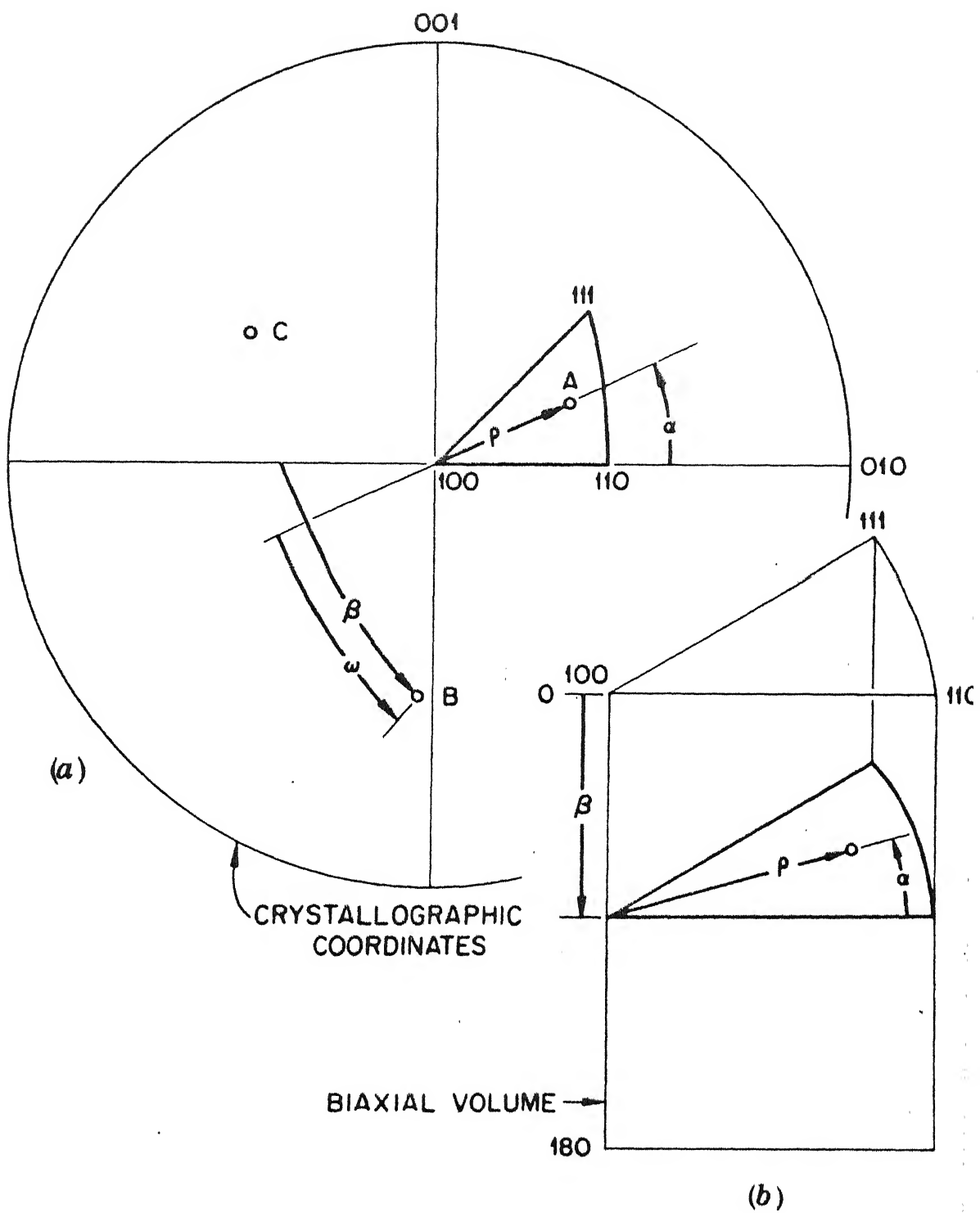
application of the method to the recrystallisation of heavily rolled copper. They demand that this technique compares favourably to the standard methods in this field.

2.4.3. Rolling textures of f.c.c. metals

A random polycrystalline aggregate will develop a preferred orientations or textures, upon sufficient plastic deformation. The nature of the deformation texture depends essentially on the crystal structure of metal and its flow characteristics. The resulting texture may be affected to some extent by many other factors such as the initial textures, the chemical composition, the previous thermal or mechanical treatments, the temperature, rate or physical constraints during deformation, etc. Many theories have been proposed to date to explain the formation of textures in polycrystalline aggregates. However, the complexity of the deformation process of the individual grains in a polycrystal, particularly at large strains, and the usual complexity of the poly-crystalline texture itself impose great difficulty in the derivation of a theory on rigorous grounds. As a first step towards the understanding of texture formation in polycrystals, much effort has been made in the study of texture developments in single crystals.

2.4.3.1. Rolling textures of f.c.c. single crystals

Texture studies on single crystals have been conducted most extensively with the f.c.c. metals Cu and Al.

crystals of Ag, or f.c.c. alloys, such as brass. Most of the data available in the literature for single crystals of Cu, Al, and Ag, brass and other copper base alloys can be summarised stereographically as shown in Figure 21. This has been done in accordance with the initial orientation of the individual crystals.

Group I.

Barrett and Steadman[88], Lin and Hibbard[89] and Hibbard and Tully[90] have studied the orientational changes in copper single crystals on rolling. They found that single crystals of copper in the (110) $[\bar{1}12]$ orientation do not undergo detectable rotation even after very large reductions in thickness (>95%). Thus (110) $[\bar{1}12]$ seems to be quite a stable orientation in Cu single crystals. High stability of the initial orientation after deformation was also noted in crystals having an orientation near the stable (110) $[\bar{1}12]$ and orientation — such as (110) $[\bar{1}15]^{[88]}$ and (110) $[1\bar{1}3]^{[91]}$. Moreover, the small orientations spread noted in the deformation texture of single crystals of these orientations indicated that the trend of lattice rotation was towards the (110) $[\bar{1}12]$ an end orientation. For (110) $[001]$ single crystals of Cu, the trend of the orientational changes upon rolling was also found to be toward the stable end orientation (110) $[\bar{1}12]$.

Hu, Cline and Goodman[6] compare the textures developed (110) $[1\bar{1}2]$ crystals of high purity Cu and Cu-4% Al alloy after rolling unidirectionally at room temperature
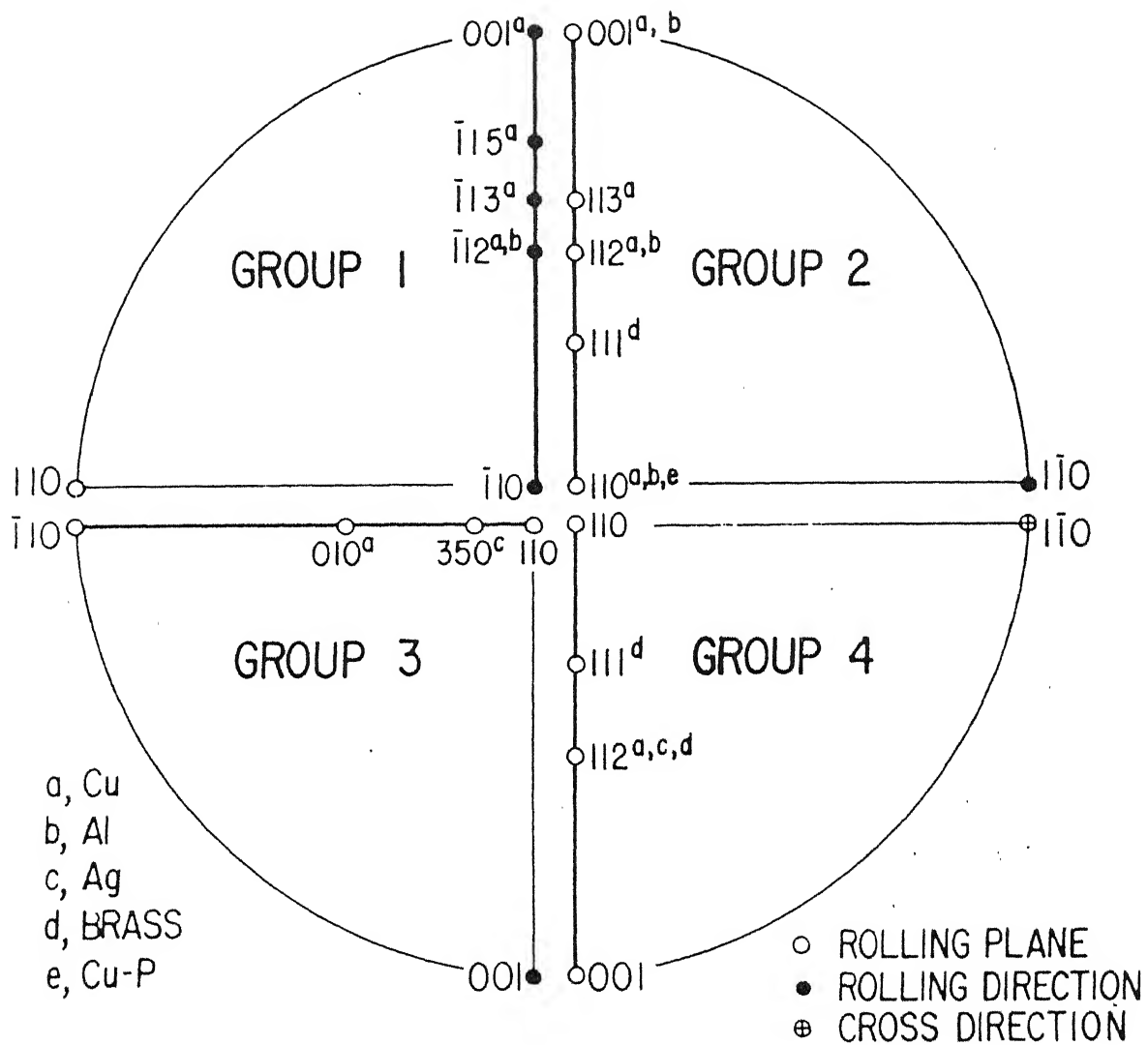
to 95% reduction in thickness. No essential change in orientation was observed in either crystal at this level of deformation. The texture of the high purity Cu crystal was remarkably sharp, whereas Cu-4% Al crystal showed a comparatively a larger orientation spread. The maximum intensity for the Cu-4% Al crystal was substantially lower than that observed in the pure Cu crystals. After 99% reduction, while the texture of the Cu-crystal retained a high degree of sharpness, that of the Cu-4% Al crystal already assumed a double (110) [112] orientation which closely resembles the polycrystalline texture of α-brass.

Group 2.

Among the Group 2 crystals, the rolling textures of (110) [Ī10] single crystals of Al, Cu and Cu-0.05% P were examined by Verbraak[92]. After being rolled to 99%, the principal orientations of the rolling textures in each of these crystals were found to be essentially the same. As shown in Figure 22, the main components of the rolling texture in all 3 cases were a pair of complementary (112) [111] orientations — the range of orientations spread differing considerably amongst the three. The Cu-0.05% P crystal had the most extensive orientation spread whereas the Al crystal had the least orientation spread with Cu lying in between these two extremes. Verbraak described the orientation spread in the Cu-single crystal approximately as a rotation around the most favourable slip direction, [110] after the (112) [111] type orientation was developed.

(111)

(a) Al
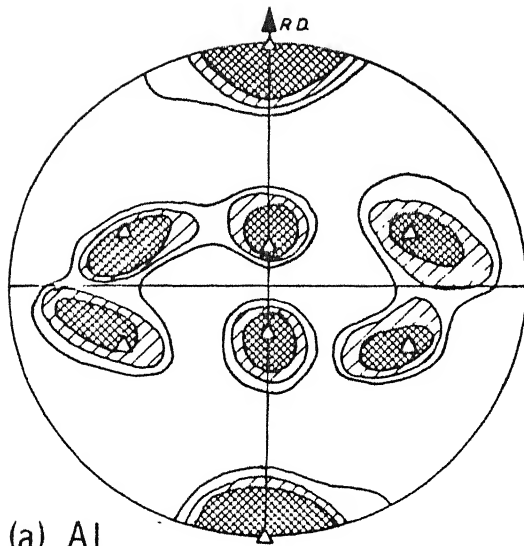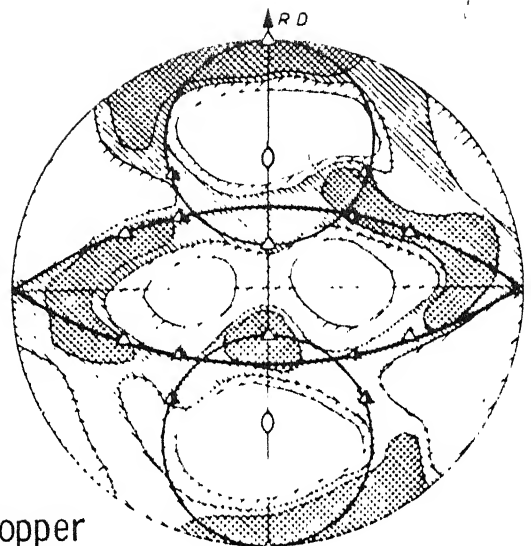
(b) Copper

△ {112} <111>

▲ {112} <111>

() Most favorable
slip directions
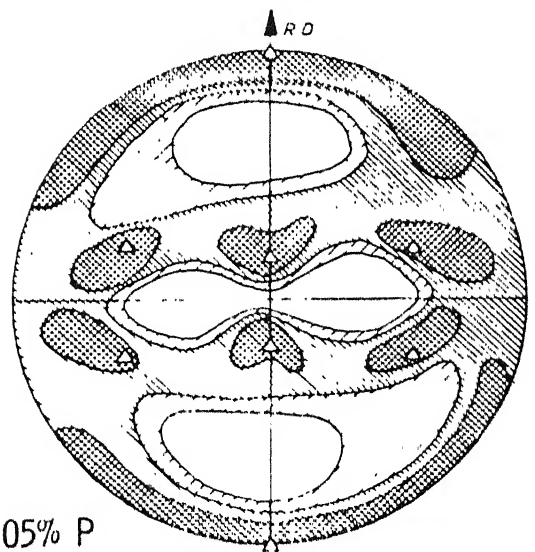
(c) Cu - 0. 05% P

The results of textures studies made on Cu-single crystals of (112) [$\bar{1}$10]$^{(88-92)}$ and (113) [$\bar{1}$10]$^{(88)}$ orientations after rolling were largely similar to those having (110) [$\bar{1}$10] initial orientations. The rollings texture of the (001) [110] oriented single crystals of Cu was found to consist of a (110) [001] component in addition to the two complementary (112) [111]$^{(78)}$ orientations. The textures components are related to the initial orientation of the crystal by rotation around the [$\bar{1}$10] axis in the transverse direction. Burgers and Louwerse$^{(93)}$ have obtained similar results for an Al single crystal rolled in the (001) [110] orientation.

Group 3.

Among crystals having orientations represented by the Group 3 the most extensive investigations have been made on (001) [100] crystals of Cu.$^{(88,91,92)}$ The results obtained by all these workers were essentially the same. It was found that {001}<100> crystals of Cu, after rolling, developed a texture that virtually corresponded to the polycrystalline texture of Cu with a strong cube-orientation component.

The development of rolling texture in a {350} <001> oriented single crystal of α-brass was examined at various stages of rolling by Brick$^{(94)}$. The change in orientation during rolling was found to be from (350) <001> to (110) [$\bar{1}$17] after 85% reduction, then to a pair of complementary (110) [113] orientation after 99% reduction. Thus it was clearly indicated that rotation toward the (110) [112] end orienta-

Group 4.

The most widely studied crystals belonging to this group were the ones having the orientations (111) [112] and (112) [111]. The results obtained by Barrett and Steadman[88] and Verbraak[92] on (112) [111] Cu-crystals are in agreement that the crystals of this orientation, after being rolled to 96 and 99% reductions, develop the complementary (112) [111] orientations. Hibbard and Tully[80], however, have not reported any complementary orientation in their crystal rolled 95%. Hu, Cline, and Goodman[6] have reported a comparative study of texture development on rolling in (112) [11$\bar{1}$] oriented crystals of high purity Cu and Cu-4% Al alloy. They observed a marked difference in rolling textures of the pure metal and its alloy even at a low deformation level (50% reduction) as shown in Figure 23. While the Cu-crystal was found to retain its initial orientation and showed a very sharp texture, the Cu-4% Al crystal developed a large orientation spread and a strong component of (552) [$\bar{1}\bar{1}$5] orientation which is a twin orientation of (112) [11$\bar{1}$]. After further reduction upto 95%, a minor component of the (552) [$\bar{1}\bar{1}$5] twin orientation was developed in the Cu-crystal, whereas the texture of the Cu-4% Al crystal showed further changes from both the matrix and the twin orientations to the (111) [11$\bar{2}$] and (110) [001] orientations respectively (Figure 24).

The behaviour of rolled Ag single crystals of the (112) [11$\bar{1}$] orientation was found to be quite different from that of Cu-crystals of the same orientations rolled at room

(a)

(111)

R. D

C D

0.5
2.5
10
40
80

▲ (112) [11ī]

(b)

(111)

R. D

C.D.

0.5
1
2.5
5
10
20
40

▲ (112) [11ī]
▲ (552) [ī15]

(a)

(111)

R D

C D

0.5
1
2.5
5
10
15
20

△ (112) [11ī]
▲ (552) [ī15]

(b)

(111)

R D

C D

0.5
1
2
3
5
6

▲ (110) [001]
▲ (111) [11̄2]
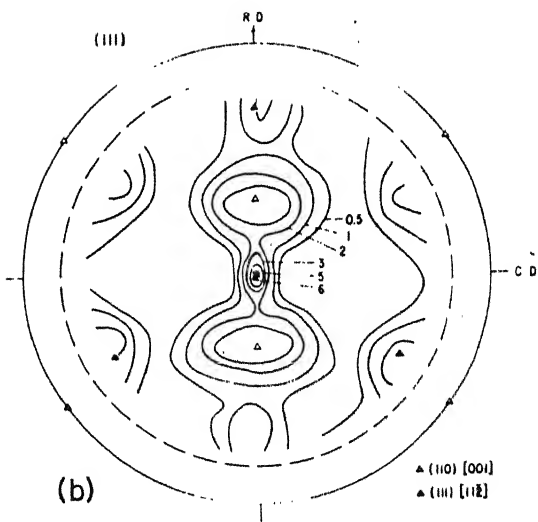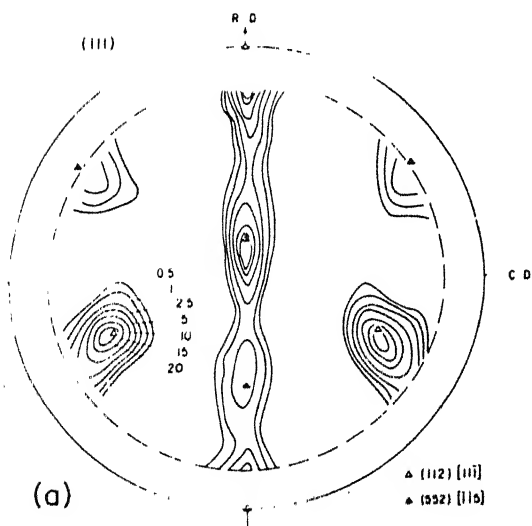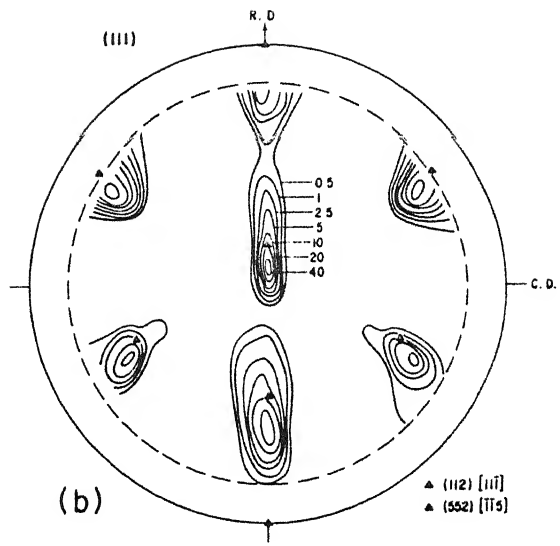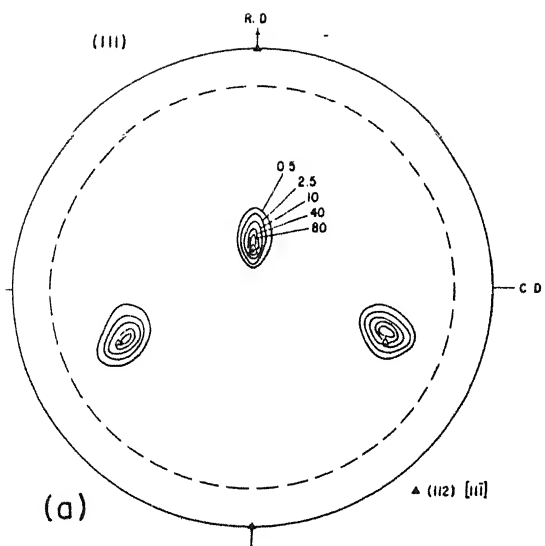
temperature. Verbraak[92] measured the peak intensities of three different reflections, from planes parallel to the rolling plane, of a Ag crystal with the (112) [11$\bar{1}$] orientation, after rolling at various reductions. From his results, he suggested that during deformation crystal rotated around the cross-rolling direction from the initial (112) position in the rolling plane through the (111) plane, and finally to the (110) positions with increasing reduction. In order to explain the observed difference in the rolling textures of Cu and Ag single crystals of the same orientation, namely (112) [11$\bar{1}$], Verbraak postulated that in a (112) [11$\bar{1}$] Cu-crystal, slip is possible on cube planes, that is (001) [110] slip is operative; but in Ag only the (111) [$\bar{1}$01] and (111) [0$\bar{1}$1] slip systems are operative, hence the crystal rotates in one direction only.

Hu, Cline and Goodman[6] pointed out that Verbraak's interpretation was not consistent with the results they obtained for the Cu-4% Al crystal, since the (110) [001] orientation tion in the Cu-4% Al crystal was derived from the twin orientation rather than from the matrix orientation by a large angle rotation. They suggested that their results were in good agreement with the observations of Ahlborn, Grewen and Wassermann[95] on a (112) [11$\bar{1}$] Ag crystal. The results of the later workers indicated that the (112) [11$\bar{1}$] Ag-crystal, after 30% reduction developed a new component of the (552) [$\bar{1}\bar{1}$5] orientation in the texture and that upon further deformation this component rotated into (110) [001].

Formation of rolling texture was also studied in (111) [11$\bar{2}$] oriented crystals of Cu and α-brass. Vacher[96] found that the texture of a (111) [11$\bar{2}$] crystal of Cu-rolled 90% was (110) [112] + (112) [111] with their complementary orientations. Brick and Williamson[97] showed that a (111) [11$\bar{2}$] crystal of α-brass developed the (110) [001] texture after 80% reduction, and a double (110) [112] end texture after 99% reduction.

Single crystals of Cu and Al of a few special initial orientations were also studied by various workers to determine their textural behaviour. These include the (123) [$\bar{4}\bar{1}2$] oriented crystals of Cu[90] and Al[98] and the (3$\bar{5}$8) [$\bar{5}$23] oriented crystal of Cu[90]. It has been found that all these orientations were essentially retained with a reasonable scatter-up to high rolling reductions. The textures of Cu and α-brass single crystals rolled in various irrational orientations have also been determined by several workers[91,99,96].

2.4.3.2. Rolling textures of f.c.c. metals and alloys

In general, two types of rolling textures are normally recognised in f.c.c. metals and alloys. Quantitative texture determination were made by Beck and his co-workers[100,101] on Cu, Al and α-brass after 96% cold reduction. They found that the rolling textures of Cu and Al were similar and at the same time different from the texture of α-brass (Figure 25). The α-brass texture could be adequately characterised by the ideal orientations (110) [112] plus a

minor (110) [001] component. The Cu and Al textures could
not, however, be so readily described and the texture shown
in Figure 25 for Cu has been called an irrational texture.
Hu, Sperry and Beck[101] using quantitative pole figures,
suggested an 'ideal orientation' of approximately (123) [$\bar{4}\bar{1}2$]
to designate the type of texture encountered in Cu and Al.
To account for the intensity maxima on the pole figures, a
second ideal orientation of near (146) [$21\bar{1}$] was also used to
describe the texture of Cu. Results from a number of quanti-
tative texture studied[102-109] indicate that the textures of
most f.c.c. metals (except Ag) are of the Cu-type whereas
those of the Ag and most f.c.c. alloys are of the brass-type.

There are some indirect evidences which indicate that
the rolling texture of polycrystalline Cu can be better
described as (110) [112] plus (112) [111] rather than by the
single 'ideal orientation' (123) [$\bar{4}\bar{1}2$]. In an elastically
anisotropic material, such as Cu, for which accurate single
crystal moduli are available, measurements of Young's modulus
may be used to interprate texture data. With this in mind,
Weerts[80] calculated the variation of Young's modulus with
direction, assuming the texture of Cu to consist of equal
volumes of (110) [112] and (112) [111], and obtained reason-
ably good agreement with the measured variation. Again, as
Jones and Fell[110] deduced, the theoretical modulus variation
with direction for the ideal orientation (123) [$\bar{4}\bar{1}2$] did not
fit the experimental data. They also preferred to describe
the rolling texture of Cu as a mixture of (110) [112] and
(112) [$11\bar{1}$].

Another way of describing the texture of f.c.c. metals was suggested by Dillamore and Roberts.[111] This was indicated by descrete ideal orientation representing a continuous spread and is shown in Figure 26.

A useful contribution to the study of textures of polycrystalline f.c.c. metals has been made independently by Lucke, Perlwitz, and Pitsch[112] and by Haessner, Jakubowski and Wilkens.[113] These workers made orientation determination by selected **area** electron diffraction techniques of the crystallites in a polycrystalline Cu-sheet rolled to 95% reduction. Measurements were actually made on several hundred spots over a large area of the sample, and the orientation distribution was analysed statistically. The distribution of poles as deduced from the SAD data was found to be in essential agreement with the X-ray pole-figures.

2.4.3.3. Texture transition in f.c.c. metals and alloys

The effect of solute additions on the deformation textures of a number of f.c.c. metals has been investigated extensively by Smallman[102-109], Liu and Richman[107-108] and others. Smallman[102] showed that the texture transition from Cu to α-brass type was caused by the addition of elements like Al, Zn, Ge. Liu and Richman confirmed the transition for the elements P, As, Sb, Ge and Sn in copper. Clark et. al.[114] have shown that pure Ni has a texture similar to that of Cu. However, a gradual transition have been found to an α-brass type of texture where Co is added to Ni in
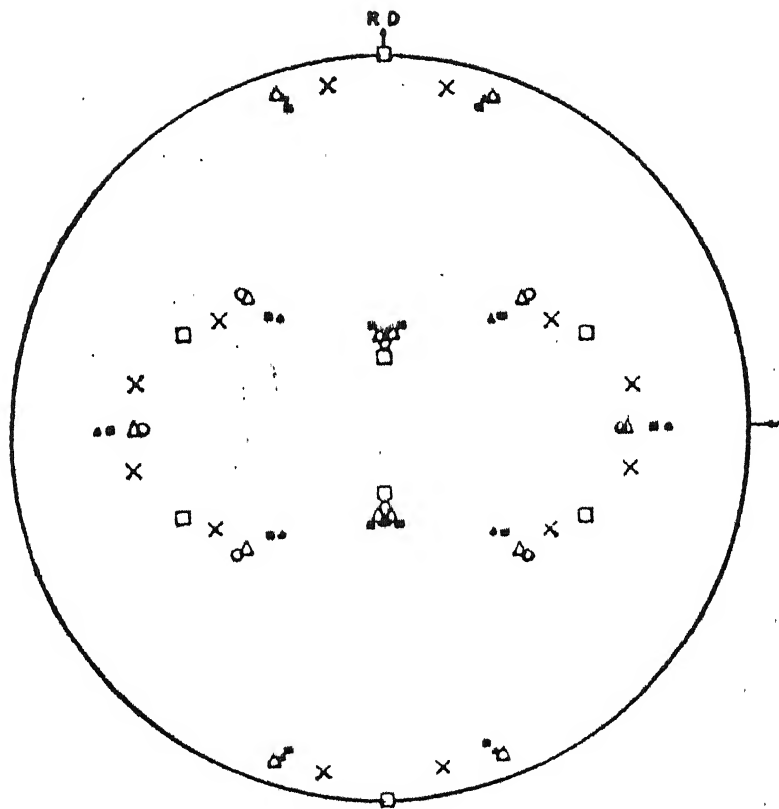
solid solution.[104,115]

Smallman and Lin, and Richman showed that for a given solute, a minimum amount is required to initiate texture transition, and the degree of transition increases with increase in solute concentration. For complete transition a characteristic amount of the solute is required, which varies from solute to solute. Further addition of solute does not change the texture. Smallman[102] tried to correlate the amount of solute requirement for complete transition with the atomic misfit between the solute and the solvent elements. He suggested that for a given solvent metal, the greater the misfit the solute atoms in the solvent lattice, the lower is the solute concentration required to complete the texture transition. Thus, according to Smallman, elastic interaction between the solvent and the solute atoms is the most important factor in affecting the mode of deformation and hence the resulting texture. Lin and Richman[107,108] on the other hand, suggested that the combination of electronic and ion-core interaction might be more important than elastic interactions in initiating a texture transition. A typical example of texture transition of Cu to α-brass type, on the addition of increasing amounts of Zn to Cu, is shown in Figure 27.

In an attempt to characterise f.c.c. preferred orientations over the range from the 'pure metal' of Cu-type to the 'alloy' or α-brass type of texture, a number of parameters have been devised. Parameters suggested by Smallman[102] was based on a ratio of intensities near the centre of the (111)

Table-1 Effect of Alloying on Texture (Ref.125).

Metal	Texture	$\frac{I_{TD}}{I_{20}}$	At.-% Solute to Transform to "Alloy" Texture for 95% Deformation
Aluminium	"Pure-metal"	0·42	—
Copper	"Pure-metal"	0·72	20% zinc 8% aluminium 4% germanium 3·5% tin 2% phosphorus 3% arsenic 1·5% antimony
Gold	"Pure-metal"	0·75	8% zinc
Lead–2% Calcium	"Pure-metal"		—
Nickel	"Pure-metal"	0·49	50% cobalt 10% molybdenum
Palladium	"Pure-metal"	0·55	—
Platinum	Intermediate	0·94	—
Rhodium	"Pure-metal"	0·67	—
Silver	"Alloy"	1·31	—
Thorium	"Pure-metal"	∼0·7	90% cerium
Ytterbium	"Alloy"	1·30	—

pole figure. A second parameter proposed by Liu and Richman[108] was based on the ratio of intensities on the periphery of the (111) pole figure at the transverse direction (I_{TD}) to that 20° from the rolling direction (I_{20}). This parameter was supposed to be more sensitive than the Smallman's and was used by Dillamore et.al.[116] Textures of various f.c.c. pure metals rolled 95% at room temperature are listed in Table I with a qualitative as well as a quantitative description in terms of the parameter (I_{TD}/I_{20}). The amounts of various solute elements required for complete texture transition from 'pure metal' type to 'alloy' type in all these metals are also indicated in this table.

Transition of rolling texture from pure metal to alloy type in the f.c.c. metals can also be affected by changing the temperature of deformation. Muller[117] first reported that rolling texture of electrolytic copper, when deformed at -183°C, resembles the α-brass texture.

From the works done by various workers, temperature dependence of texture transition was found to be very sensitive to impurity contents, e.g., no essential change in texture was observed in high purity copper (99.999%) by rolling at -196°C.[118] The change in texture in 99.99% pure Cu rolled at -196°C was found to be somewhat less pronounced than that found in electrolytic copper.[119]

There is evidence to show that raising the temperature of deformation above room temperature can also affect texture transition. One such example is the pure metal Ag.

(III)
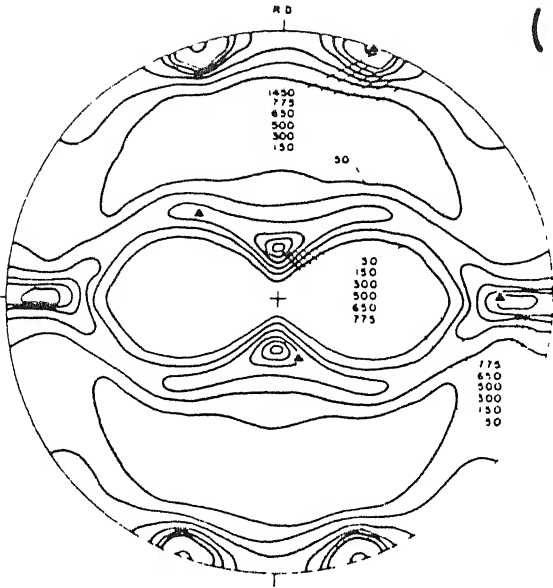
(a) 3% Zn
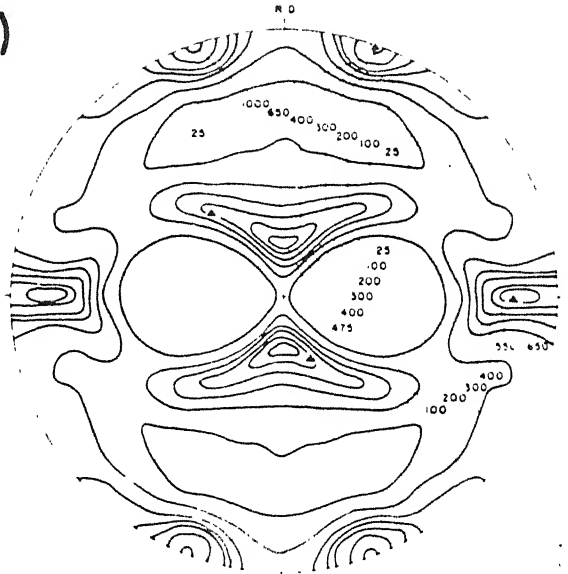
(b) 6% Zn
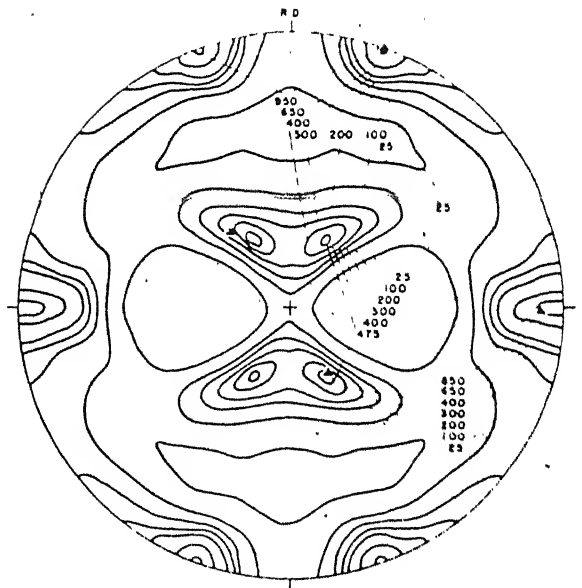
(c) 10% Zn

Pure Ag has been found to develop a texture similar to that of α-brass when rolled at room temperature, whereas when rolled at elevated temperatures, it assumes a texture similar to that of pure Cu.[120,121]

Hu and co-workers[121-123] suggested a general correlation between the temperature dependence of rolling texture transition and of the stacking fault frequency or probability, α, as determined from the X-ray pick-shift measurements. According to them, the brass-type textures are associated with high stacking-fault frequencies, whereas the copper type textures are associated with relatively low stacking fault frequencies. Smallman and Green[118] followed the transition from the Cu-type to the brass type texture that occurs on alloying and related this to a decrease in stacking fault energy, using Cu-Al and Cu-Ge alloys. Haessner[104,115] employed a similar correlation for the texture transition that takes place when cobalt is added to nickel.

2.4.3.4. Theories of texture development in f.c.c. metals and alloys

Barret[80] and Underwood[124] have adequately reviewed the earlier theories of deformation texture due to Wever and Schmid, Boas and Schmid, Pickns and Mathewson, Taylor, and Hibbard and Yen. The later theories have been reviewed in detail by Dillamore and Roberts,[125] Hu, Cline and Goodman[6] and Haessner.[126]

The four more recent theories of texture formation of f.c.c. metals and alloys have, in one way or another,

inherited some of the basic principles or method of analysis used in earlier theories of deformation textures. In all four theories, more or less obvious use was made of the concept of stacking fault energy in the development of texture. Haessner[127] proposed that texture transition in f.c.c. metals and alloys is caused by non-octahedral slip. According to him, normal octahedral slip will lead to the (110) $[\bar{1}12]$ or brass type texture. Cu-type texture will be developed if slip can also occur on the $\{100\}$ planes in the $\langle 110 \rangle$ direction as an additional deformation mode to $\{111\}$ slip. Haessner's proposition is similar to the mechanism suggested earlier by Richards and Pugh[128] to explain the ideal orientation (112) $[11\bar{1}]$. They assumed that a second shear in the $\{100\}$ $\langle 110 \rangle$ system following normal octahedral slip would change the (110) $[\bar{1}12]$ orientation into (112) $[11\bar{1}]$. It was further proposed by Haessner that for metals with low stacking fault energy, cubic slip will become more difficult as the separation of the particles in the $\{111\}$ planes become wider.

A theory based on dislocation interaction has been proposed by Liu[129] to explain the formation of rolling textures in f.c.c. metals and alloys. He considered that during deformation the slip systems which operate are deter-mined by the ability of dislocations on these slip systems to interact producing a net reduction of energy. Having determined which sets of four slip systems give the greatest reduction in energy, the end texture is the orientation at

which the slip rotations on the operating systems cancel out. On this basis, Liu predicted that for metals of low stacking fault energy, the ideal orientations were (110) [$\bar{1}$12] plus an orientation spread with (110) in the rolling plane. The ideal end orientation for metals of relatively high stacking fault energy was shown to be close to (358) [52$\bar{3}$].

Hu et.al.[6] pointed out that although these results were in essential agreement with the two types of rolling textures observed in f.c.c. metals or alloys, the (112) [11$\bar{1}$] orientation of the Cu-type texture was not predicted from Liu's analysis. This theory has also been criticised on the grounds that there would, in fact, be no net reduction in internal energy due to interactions of dislocations on the operating systems. The main difficulty with Liu's theory is that it is highly hypothetical and the present scientific knowledge and experimental techniques available are not suff-icient to test the validity of the postulates of this theory.

Dillamore and Roberts[111] proposed their cross-slip hypothesis in order to explain the deformation textures in f.c.c. metals and alloys. They suggested that all f.c.c. metals first develop the (110) [$\bar{1}$12] or the brass-type texture by normal slip. The Cu-type pure metal texture is formed if, in addition to {111} slip on the primary and the secondary systems, large amounts of cross-slip also takes place on other planes.

A strong objection to the cross-slip hypothesis was put forward by Haessner. He pointed out[126] that the internal

stress attained in rolling is largely dependent of the stacking fault energy of the material and is much higher than $\tau_{11}(0)$, the stress at which cross-slip starts to occur in single crystals at 0°K. He based his arguments on the cross-slip models of Schoek, Seeger and Wolf[130,131] and also on that of Hirsch.[132]

Geometrically, equal proportions of slip on two {111} planes, e.g. the primary and the cross-slip plane is equivalent to cubic slip. Thus the theories of Haessner and Dillamore and Roberts lead to essentially the same model that is capable of explaining the textures in f.c.c. metals and alloys geometrically.

The 'twin hypothesis' of Wassermann[133] is quite different from 3 slip theories already mentioned. In this theory mechanical twinning is supposed to be responsible for the observed textured transition in f.c.c. metals and alloys. He assumed that during deformation, all metals tend to develop the Cu-type 'pure metal' texture by means of slip on {111} planes. For the development of brass type texture, mechanical twinning, as an additional deformation mode is essential. He proposed that the rolling texture of f.c.c. metals can be considered as being composed two limited fibre textures centred on the orientation {110} <112> and {112} <11l>. If mechanical twinning in the systems {111} <211> is considered as a possible deformation mode additional to normal slip, then the material in the {112} <11l> orientation may be transformed by twinning to the {552} <115> orientation (Figure 28), which rotates into the {110} <001> orientation by

R.D

⟨111⟩ ℓ

⟨221⟩ m

⟨331⟩ ℓ

⟨211⟩ m

⟨211⟩ ℓ

⟨411⟩ ℓ

⟨110⟩ m

⟨211⟩ ℓ

⟨111⟩ ℓ ⟨552⟩ m
= 0.707

N.D.

⟨552⟩ ℓ ⟨111⟩ m

⟨211⟩ m

⟨110⟩ ℓ

⟨411⟩ m

⟨221⟩ ℓ

⟨100⟩ m

⟨111⟩ ℓ

⟨511⟩ m

⟨211⟩ ℓ

⟨211⟩ m
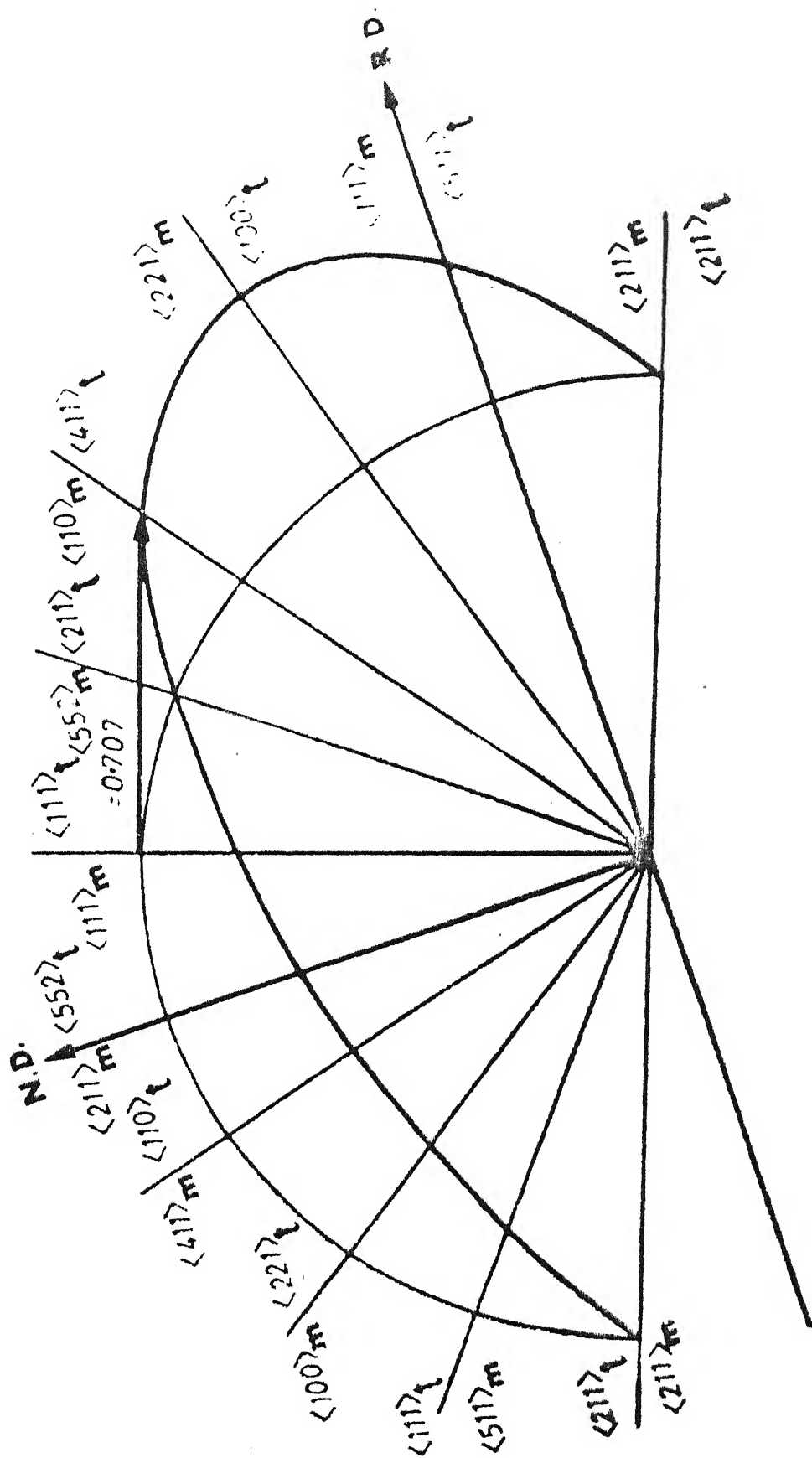
subsequent slip. Wassermann argued that {110} <112> orientation does not change during deformation, because twinning of this orientation would lead to shape change that do not meet the strain requirements of the rolling process. The proposed mechanism is in agreement with the observation that metals of low stacking fault energy may deform by mechanical twinning[134] and it is these metals which exhibit the 'alloy' texture. The theory is also consistent with the observations on the temperature dependence of twinning in f.c.c. single crystals.

2.4.4. Recrystallisation textures of f.c.c. metals and alloys

2.4.4.1. Recrystallisation textures of rolled f.c.c. single crystals

Most of the work in this field has been confined to Cu single crystals of various orientations. In a rolled Cu single crystal of the (110) [1$\bar{1}$2] orientation, Liu and Hibbard[89] found, after annealing, a recrystallisation texture where the individual components were related to the deformation orientation by 30° rotations, clockwise and anticlockwise, about common <111> poles. They observed that for annealing temperatures of 400°C and below, all the four <111> poles of the deformed crystal acted as axis of rotation, whereas above 400°C, only three could be found. The (111) pole figure obtained by Liu and Hibbard for the (110) [1$\bar{1}$2] Cu crystals cold-rolled and recrystallised at 400°C together with a stereographic projection of 30° <111> rotations of {111} poles for crystal in (110) [1$\bar{1}$2] orientation are shown in Figure 29.

R.D.

R.D.

I

II

III

IV
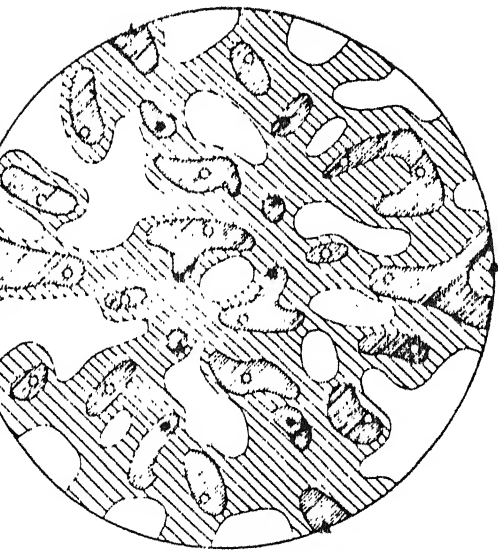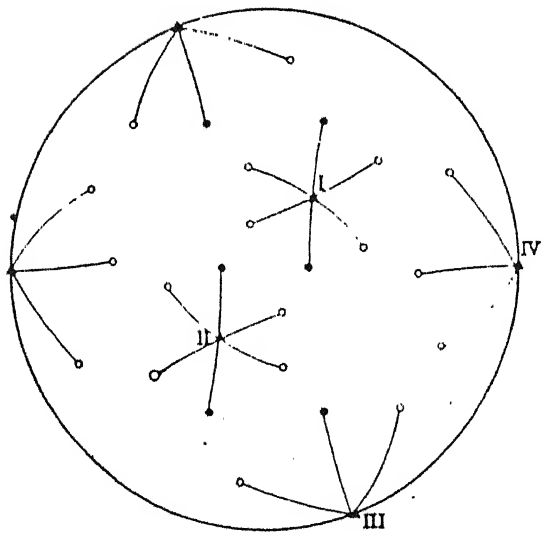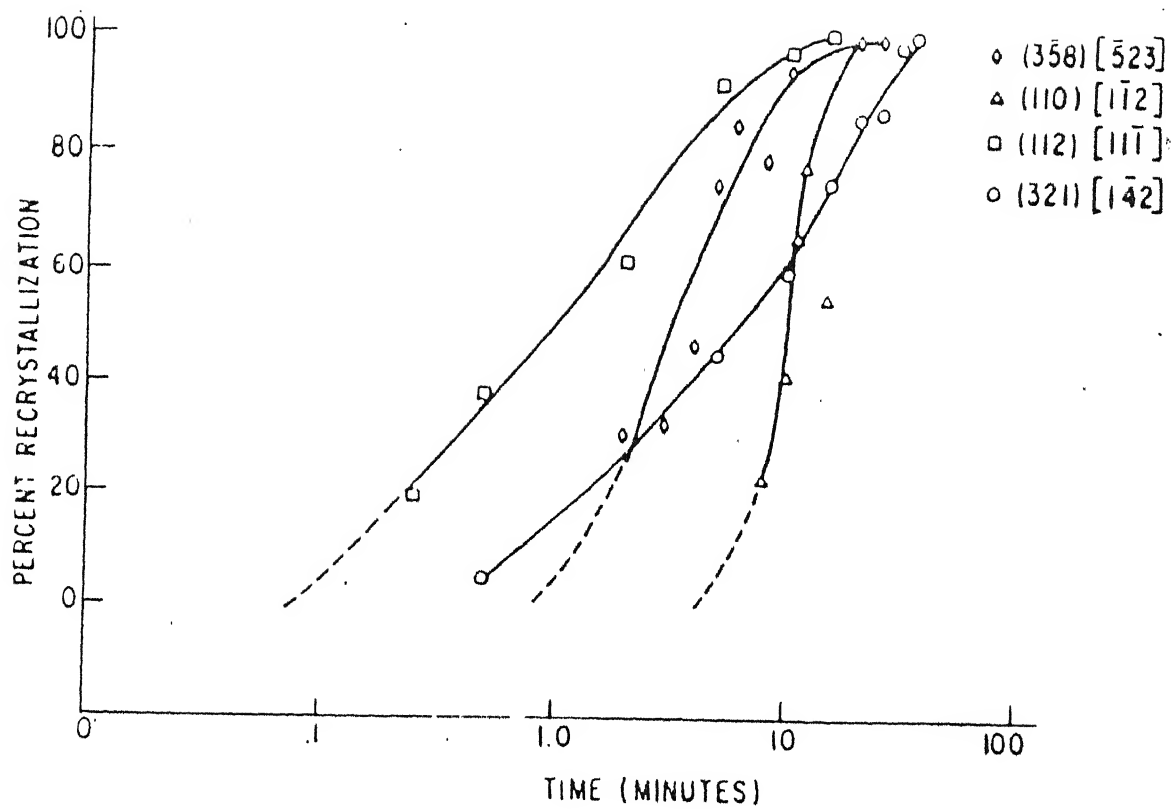
Liu[135] rolled a single crystal of Cu having the modified (358) [3$\bar{5}$2] orientation by 80 to 95% and on annealing the recrystallisation texture components were found to be 7° off the ideal cube texture (100) [001], together with twins of this off-cube component. Verbraak[136,137] rolled the same orientation crystal by 99% and found a similar annealing texture to that of Liu but 15° from the cube orientation.

Hibbard and Tully[90] studied the recrystallisation kinetics of single crystals of copper of various orientations which together represent the rolling texture components of polycrystalline Cu. They found that of the four orientations, (358) [5$\bar{2}$3], (110) [$\bar{1}$12], (112) [11$\bar{1}$] and (123) [41$\bar{2}$], all of which had been rolled 95%, (112) [11$\bar{1}$] recrystallised most rapidly and (110) [$\bar{1}$12] was the slowest to recrystallisation (Figure 30).

In addition to the studies made on Cu-single crystals, work on the recrystallisation behaviour of rolled Al-single crystals of various orientations has also been reported by a number of investigators. Liu and Hibbard[138] rolled an Al-single crystal having the (110) [$\bar{1}$12] orientation. This orientation, though remained reasonably stable during deformation, showed some spread after 99.5% reduction. After annealing at temperatures ranging from 400°C to 600°C, the recrystallisation components were found to be related to the deformation orientation by 40° unidirectional rotation about 3 of the 4 octahedral poles and 30° unidirectional rotation about three <110> poles. On annealing at 650°C, only 3 of these components

were present, two of which where found to bear the <110>
rotational relationships.

2.4.4.2. Recrystallisation textures of polycrystalline f.c.c. metals and alloys

Extensive work has been done in order to determine
the recrystallisation texture of such polycrystalline f.c.c.
metals as Cu, Al, Ni and their various alloys. As in the case
of deformation textures, the most completely documented mater-
ial is Cu and its alloys. The particularly sharp cube texture,
(100) [001] which is found in deformed pure Cu after recrysta-
llisation is a phenomenon of both practical and scientific
interest and this has stimulated a large number of investiga-
tions into the formation of annealing textures in Cu.

It is now known[80] that in pure polycrystalline Cu
the recrystallisation texture is almost random after prior
deformations of upto 50%. The annealing texture resembles
the deformation texture after 90% deformation. Finally, at
higher amounts of deformation the texture consists of the
cube components {100} <001> and its twin {122} <212> (Figure
31). A large body of work[92,107,108,136,139-142] has infor-
med that the cube texture is more perfect and twin density
lower for fine-grained starting material and a high annealing
temperature. The cube texture was found to become more
sharp for deformations between 95 and 99.9%[143] but at
higher amounts of deformation the sharpness decreased. Kamijo
and Yamamoto[141,144] examined the effect of a secondary
reduction at either 45° or 90° to the original rolling

a   b
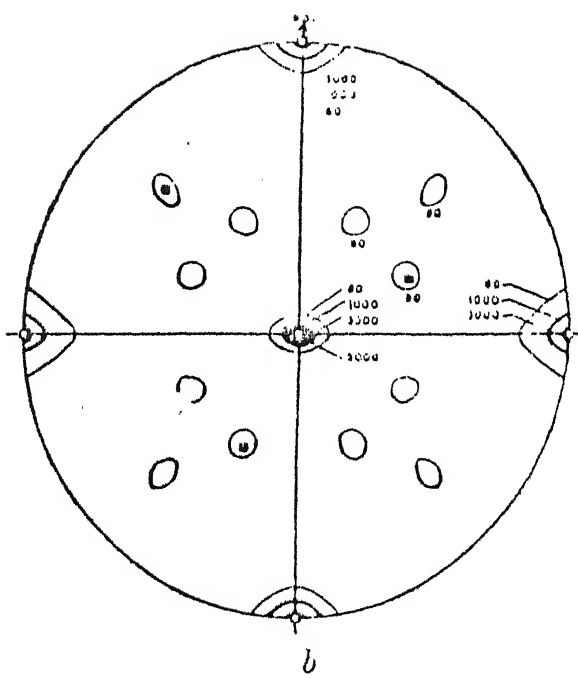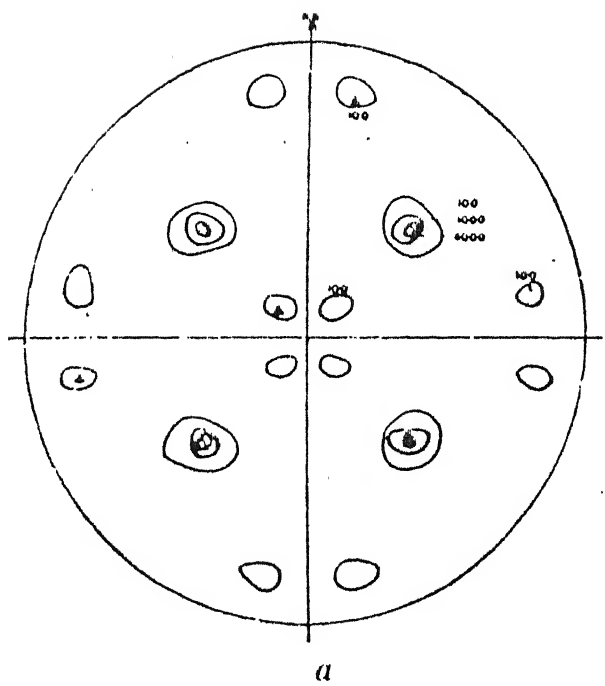
direction, after a primary reduction to a texture which gives rise to the cube texture on recrystallisation. It was found out that low secondary reductions caused increasing spread about the cube texture and its eventual loss. At high secondary reductions cube texture was again obtained after annealing.

The recrystallisation textures in Ni and its alloys have also been extensively investigated. Detert et.al.[106] found that in Ni of 99.5% purity which had been rolled to 97.5% reduction, recrystallisation occurs at 550°C giving rise to a texture similar to that of annealed pure Al but with the cube component for more prominent (for Al of 99.99% purity and about, the recrystallisation textures are similar to those for Cu, with the exception that it is rather more difficult here to produce 100% cube texture[128,139,145,146]). A texture consisting entirely of the cube orientation was produced when the rolled material was annealed at 1050°C for 90 minutes.

A large number of investigations have also been made on the effect of alloying on textures in Ni. Annealing textures of Ni-Fe alloys, in particular, have been extensively studied[143,147-151] on alloys containing from 50% to 70% Fe. It has been found that deformation textures of Ni is not greatly affected by the addition of upto 70% Fe and on recrystallisation the cube texture is the most important component. An higher annealing temperature is thought to be beneficial in raising the proportion of cube orientation in the final annealing texture. Detert et.al.[106] have reported that

addition of Co and Mo to Ni affects its deformation texture — the transition from the pure Ni to the alloy type texture takes place when either 10% Mo or 50% Co is added to Ni. The rolling texture transition then produces a change in the annealing texture as is found in brass. In the same investigation Detert et.al.[106] observed the addition of 50% Fe, 15% Cr or 1% Ta had no effect on the deformation or recrystallisation texture of Ni.

Clark and Mee[114] have reported on the recrystallisation textures in commercial Ni and some solution — and precipitation hardening Ni — alloy in the Nimonic series. The reductions used were, however, rather low and the textures were either random or of retained rolling texture type.

2.4.4.3. Theories of the formation of recrystallisation textures

Since primary recrystallisation involves nucleation of a new set of strain-free grains and their subsequent growth, it is clear that orientation present in the fully recrystallised material require both the presence of nuclei in these orientations and the ability of recrystallisation grains of the orientations in question to grow during the annealing process. In search for the origin of recrystallisation textures, one of the principal questions to be decided is whether the orientations absent from (or only weakly represented in) the recrystallisation texture are suppressed because of the unavailability of nuclei in these orientations or because of the inability of such nuclei to grow to an

appreciable volume in competition with nuclei of other orien-
tations. These two ideas from the basis of two theories that
have been put forward to explain the development of primary
recrystallisation texture. In the 'oriented nucleation' theory
the nucleation process is supposed to be of primary importance
in determining the range of available nuclei which can contri-
bute to the recrystallisation texture. In the 'oriented growth'
theory, on the other hand, the recrystallisation texture is
supposed to be result of growth selection due to the orienta-
tion dependence of the rate of grain boundary mobility.

The first attempt at rationalising the orientation
relationship between recrystallised grains and the deformed
matrix in which they grow was made by Bergers[93] who has also
been the main proponent of the oriented nucleation theory.
Following the concept that the preferred orientation of the
recrystallised grains is determined by the orientation of the
available nuclei, Burgers tried to relate the nucleas orien-
tations in turn to a model of the structure of his compressed
Al single crystal specimens. He assumed that on annealing the
deformed crystal, the nuclei of the recrystallised grains
developed from the most heavily deformed fragments which were
located in the vicinity of active glide planes. Burgers
considered that these fragments or highly deformed elements
were rotated with respect to the main body of the crystal
around <112> axes parallel to the active slip planes and
normal to the active slip direction in each slip plane. The
sense of rotation was expected to be that corresponding to
'rollers' between neighbouring glide lamellae of the crystal

These earlier suggestions by Burgers, in effect, invokes local bending caused by edge dislocations left behind during slip and concentrated along slip planes (Figure 32).

Barrett[152] made orientation determinations on fifty recrystallised grains in a compressed Al single crystal and found the orientation to correspond to approximately 45° rotations around <111> axes with respect to the orientation of the deformed crystal. The <111> rotational orientation relationship in primary recrystallisation of Al has been also reported by other workers.[153,154] Maddin, Mathewson and Hibbard[155] reported that the recrystallised grains formed on annealing α-brass single crystal deformed in tension were related to the respective matrix crystals by rotations around approximately common <111> axes, and that the later were normal to the primary, cross or conjugate slip planes (i.e. none of the crystals was rotated around the fourth [111] axis, which was not normal to an active slip plane). All these results, as also the results of Liu and Hibbard[89] on rolled Cu-single crystal, seemed to contradict Burgers theory of oriented nucleation. The theory also does not account for the apparent lack of preferred orientation of the recrystallised grains in slightly deformed single crystals.[156,157] Beck and Hu[158] argued that Burgers theory should have predicted the same kind of rotation for both heavily rolled and lightly deformed single crystals, with less scatter in the later case, because of the better definition of slip planes and slip directions in crystals lightly deformed in tension. In spite of these

A_{Dr}

$\vec{G}$

A_{Kr}
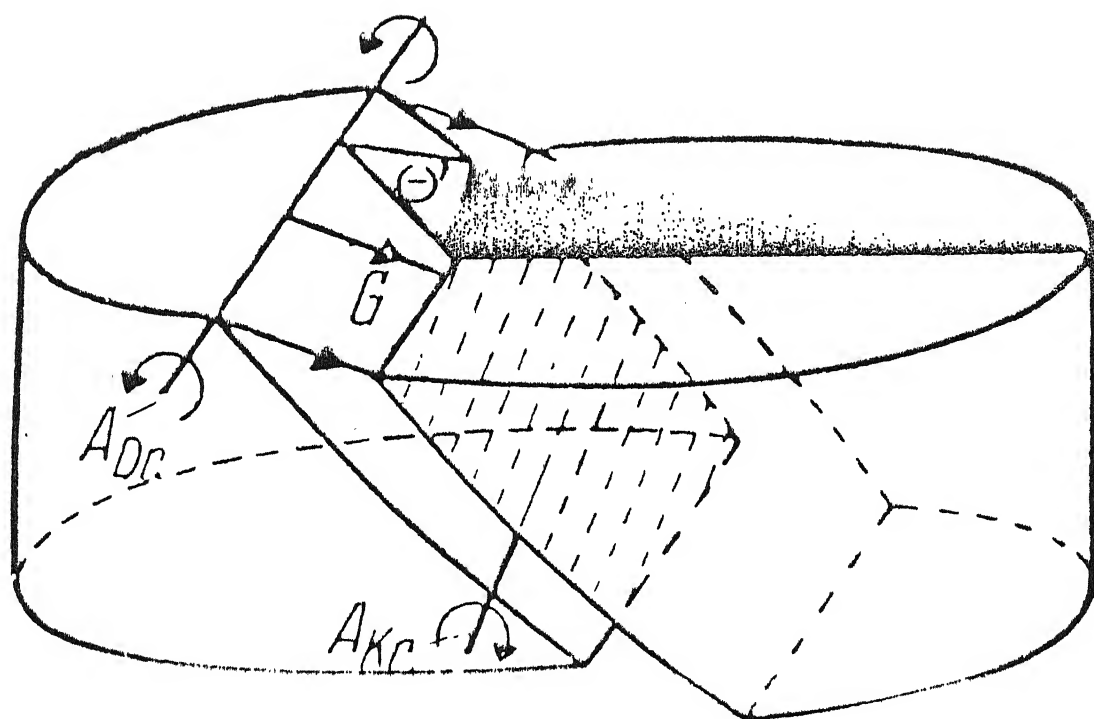
contradictions, the success of Burgers theory in some cases of
b.c.c. single crystals, particularly in predicting the sense
of rotation corresponding to the re-orientation on recrystal-
lisation, suggests the possibility that this theory may correc-
tly reflect at least certain elements of the factual situation
for highly compressed or rolled single crystal.[158]

Liu and Hibbard[89] tried to explain the application
of the oriented nucleation interpretation to the recrystallisa-
tion textures of rolled polycrystalline Cu, brass and Al,
thus going far beyond the original proposal of Burgers and
Louwerse[93] which was concerned only with the recrystallisa-
tion of uniformly compressed single crystals. Beck[159] has
observed that the application of an oriented nucleation mecha-
nism to polycrystalline metals must encounter certain diffi-
culties. Such a mechanism depends on a definite orientation
relationship between nuclei and matrix, and since the nuclei
orientation must be related to the orientation of the micro-
scopic matrix region immediately surrounding it, the range of
nucleas orientation is bound to be at least as large as that
of the matrix orientations. Thus, on the basis of oriented
nucleation theory, a complex deformation texture, such as
that of rolled polycrystalline Cu, should, on annealing, yield
an extraordinarily large number of nucleas orientations and
consequently an extremely complicated recrystallisation
texture. However, it has been found that under suitable cond-
itions only the very sharp single compounds 'cube texture'
{100} <001> is actually formed on recrystallisation in rolled

Cu. To overcome this difficulty Liu and Hibbard[160] later
assumed that the 'modified (358) [3̄5̄2]' component of polycrys-
talline deformation texture which was suggested to give rise
to the cube oriented nuclei,[138] recrystallises faster than
structural elements in any other orientation present in the
deformation texture, and, thus, the orientation of its recrys-
tallised grains dominates the recrystallisation texture.
Work by Hibbard and Tully[90] showed that the assumption of a
maximum recrystallisation rate for the (358) [3̄5̄2] orientation
in Cu is incorrect and so the proposed oriented nucleation
mechanism based on the orientation dependence of recrystalli-
sation kinetics seems to be very doubtful.

The cube texture found in Cu, Ni and other f.c.c.
metals and alloys has excited much curiosity because of its
high degree of sharpness. To explain the formation of the
cube texture in cold-rolled polycrystalline Cu after annealing,
a new oriented nucleation mechanism has been proposed by
Burgers et.al.,[161] Burgers,[162] Decker and Harker[163] and
Stadalmaier and Brown.[164] All of them assumed that in
rolled polycrystalline f.c.c. metals, like Cu, there are
present small local regions that possess the cube orientation.
These regions would then serve as the nuclei for recrystall-
isation on annealing. A nucleas in the cube orientation
would, for reasons of particular elastic anisotropy, have
the lowest possible strain energy[165]; hence it would be
favoured over all others in growing at the expense of the
matrix.

A very serious difficulty with the postulated mechanism is that it implies the formation of the cube recrystallisation texture, regardless of the deformation texture, provided that at least a small volume fraction of the deformed material is present in the cube orientation. Merlini and Beck,[166] however, observed that the cross-rolled Cu which has about twice as much cube-oriented material present as in straight rolled Cu, does not recrystallise in the cube orientation. Again, Verbraak[92] has reported that a heavily rolled Cu crystal of the {100}<001> orientation has a deformation texture very similar to that of highly rolled polycrystalline Cu, except for the relatively large volume fraction of material the single crystal retains in the cube orientation. In spite of this, the recrystallisation texture of the rolled crystal comprises only a very weak cube texture component. Results very similar to this were obtained earlier by Schmid and Thomas[143] with rolled polycrystalline cube textured Ni-Fe.

A new and quite different oriented nucleation mechanism has been suggested by Burgers and Verbraak[167] to explain the formation of the cube texture in Cu. This model, described as the martensitic nucleation of cube texture, is based on a lattice transformation suggested by Rowlands[168] and earlier by Richards.[169] Rowlands[165] described a twinning mechanism, which leads from the original single f.c.c. lattice to two new f.c.c. lattices having a twin orientation relationship with respect to one another. He showed that the homogeneous shear is necessary to accomplish this transforms

the vector [100] of the original lattice to the vector $\frac{1}{2}$ [110]

in both new lattices and also the vector [001] of the original

lattice into the vector [1$\bar{1}$2]. Accordingly, the (010) plane

of the original lattice becomes ($\bar{1}$11), parallel to the compo-

sition plane which the two twin related lattices have in

common. Burgers and Verbraak[154] suggest that adjacent twin

related lattice regions of the two {112} <111> type orienta-

tions, which are present in highly rolled polycrystalline Cu,

may undergo jointly an inverse Rowlands transformations to

convert these orientations to the cube orientation (Figure 33).

This mechanism does not require the presence of any

cube oriented regions in the cold-rolled material prior to

annealing. It may be of interest to note here that previous

experiments with rolled single crystals of the (11$\bar{2}$) [$\bar{1}$11] and

(1$\bar{1}$0) [112] orientations revealed that on annealing the former

recrystallises giving a cube component whereas the later does

not.[170] Beck and Hu[158] have objected to this model on

energy considerations. They argue that the decrease in free

energy due to the postulated untwinning process would be that

connected with disappearence of the ($\bar{1}$11) coherent twin compo-

sition boundary which obviously has a very low interfacial

energy. At the same time the newly formed cube oriented

lattice region, created as a result of the inverse Rowland

shear, must be separated from the surrounding material by

high angle boundaries which must be having high interface

energy. Thus, according to Beck and Hu, the total free energy

would increase as a result of the inverse Rowland shear process.

$\{112\}\ \langle 111\rangle$

inverse
Rowland

$\langle 100\rangle\ [001]$

N.D

T.D.
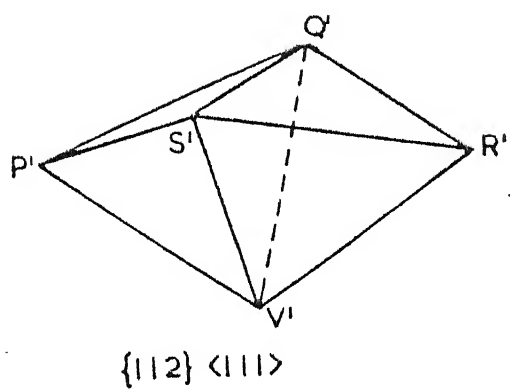
R.D
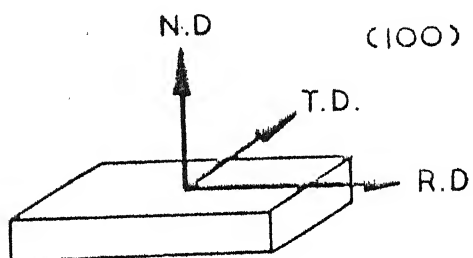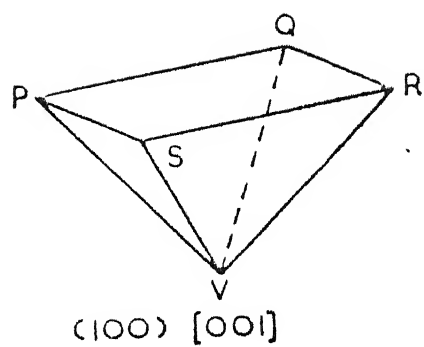
They also question Verbraak's[171] supposition that during the inverse Rowland shears a few of the 48 possible types of [112] partial dislocations are expected to be eliminated and the corresponding decrease in free energy might favour the postulated nucleation mechanism.

The main proponents of the oriented growth theory are Barrett[152] and Beck.[172] This theory is based on the well-documented dependence of growth rate on the orientation relationship between the matrix and the growing grain. Lucke and his co-workers[119,173,174] have shown that the recrystallised grains which grow at the fastest rate are related to the unrecrystallised matrix as follows:

a) Al: 40° rotation about a common <111> axis

b) Fe-3% Si: 27° rotation about a common <110> axis

c) Zn: 30° rotation about a common <0001> axis.

These results are in good agreement with those quoted by earlier workers for f.c.c., b.c.c. and h.c.p. structures, respectively.[80] However, it has been also pointed out that these orientation relationships are not necessarily obeyed by all materials having a particular crystal structure. Cu and Ag, for instance, show a 30° <111> axis whereas Al-0.5% Mn always have been found to possess a 84° <112> relationship.[125] All these works clearly indicate that grains in particular orientations have high growth rates without suggesting any reason why this is so.

Using this information, Dillamore[175] has proposed an analysis which enables the recrystallisation texture to be predicted from the deformation texture.

on a number of conditions which must be satisfied if a potential nucleas is to grow. For example, a nucleas must be positioned so that it is capable of rapid growth into two orientations, and must also be capable for long range growth. Dillamore's analysis has had considerable success in deriving the textures of annealed f.c.c. metals but rather a limited success when applied to b.c.c. metals.

Experiments in which recrystallised grains in random orientations are artificially nucleated by a highly localised inhomogeneous type of deformation, and then allowed to grow, have thrown much light on the oriented growth mechanism. Such experiments were carried out by Beck et.al.[67,98] with Al. It has shown that the orientation relationship between recrystallised grains and the matrix, obtained when the recrystallised grains are nucleated by highly localised deformations, such as pin pricks or cuts or abrasions, is similar to that obtained without such 'artificial nucleation'. In the work by Beck et.al.[67,98] Al single crystals were rolled 80% and artificial nucleation was ensured by abrasing one surface with emery paper. After short time annealing small recrystallised grains were found to form at the roughed surface. Texture studies indicated quite a random orientation of these small grains at this stage. After annealing for longer periods of time, some of these grains were seen growing selectively across the specimen thickness. This, coupled with the observation that in Al, the fastest growing grains are those having nearly 40° <111> rotational orientation relationships with

the matrix,[176] furnish satisfactory evidence of the effect-
iveness of the selective growth mechanism in giving rise to a
sharp recrystallisation texture in single crystals.[158]

Several arguments have been put forward by various
investigators against the view that primary recrystallisation
textures are controlled by the oriented growth mechanism. A
major objection was raised by Burke.[177] He pointed out that
although the components that actually occur in recrystallisa-
tion textures in f.c.c. metals do have approximately 30° or
40° [111] rotational orientation relationship with the matrix,
not all such orientations that have crystallographically equi-
valent orientational relationships with the matrix actually do
occur. Beck and Hu[158] have reasoned that the absence of
recrystallisation texture component corresponding to certain
<111> rotations are due to complexity of the deformation
texture itself. They also suggest that the observed lack of
crystallographic symmetry in the effective <111> rotation axes
may be caused by the anisotropy of boundary mobility[178] in
combination with what has been termed as 'driving force aniso-
tropy' connected with the line tension of dislocations.[179]
Thus, Beck and Hu[158] tried to show that the absence of
certain <111> rotated orientations from observed recrystall-
isation textures is quite compatible with the oriented growth
mechanism.

According to Becker,[180] the observation that
recrystallisation textures are affected by annealing history,
is incompatible with the oriented growth mechanism and must

require oriented nucleation at least as a contributing factor. However, Beck[181] pointed out that oriented growth mechanism does actually require changes in the annealing texture consequent upon the changes in the temperature-time programme of the annealing process.

Verbraak[92] and Lucke[119] have pointed to experimental evidence indicating that a) identical rolling textures can give rise on annealing to quite different recrystallisation textures, and b) different rolling textures can produce very similar recrystallisation textures. It has been suggested by them that both of these observations are incompatible with the oriented growth mechanism of the formation of annealing textures. Beck and Hu[158] have taken great pains in repudiating this claim and they argue that most of the Verbraak's data can, in fact, be satisfactorily accounted for on the oriented growth mechanism.

Finally, mention must be made about an early objection by Burgers and Tiedema[182] that the orientation dependence of boundary mobility, which forms the basis of the oriented growth theory, is not sharp enough to account for the well-defined recrystallisation textures obtained on annealing highly rolled polycrystalline metals. Indeed, Dunn's results[183] on Si-Fe indicate that the dependence of growth rate on the orientation relationships between matrix and growing grains is rather weak. However, Beck[184] has pointed out that a much sharper orientation dependence than that suggested by the relative boundary mobilities themselves

is to be expected. This is due to the fact that the distri-
bution of the fraction of recrystallised volume over the
possible nucleas orientations is proportional to the 3rd or
4th power of the corresponding relative boundary mobilities.
It has also been suggested[184,185] that grains of boundaries
with maximum mobility can grow to disproportionately larger
sizes than other grains, even if the differences in mobility
are slight, provided that the number of competing new grains
is large enough to make the competition keen. It has been
argued that[67,98] growth selectively alone can satisfactorily
explain the formation of a well-defined recrystallisation
texture in a single orientation matrix. Beck[184,185] postu-
lated that the growth rates of a recrystallised grain must be
considered into all components of the deformation texture.
The extraordinary sharpness of the cube texture in Cu has been
explained on the basis of this hypothesis. The cube orienta-
tion does not have the exact orientation relationships with
respect to all the four main rolling texture components which
give the maximum boundary mobility. However, the approximately
ideal (30° <111> rotational) orientation relationship which
it has with the main rolling texture components is quite
symmetrical, and these conditions are not very far from those
that ensure maximum boundary mobility. These ideas have been
shown pictorially in Figures 34 and 35.

Similar argument has been put forward by Beck[184]
to explain for the formation of the (225) [$73\bar{4}$] recrystallisa-
tion texture in rolled and annealed polycrystalline 70:30 brass.
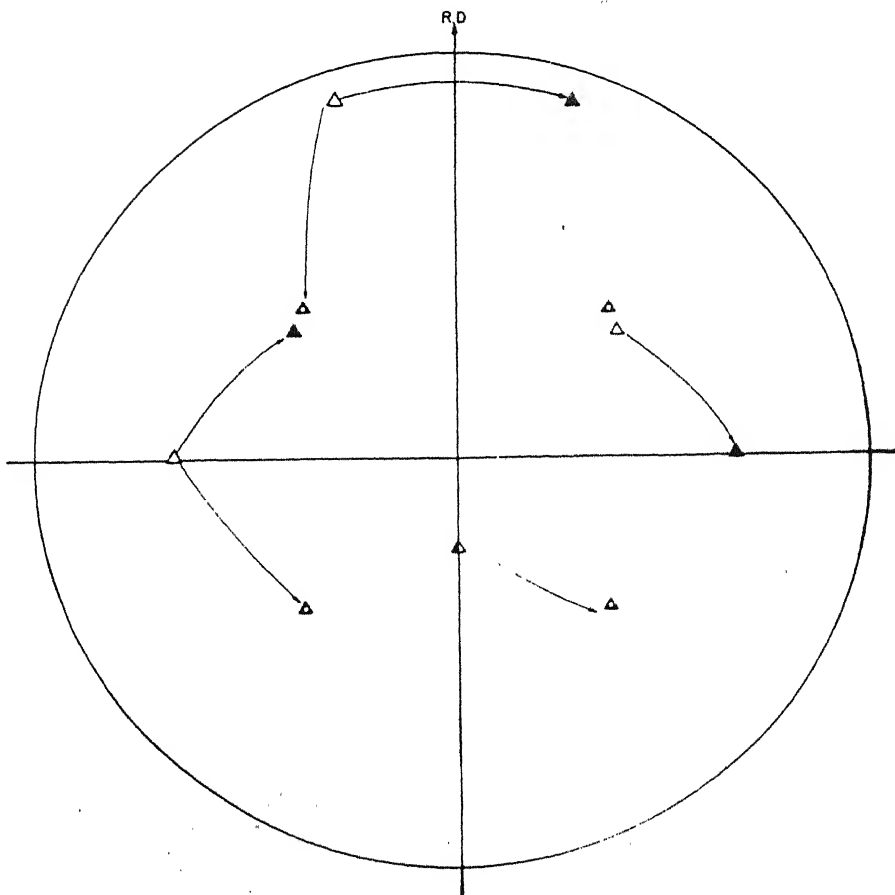
In this connection, he pointed out that not only the main matrix texture components but minor components and orientations spread also must be taken into consideration while estimating the relative order in which crystals of various orientations are preferred for growth in the matrix as a whole. Stuwe[186] elaborated the conditions put forward by Beck to account for the textures observed in annealed Al, in which a cube component coexists with a component described as a retained rolling texture. He showed that each of the four components of the rolling texture is favoured for growth into the other three, while the cube texture is capable of growth into all the four components.

For the formation of cube texture in pure metal, the presence of cube oriented nuclei in the deformed matrix seems to be essential.[76] Once a recrystallised grain comes into existence its growth by high angle boundary movement is much faster in pure metal than in the alloys of that metal.[76]

CHAPTER - 3

EXPERIMENTAL PROCEDURE

3.1 Material and Initial Treatment

The chemical composition of all the alloys (in wt. %) used in the present study are given in Table 2. All the alloys were induction melted and cast under an argon atmosphere using virgin metals of purity > 99.99%. The ingots were cylindrical in shape having a height of about 20 mm. These ingots were cold-rolled 50% to a thickness of 10 mm and then homogenisation annealed in vacuum at 1150°C for 24 hrs. These were then again cold-rolled 50% and annealed at 1150°C for a period of 3 hrs to yield the starting material of almost random texture and a grain size of ~0.1 mm.

3.2 Cold Rolling

Strips cut from the thick sheets of all the five materials were cold-rolled in 2-high laboratory rolling mill where paraffin oil was used as lubricant. The direction of the strips were reversed end to end after each pass. In between any two successive passes, the strips were dipped into cold water bath to minimise any unwanted rise in temperature. The change in thickness after each pass was noted. All the materials were rolled to 95% deformation. The same rolling schedule was followed for all the alloys.

TABLE 2

Chemical compositions of alloys (wt. %)

Alloy designation	Weight percent alloying element						
	C	Si	Mn.	P	S	Ni	Co
Alloy A	0.006	< 0.03	< 0.03	0.005	0.003	88.40	11.15
Alloy B	0.007	0.06	< 0.03	0.005	0.003	76.90	22.85
Alloy C	0.006	< 0.03	< 0.03	0.004	0.003	68.85	30.90
Alloy D	0.006	0.03	< 0.03	0.003	0.004	58.70	41.05
Alloy E	0.006	0.06	< 0.03	0.003	0.004	39.20	60.50

Specimens for electron microscopy were made from both cold-worked and recrystallised samples of all the alloys.

Foils were made from the conventional rolling plane section of the thin sheets. Since the 95% cold-rolled materials are only 0.25 mm thick, it was found impossible to prepare the foils from the cross sections as such.

For preparation of oils thin strips were sectioned along transverse direction into rectangular foils. These foils were thinned down to 0.01 mm by chemical polishing in a solution of HF and HNO_3 in the ratio of 1:8. Then they were further thinned down to the extent of 1000 Å by electropolishing. The electrolyte used was a mixture of $HClO_3$ and CH_3COOH in the ratio of 7:93 by volume. The electrode and voltage used were stainless steel and 30-35 volts respectively. The temperature of the bath was maintained at about 10°C. During electropolishing the sample was found to be eaten away from the lower end. The foils were cut from this end with the help of a sterile scalpel blade in a manner so that the cut edge represented the rolling direction.

The foils so made were enclosed within folding grids and then examined under the microscope. The micrographs and the corresponding selected area diffraction patterns from different parts of a number of selected foils were then studied under the TEM and recorded into 35 mm films. The photographs were finally printed, the rolling directions marked on each of them, the S.A.D.'s were analysed and finally the orientations in different areas of the

micrographs were determined after taking into consideration the relative rotation between the micrographs and the corresponding S.A.D.'s.

3.6 Texture Measurement

Texture measurements were made on specimens taken from all the cold worked materials and some recrystallised samples. Specimens of the size (25 mm x 15 mm) were cut from the rolled sheets for this purpose. All the texture specimens were lacquered on one face and a half of the thickness was removed from each of them chemically in a solution of 11% HF and 89% HNO_3. Mostly {200} and in a few cases {111} pole figures were determined by the Schultz reflection method.[65] using Cu-K radiation. The diffracted intensity was measured with a scintillation counter. The intensity data in terms of counts were taken from the display for count time of 10 secs.

Intensity levels on pole figures were determined by comparison with a solid specimen of pure nickel which had been randomised by repeated deformation and annealing.

CHAPTER - 4

RESULTS AND DISCUSSION

4.1 The Cold-Worked State

4.1.1 Rolling Texture

The {200} pole-figures of all the five alloys A to E
are shown in Figures 36-40. The pole-figures for the alloys
A, B and C clearly show that the deformation textures in
these three materials are rather similar. The texture in each
case may be described as copper-type or pure metal-type comp-
rising of the two major components, {112} <111> and {110} <112>.

The deformation texture of alloy D (Figure 39) shows
that the major component of texture here is {110} <112> with
a minor {112} <111> component. On the other hand, the defor-
mation texture of alloy E (Figure 40) is found to comprise
almost wholly of the component {110} <112> indicating that
this texture is brass-type or alloy type.

4.1.2 Electron Microstructures

Transmission Electron Microscope observations for
the various structural features of all the cold-worked alloys
together with the corresponding S.A.D.'s are shown in Figures
41(a) to 48(b). All the microstructures show typical cold-
worked state with very high dislocation density at the cell
walls with relatively dislocation free cell interiors. Some
deformation twins are also observed in case of alloy E.

The dislocation density in the cell interiors of the alloys A, B and C seem to be a bit less with respect to the alloys D and E.

All the samples were thoroughly scanned under the electron microscope to find out the presence of cube-oriented regions. However no such regions could be located. For alloy A, Figures 41(b) and 42(b) show {112} <110> and {110} <112> orientations respectively. For alloy B, Figures 43(b) and 44(b) show {111} <110 > and {112} <110> orientations respectively. For alloy C, Figures 45(b) and 46(b) show the { 112} < 122> and {100 } <120> orientation respectively. In case of alloy D, { 112} <120> orientation and for alloy E, the {110} < 113> orientation are shown in Figures 47(b) and 48(b) respectively.

4.2   General Observations on Annealing

4.2.1   Annealing Textures

The {200} pole-figures for the alloys A to E in the fully recrystallised condition are shown in Figures 49 to 53. The pole-figures for the alloys A and B (Figures 49 and 50) are found to be rather similar. Both seem to contain a sharp enough cube texture together with weak poles for the major twin-orientation of the cube, {122} <212>.

The recrystallisation texture of the alloy C also contains the cube-component but this is not as sharp as in case of the alloys A and B. In contrast to the alloys A and B, however, here the twin component of the cube has been

found to be a bit stronger.

The recrystallisation texture in case of the alloy D is found to be somewhat unique in the sense that the general level of pole intensities are found to be quite weak here. The intensity of the cube texture is also very weak.

Practically no cube component could be observed in the recrystallisation texture of the alloy E. The texture here can be described as strongly Goss-type $\{110\} <001>$ with a minor $\{112\} <111>$ component.

4.2.2   Electron Microscopic Observations

An extensive transmission electron microscopy was carried out to find out structural changes that take place during recrystallisation of all the alloys. Recrystallisation was carried out at a temperature of 800°C for various lengths of time. Complete recrystallisation was found to occur after about 8 minutes annealing for all the alloys.

An idea about the microstructural changes during annealing can be had from a number of typical electron micrographs with their corresponding SADs shown in Figures 54(a) to 83.

Figures 54(a) and 55(a) show the initial stage of formation of subgrain from the previous cold-worked cell structure in alloy A after 5 minutes of annealing time. The dislocation density within the cell interior has come down although the dislocation density at the boundaries seem to have changed very little. Their corresponding SADs, Figures 54(b) and 55(b) contain the microscopic orientations $\{110\} <110>$

and {112} <122> respectively. Figure 56(a) shows the formation of a distinct subgrain after 6 minutes of annealing time. The corresponding SAD, Figure 56(b), shows a major {110} <111> and other two minor {310} <111> and weak {123} <111> orientations. Growth of subgrains with annealing time is shown typically in Figure 57(a). Here the grain A has the orientation {110} <111> (Figure 57(b)) and grain B has {112} <111> orientation (Figure 57(c)). This micrograph may be taken as showing the start of formation of recrystallised grains. Figure 58(a) shows a recrystallised grain surrounded by a few small subgrain and cells. The SAD's from regions A and B are shown in Figures 58(b) and 58(c). Both the orientations have been found out to be near {110} <111>. It is clear that there is hardly any misorientation between the recrystallised grain and its surrounding.

Figure 59(a) shows the nucleation of subgrain and start of the recovery process in alloy B after an annealing time of 5 minutes. The corresponding SAD (Figure 59(b)) shows a brass orientation. With annealing time slightly increased to 6½ minutes, subgrain growth starts taking place. In Figure 60(a), the central subgrain is found to grow very quickly under the impact of the electron beam in the electron microscope. The whole sequence of subgrain growth is depicted in Figures 61, 62 and 63. The corresponding SADs of Figure 60(a) are shown through Figures 60(b) to 60(f). Regions 'A', 'B' and 'C' show {100} <110> orientation Figures 60(b), 60(d) and 60(e); region 'D' shows {110} <100 >orientation (Figure 60(c));

region 'E' shows {310} <331> orient-tion (Figure (60f)).
With annealing time increased to 7 minutes, a large number of
subgrains were seen to be formed and these seemed to grow by
subgrain coalescence as shown in Figure 64(a). Here regions
'A' and 'D' show {111} <110> orientations (Figure 64(d) and
64(e)), and B and C show {112} <120> and {110} <100> orienta-
tions (Figures 64(b) and 64(c)).

In case of alloy C, subgrains (Figure 65(a)) were
found to form after an annealing time of 5 minutes. The corr-
esponding SAD (Figure 65(b)) shows {110} <111> orientation.
In Figure 66(a), subgrains were observed to grow by some kind
of boundary coalescence. The corresponding SAD (Figure 66(b))
shows a cube orientation. It may be taken as the start of the
recrystallisation process. Figure 67(a) again shows subgrain
growth by coalescenfe of boundaries. Figures 67(b), 67(d)
and 67(f) show cube oriented regions 'A', 'C' and 'E' whereas
region 'D' (Figure 67(c)) shows brass and region 'B' shows
{111} <112 >orientation. With annealing time increased to
8 minutes, completely recrystallised grains have been found to
form (Figure 68(a)). Its SAD (Figure 68(b)) shows {100} < 110>
orientation.

In case of alloy D, Figure 69(a) and Figure 70(a)
show the start of recovery process and formation of a number
of small sized subgrains. There exists complex dislocation
tangles throughout the structure. Its SAD pattern (Figure
69(b)) shows gross orientation. The SAD (Figure 70(b)) of
Figure 70(a) shows a {100} < 100> orientation. One of the

subgrains in Figure 71(a) was made to grow under the impact
of the electron beam within the electron microscope. This
in-situ process is portrayed through the Figures 71(a), 73 and
74. Regions A, B, C and F show cube orientation. (Figures
71(b) to 71(d) and 71(g)) whereas regions D and E
(Figures 71(e) and 71(f)) show {211} < 113> and {110} <110 >
orientations respectively. SAD taken from centre of Figure
72(a) shows {110} <113 > orientation (Figure 72(b)). With the
annealing time increased to 8 minutes complete recrystallisa-
tion is found to occur. Grains A and D in Figure 75(a) show
{100} <110> and {110 } <100> orientations respectively (Figures
75(b) and 75(c)) respectively.

In case of alloy E, recovery process has been found to
start within 5 minutes of annealing time (Figures 76(a) and
77(a)). The corresponding SADs (Figures 76(b) and 77(b))
contain {112} <111> and {111} <110> orientations respectively.
With the annealing time increased to 6½ minutes, a large number
of subgrains formed and grew, the dislocation density inside
the subgrains coming down to a lower value. Figures 78(a) to
78(d) show the microstructures and SADs for different sub-
grains A, B and C, all of them show negligible orientational
differences. All of them show nearly {110} <113 > orientation.
For annealing time of 7 minutes (Figures 79(a) and 80(a))
recrystallisation was found to be almost half way through.
Some annealing twins are visible in Figure 79(a), its SAD
(Figure 79(b)) showing {110} < 511> orientation. The cold-
worked area (region A), in Figure 80(a) shows {112 } <113>

orientation (Figure 80(b)) which is quite different from that
of the recrystallised area (region B), {123} <112> (Figure
80(c)). With the annealing time slightly increased to 8 minutes,
almost complete recrystallisation occurred (Figure 81(a)).
Grains A, B and C were found to have the orientations {100}
<110>, {110} <111> and {310} <131> respectively as shown in
Figures 81(b) to 81(d). Figure 82(a) shows a number of
recrystallised grains. Grains 'A', 'B', 'C' and 'D' have the
orientations {100} <110>, {112} <110>, {110} <112> and
{110} <112> respectively as shown in Figures 82(b) to 82(e).
Figure 83 shows one typical recrystallisation grain structure
with some twins and stacking faults.

4.2.3 Optical Microscopic Observations and Grain Size Measurements

To ascertain the grain size of the recrystallised
samples, optical microscopy of polished and etched specimens
were carried out. Grain sizes were measured by the linear
analysis method. Grain growth rate after recrystallisation
has been found out by plotting grain diameter (μm) against
log time (sec.) and this is shown in Figures 84 to 88. Vari-
ation of grain size with annealing time is also given in a
tabular form in Table 3. It has been noticed (Figures 84 to
88) that the rate of grain growth decreases with increased
amount of cobalt content. Not only that the average size of
the recrystallised grains has been found to decrease steadily
with increase in the cobalt content of the alloy (Figures 89
to 93). A few typical optical microstructures are shown in
Figures 89 to 93).

TABLE 3

Variation of recrystallised grain size in (μm) with annealing time for all the alloys are shown below

Alloy	7 mts	8 mts	15 mts	1 hr	3 hrs	10 hrs	20 hrs	50 hrs
A	12.17	24.41	42.94	83.48	142.54	198.01	224.09	286.04
B	6.94	18.14	37.98	82.09	134.02	160.17	173.51	260.57
C	6.04	8.97	29.87	73.54	107.98	141.09	150.98	208.01
D	5.52	7.59	15.82	70.82	92.08	119.98	139.92	199.04
E	3.02	4.85	9.98	63.74	75.02	84.78	100.07	167.76

4.3 Discussion of Results

The above results clearly indicate that there is a distinct and systematic change of the deformation texture as a function of the cobalt content of the alloys. Although alloys A, B and C show distinct pure metal type texture, the start of the change over from pure metal type of alloy type is clearly discernible for alloy D. On the other hand, alloy E shows a clear-cut alloy type or brass-type texture.

It is known that two different types of deformation texture - namely copper type (or pure metal type) and brass type (or alloy type) - can be obtained in fcc metals and alloys depending on the stacking fault energy. The former type of texture is normally found in high stacking fault energy materials, whereas the latter type is found in materials with low stacking fault energy.

The stacking fault energy of pure nickel is supposed to be rather high. Addition of cobalt to nickel is known to decrease the stacking fault energy of the latter very effectively. Thus the Ni-Co alloys in the present investigation have different stacking fault energies from very high (in case of alloy A) to rather low (alloy E). This explains the two different types of deformation texture that is exhibited by this series of alloys as a function of their cobalt content. The alloy D (with 40% Co) possibly lies in a transition zone - thus showing a texture in between the two extremes.

So far as the recrystallisation textures of the alloys is concerned, again, a distinct difference in the

texture has been obtained in these materials as a function of cobalt content. Alloys A, B and C, with a pure metal type deformation texture, have, upon recrystallisation, produced a texture which is similar to the recrystallisation texture of high stacking fault energy materials like pure copper. The major component of this texture is the cube, {100} <001>. Although no cube oriented region could be detected in the foils of the cold-worked alloys, a few small cube regions could actually be observed in some of the alloys during the recovery stage. Presumably the final cube texture has been produced in these materials by way of growth of the pre-existing cube nuclei in the cold-deformed condition. However the intensity of the cube texture has been found to diminish in these alloys as a function of increasing cobalt content. The intensity of the cube component came down very drastically for alloy D (with 40% Co) which showed a very weak cube component and a rather weak general texture all throughout. In fact, the recrystallisation texture in this alloy can be described more or less as something near a random texture.

The alloy E showing a perfect alloy-type deformation texture, does not exhibit any cube texture at all, but a rather strong Goss component {110} <001> upon recrystallisation.

During the present investigation it has been observed that the average size of the recrystallised grains decreases as a function of cobalt content of the alloys. Not only that, the rate of grain-growth has also been found to decrease

as a function of cobalt content. These observations can be
rationalised on the basis that the substitutional cobalt
atoms produces a retarding effect on the movement of the high-
angle grain boundaries.
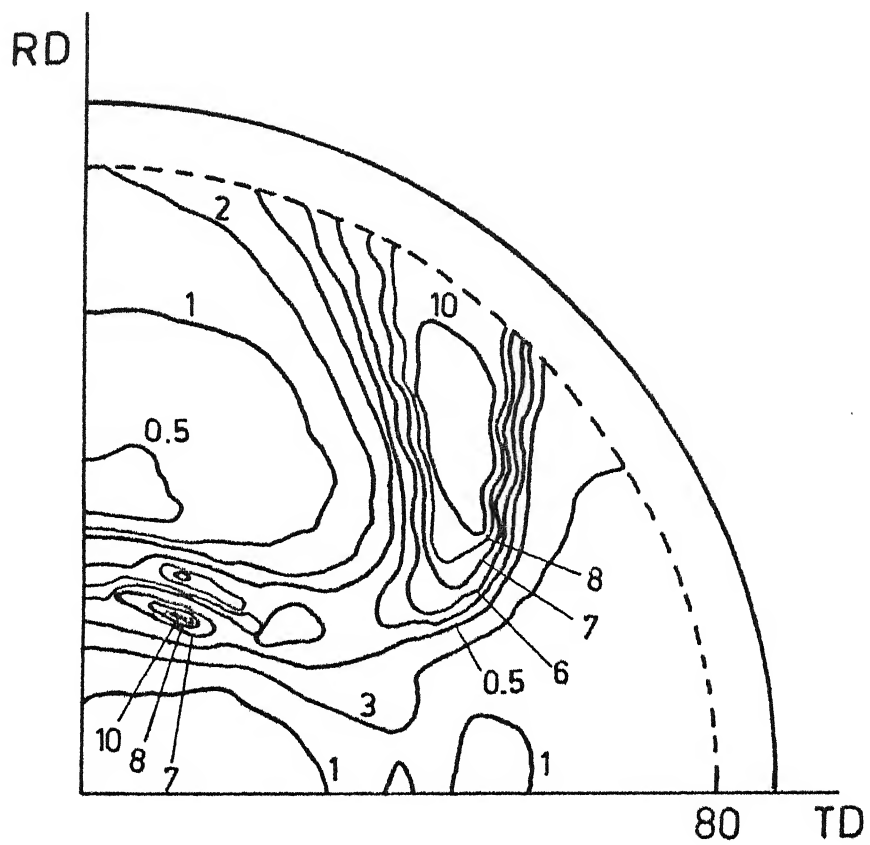
Fig. 36 {200} pole figure of alloy A cold-worked
         for 95 %.
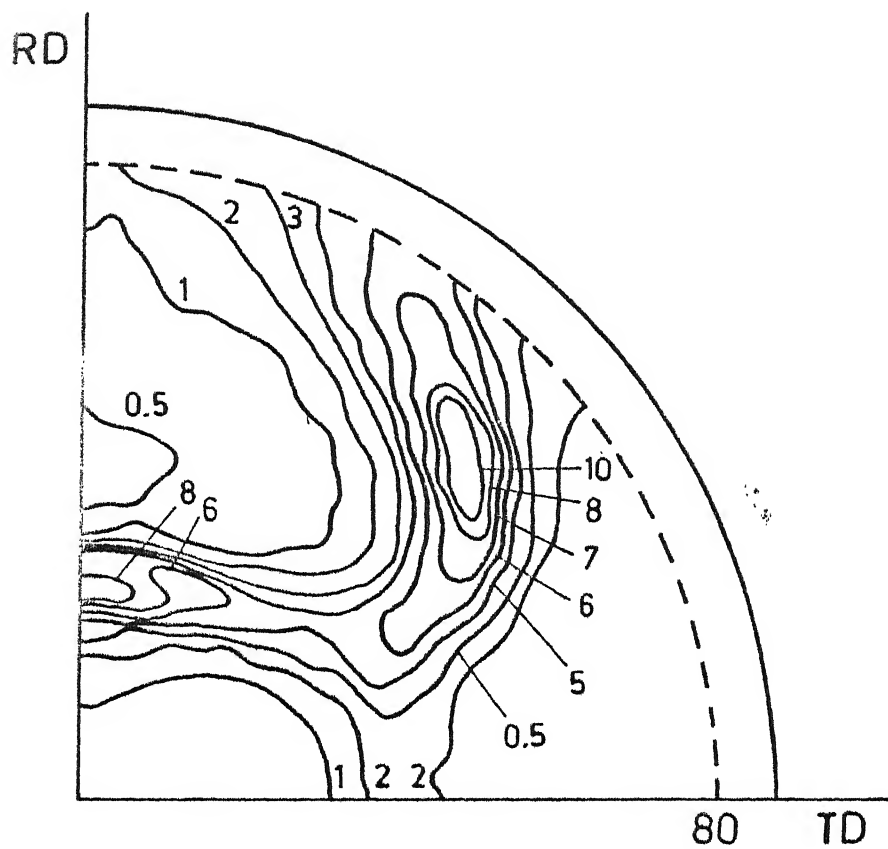
Fig. 37 {200} pole figure of alloy B cold-worked
for 95%.
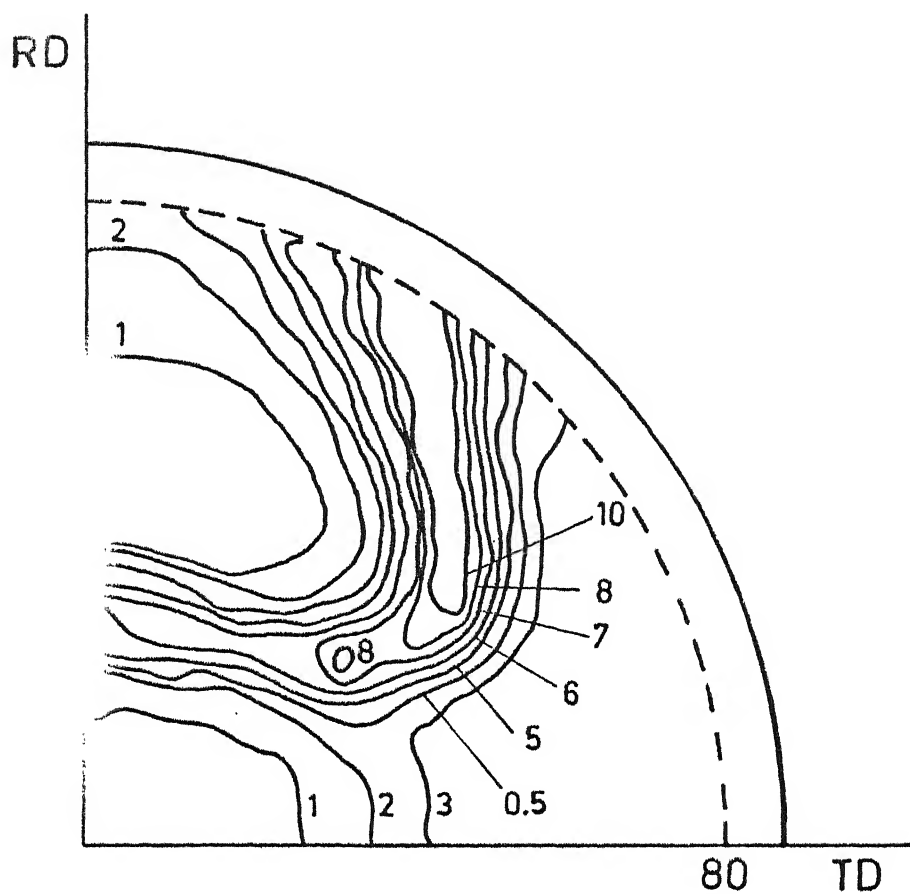
Fig. 38 {200} pole figure of alloy C cold-worked for 95%.
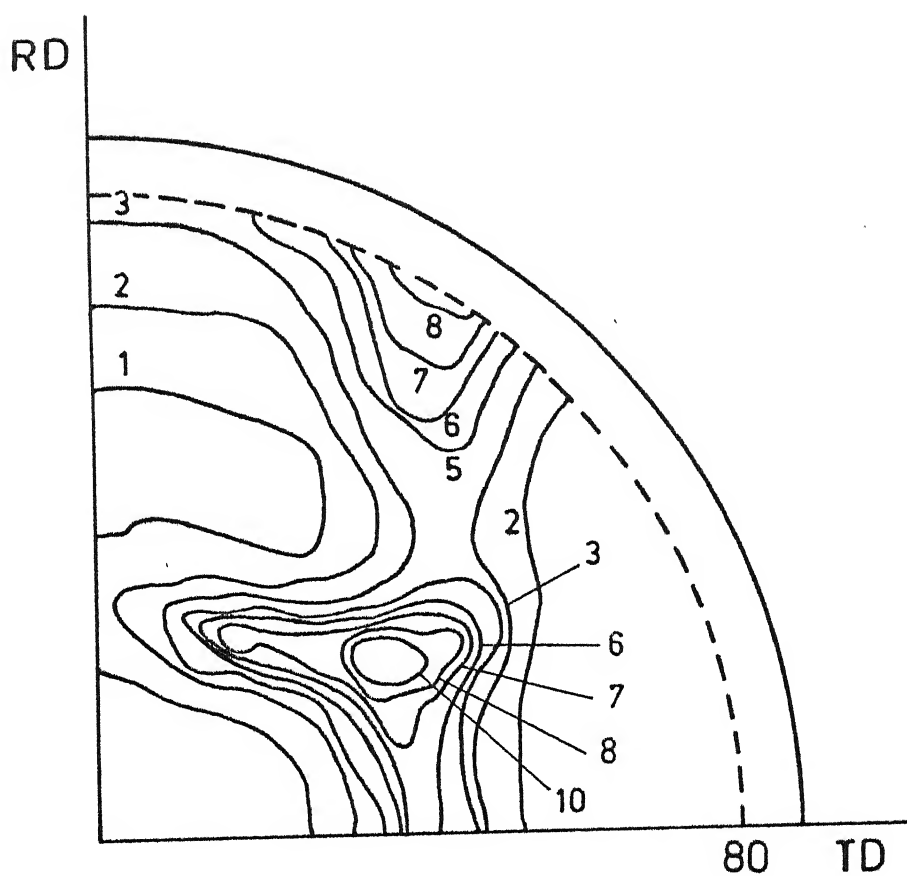
Fig. 39 {200} pole figure of alloy D cold-worked for 95%.
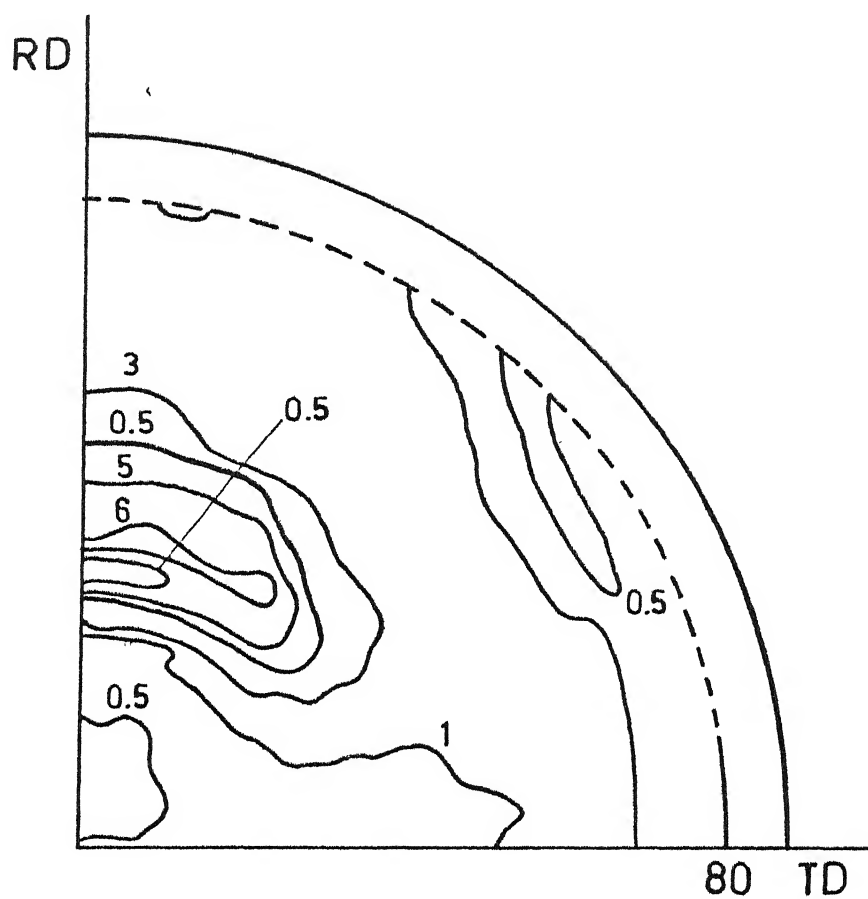
Fig. 40 {200} pole figure of alloy E cold-worked
for 95 %.

Fig. 4.1(a) Alloy A (cold-worked)
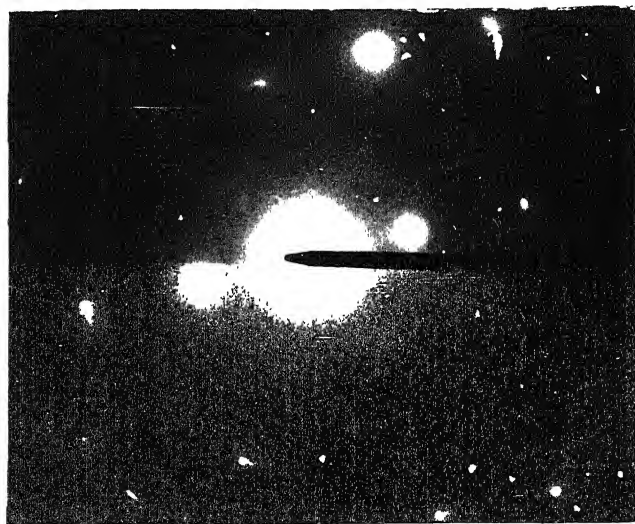
Fig. 41(b) SAD of Fig. 41(a)
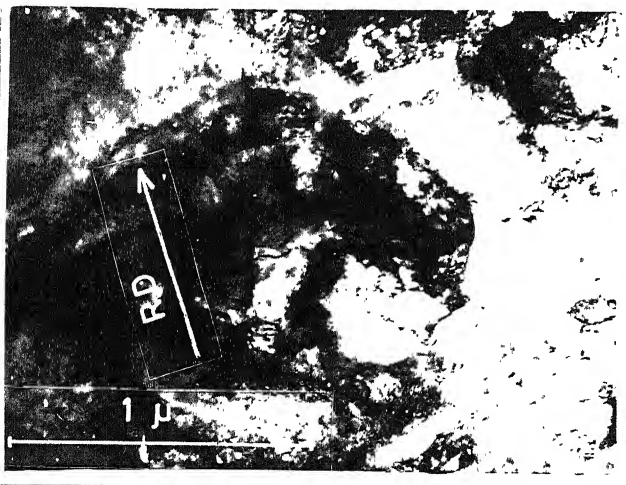
Fig. 42(a) Alloy A (cold-worked)
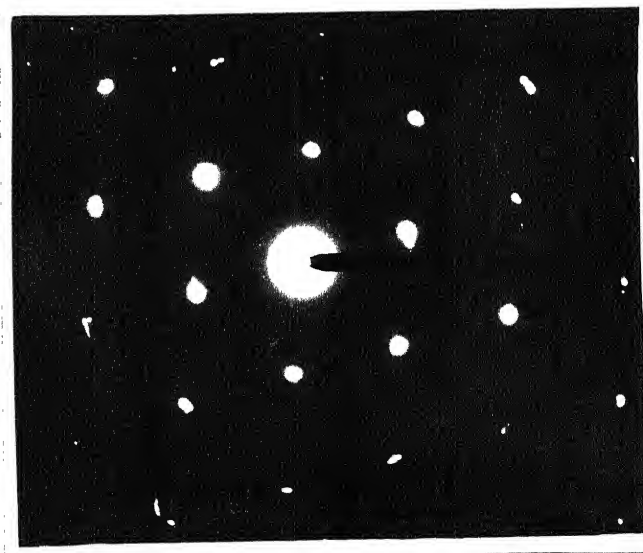
Fig. 42(b) SAD of Fig. 42(a)
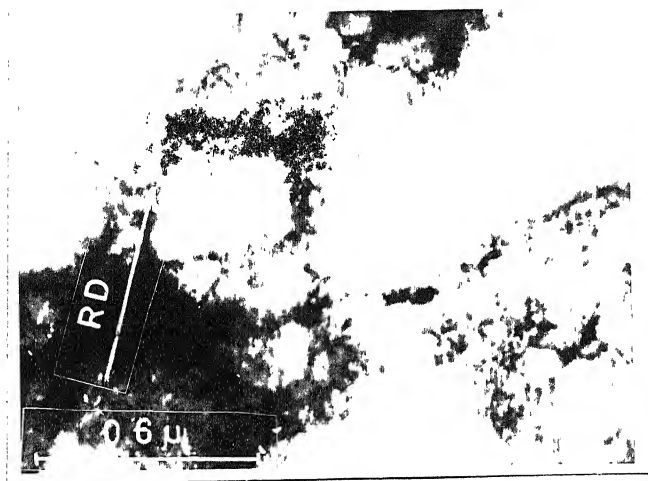
Fig. 43(a)   Alloy B (cold-
worked)
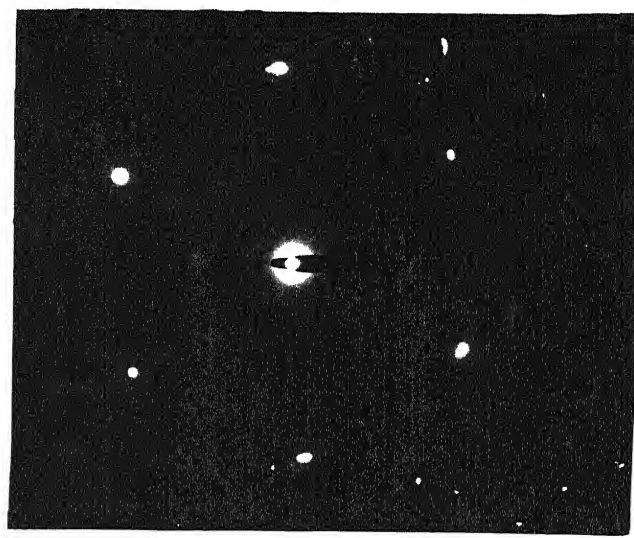
Fig. 43(b)   SAD of Fig. 43(a)
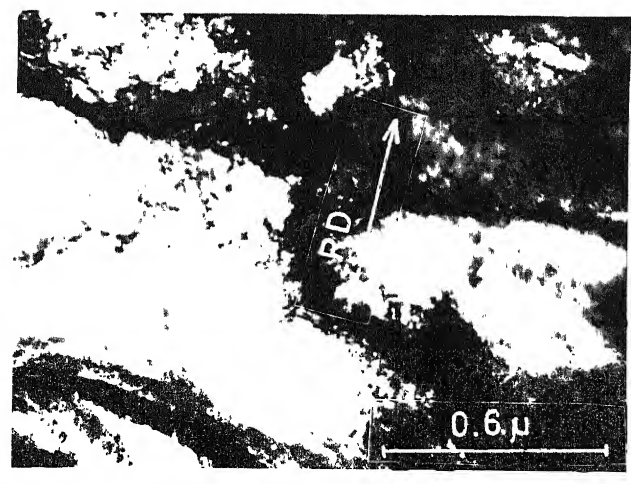
Fig. 44(a)   Alloy B (cold-
worked)
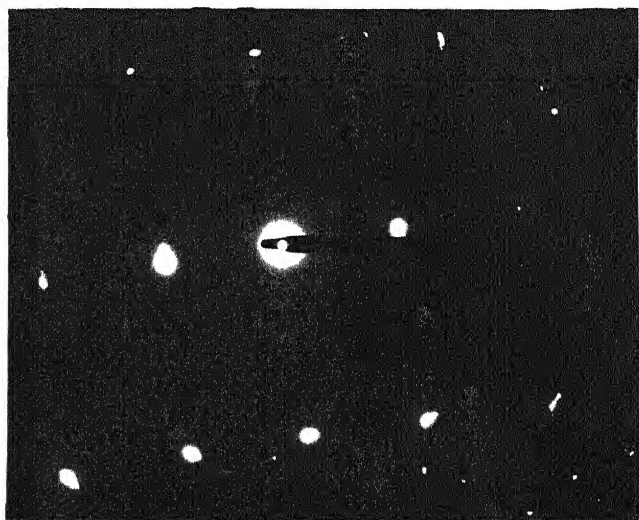
Fig. 44(b)   SAD of Fig. 44(a)
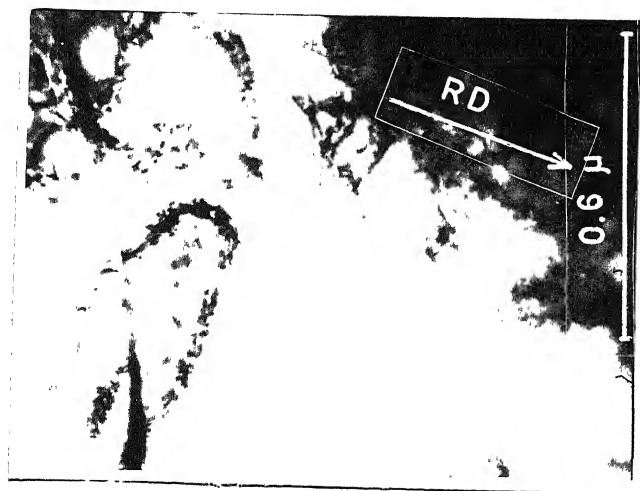
Fig. 45(a)   Alloy C (cold-
worked)
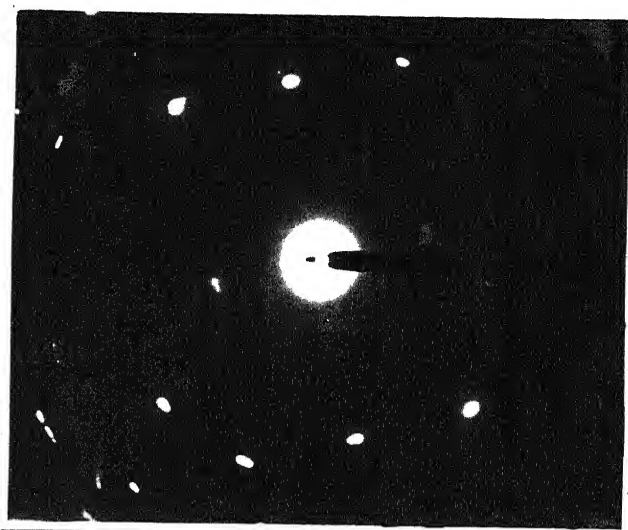
Fig. 45(b)   SAD of Fig. 45(a)
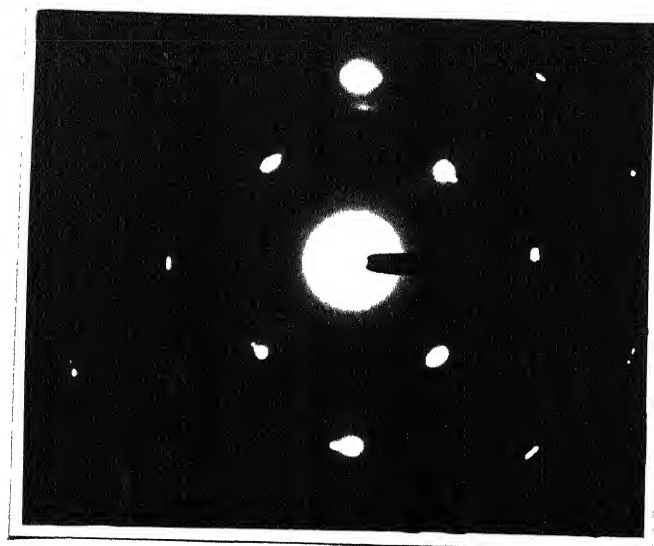
Fig. 46(a)   Alloy C (cold-
worked)
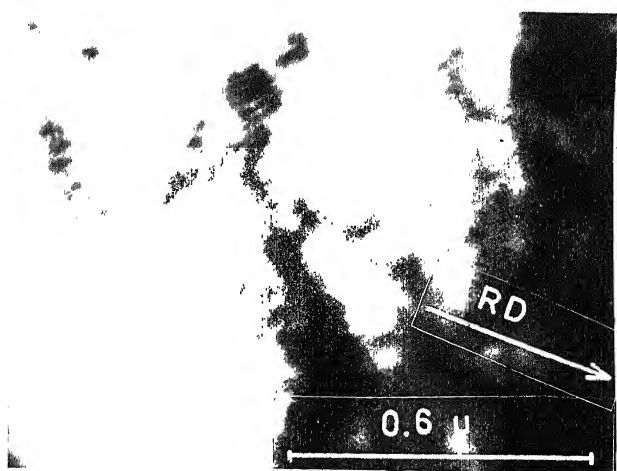
Fig. 46(b)   SAD of Fig. 46(a)
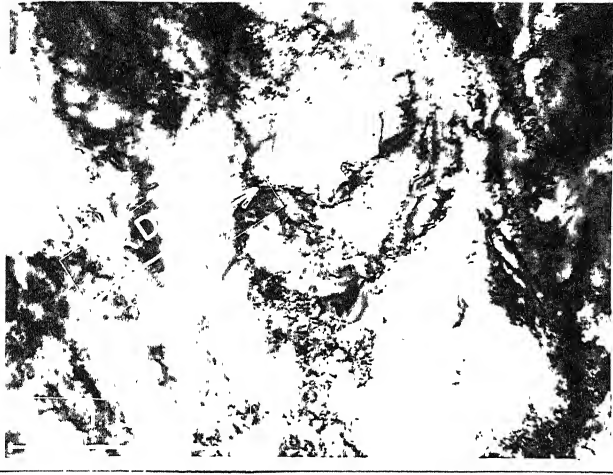
Fig. 47(a) Alloy D (cold-
worked)
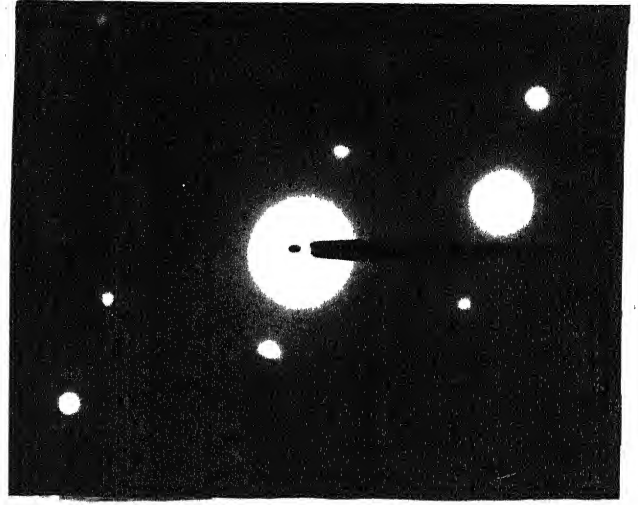
Fig. 47(b) SAD of Fig. 47(a)
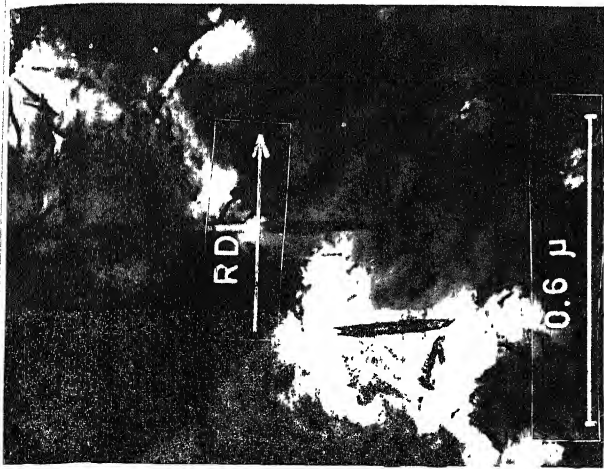
Fig. 48(a) Alloy E (cold-
worked)
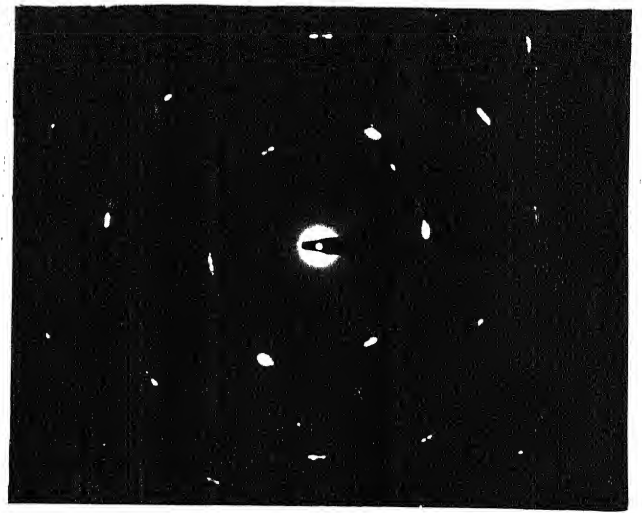
Fig. 48(b) SAD of Fig. 48(a)
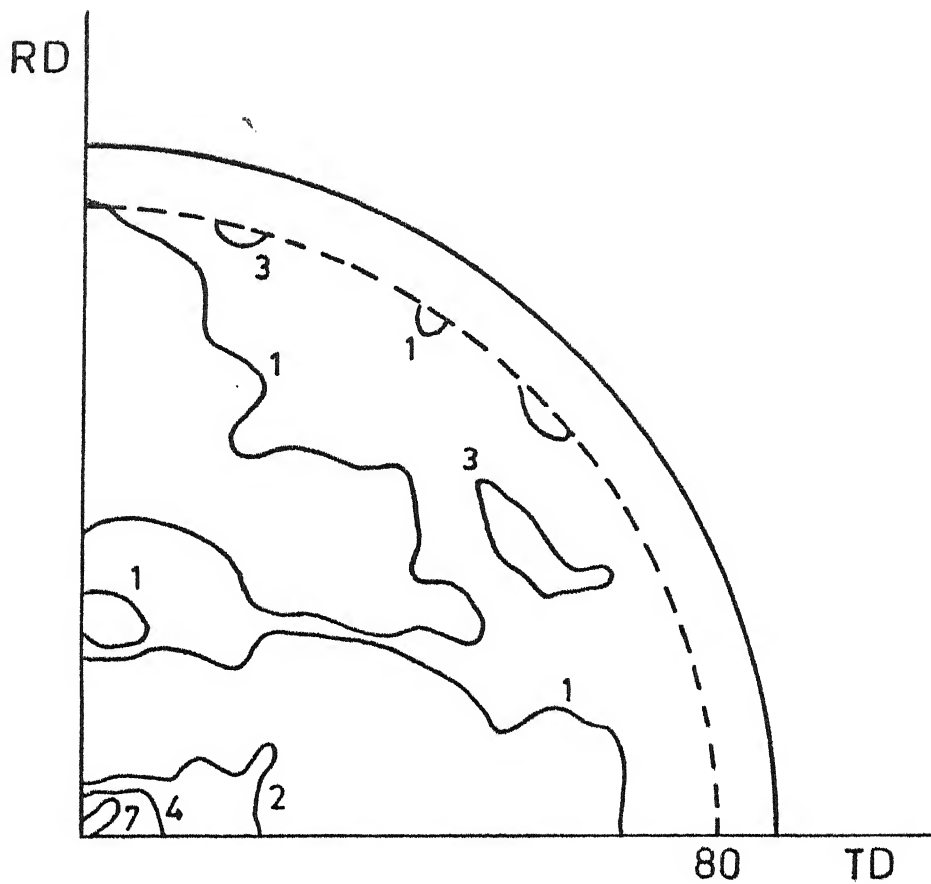
Fig. 49 {200} pole figure of alloy A recrystallised
at 800°C for 1hr.
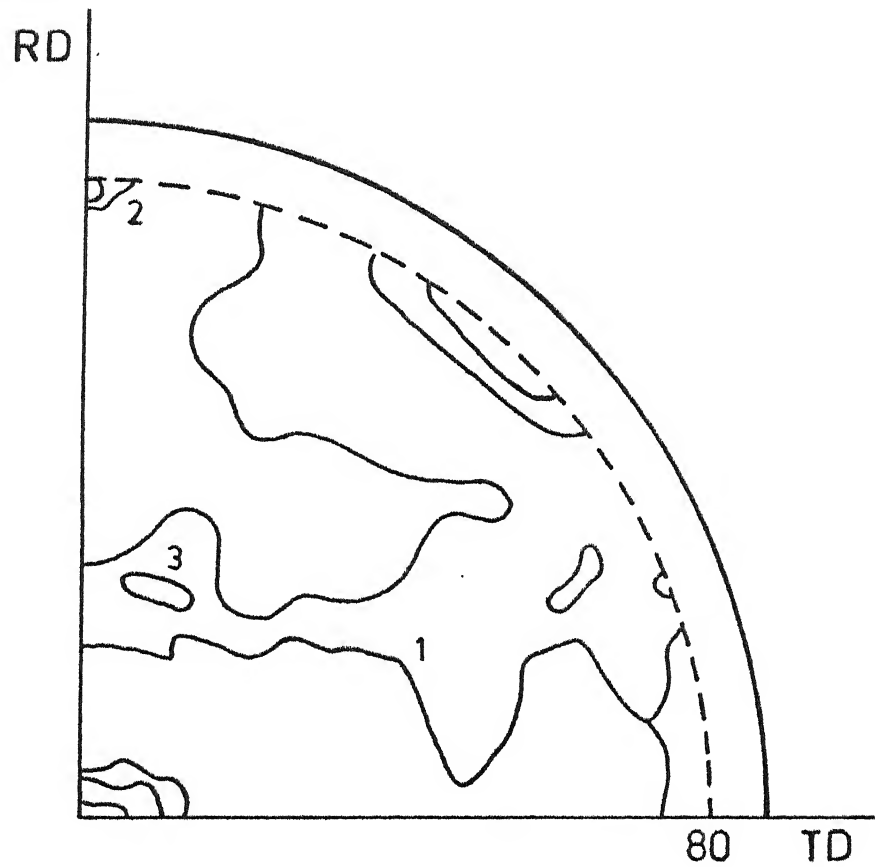
Fig. 50 {200} pole figure of alloy B recrystallised
at 800°C for 1hr.
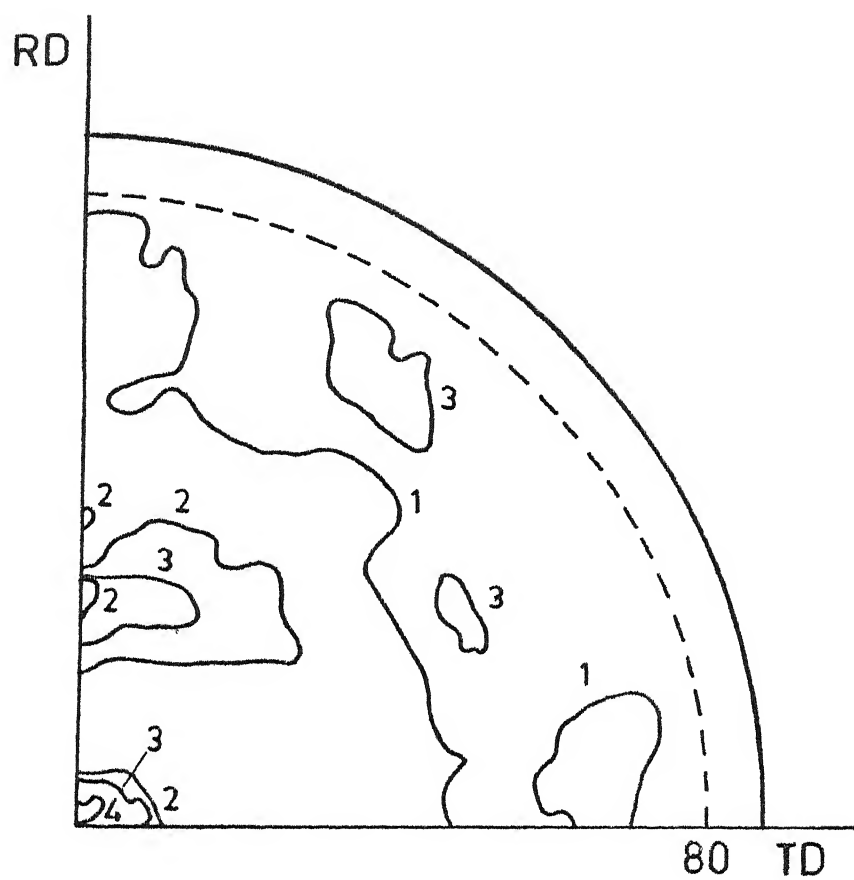
Fig. 51 {200} pole figure of alloy C recrystallised
at 800°C for 3hrs.
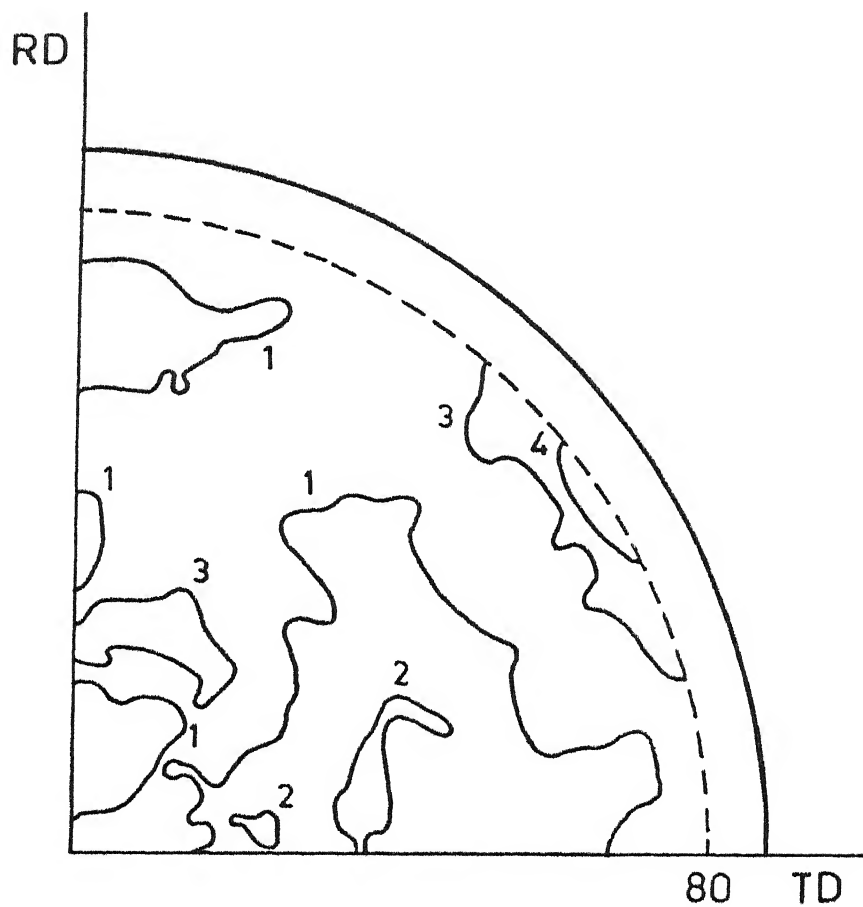
Fig. 52 {200} pole figure of alloy D recrystallised at 800°C for 1hr.
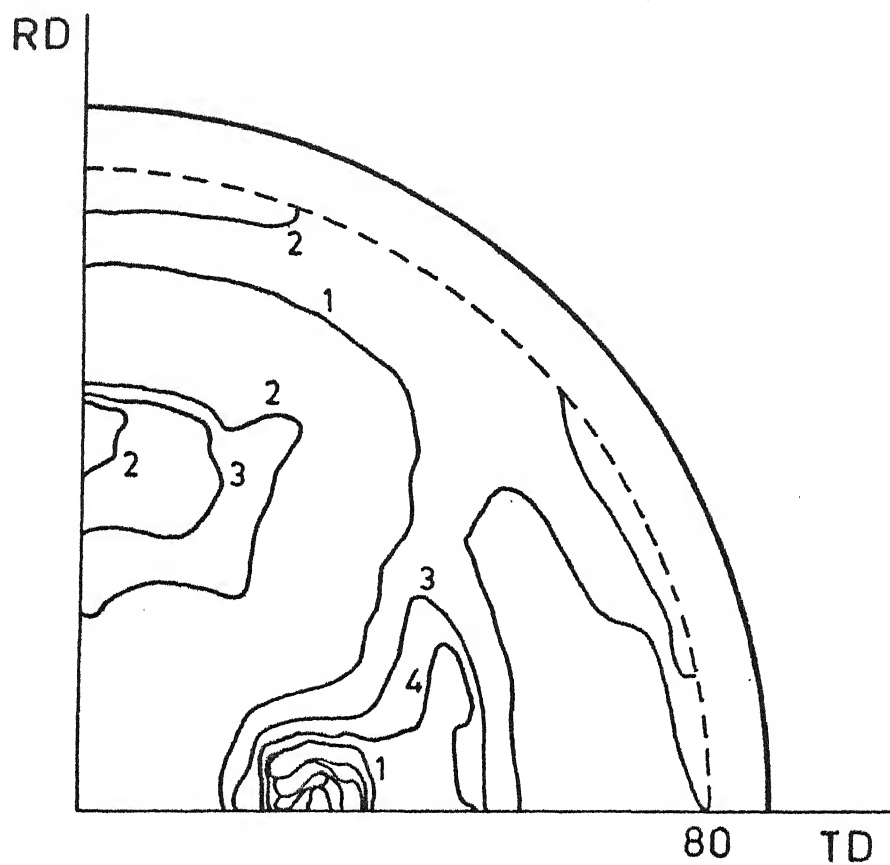
Fig. 53 {200} pole figure of alloy E recrystallised at 800°C for 1hr.
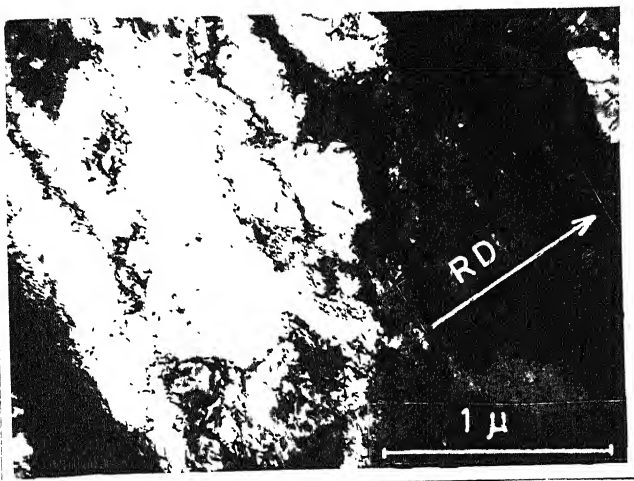
Fig. 54(a)   Alloy A
(annealed, 5 minutes)
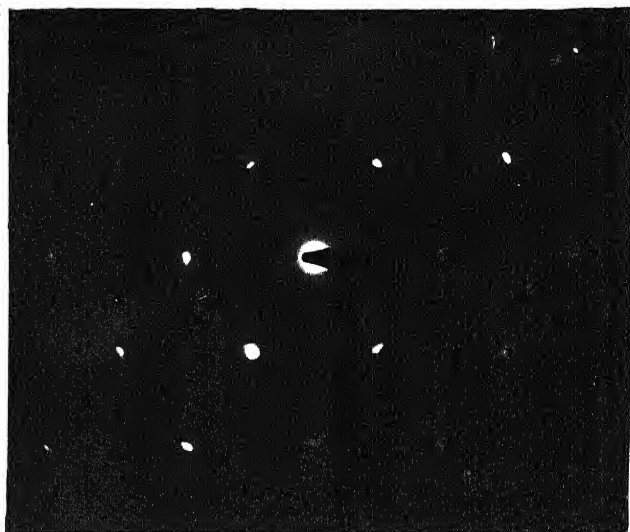
Fig. 54(b)   SAD of Fig. 54(a)
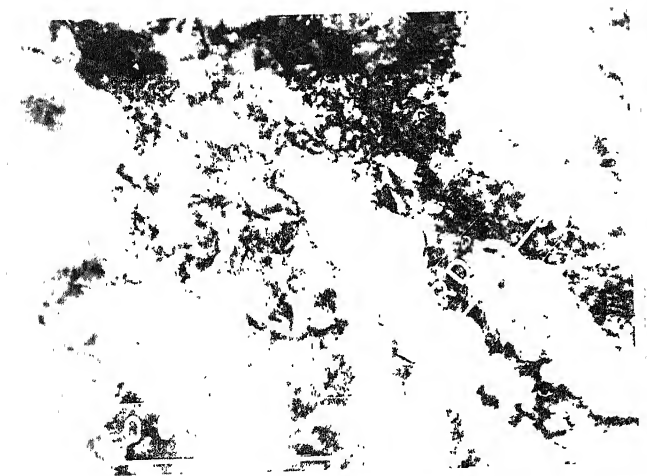
Fig. 55(a)   Alloy A
(annealed, 5 minutes)
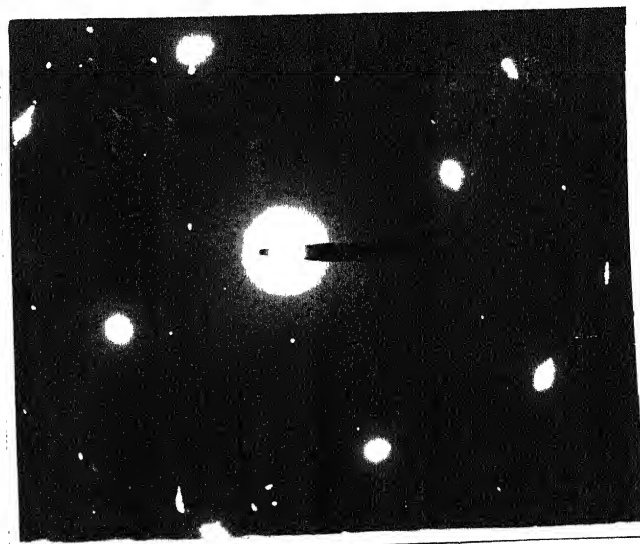
Fig. 55(b)   SAD of Fig. 55(a)
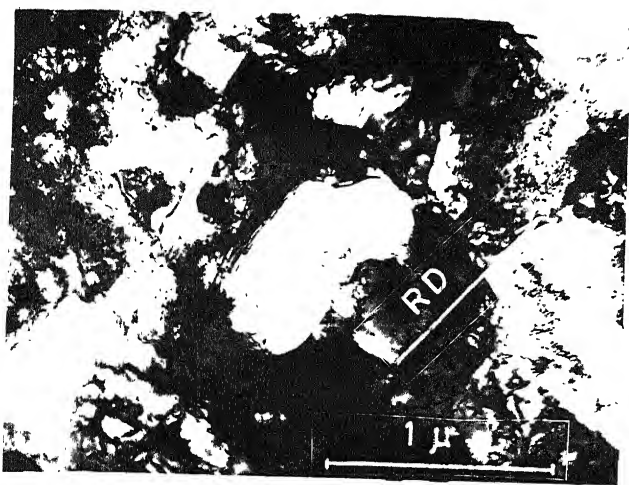
Fig. 56(a)   Alloy A
(annealed, 6 minutes)
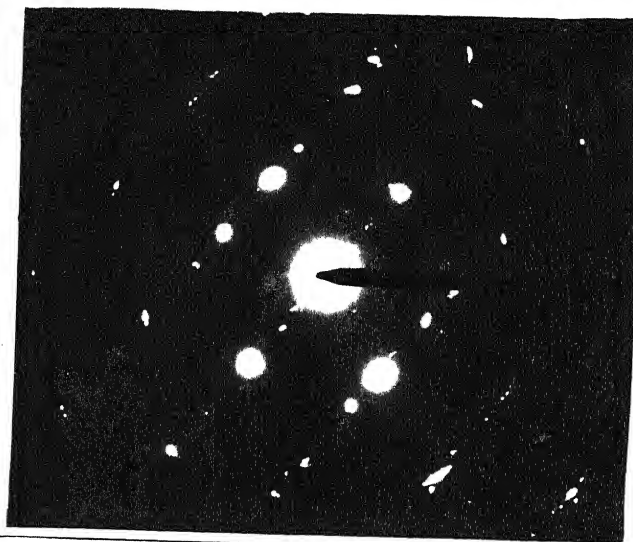
Fig. 56(b)   SAD of Fig. 56(a)
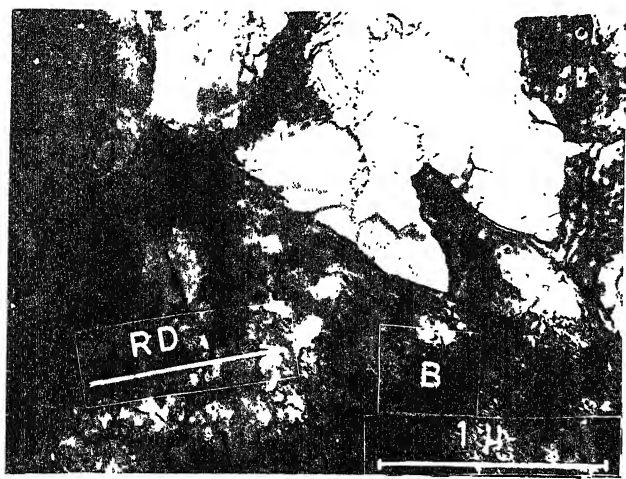
Fig. 57(a)   Alloy A
(annealed, 6½ minutes)
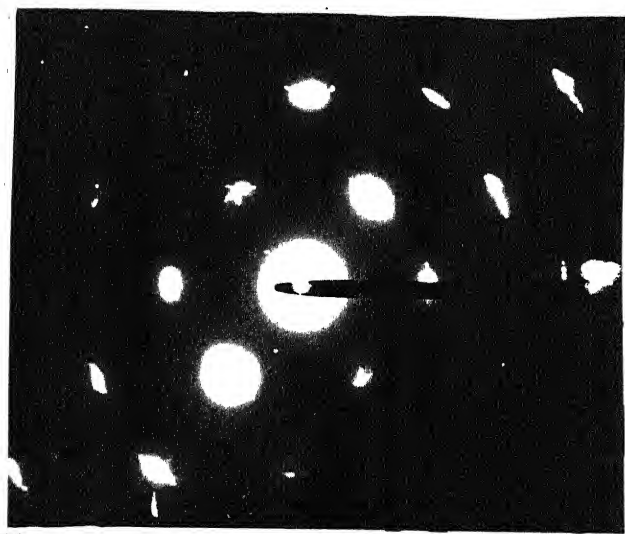
Fig. 57(b)   SAD of grain A of
Fig. 57(a)
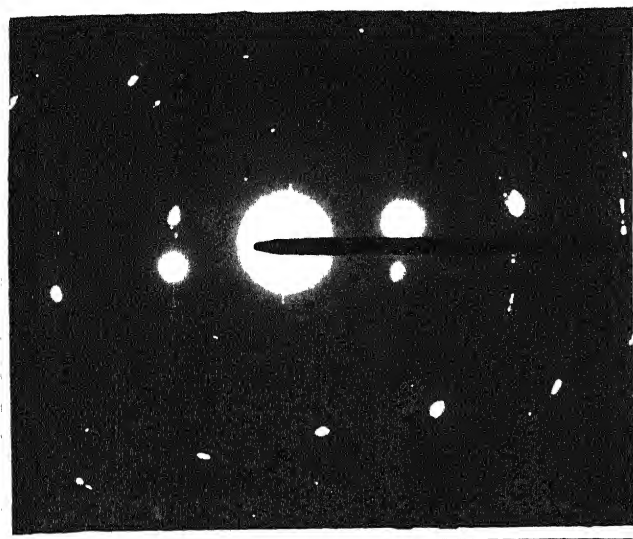
Fig. 57(c)   SAD of grain 'B' in Fig. 57(a)
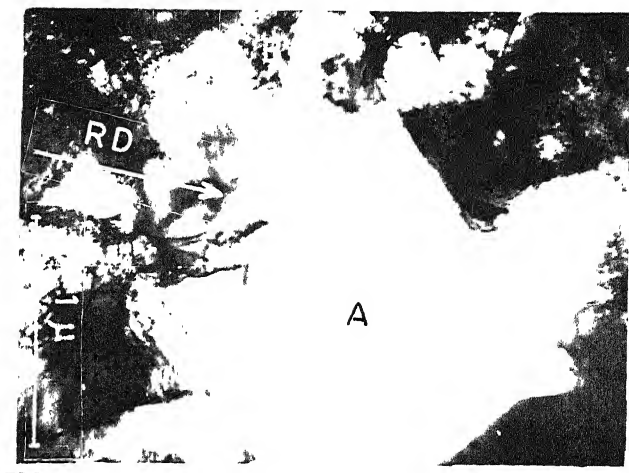
Fig. 58(a)   Alloy A (annealed, 7 minutes)
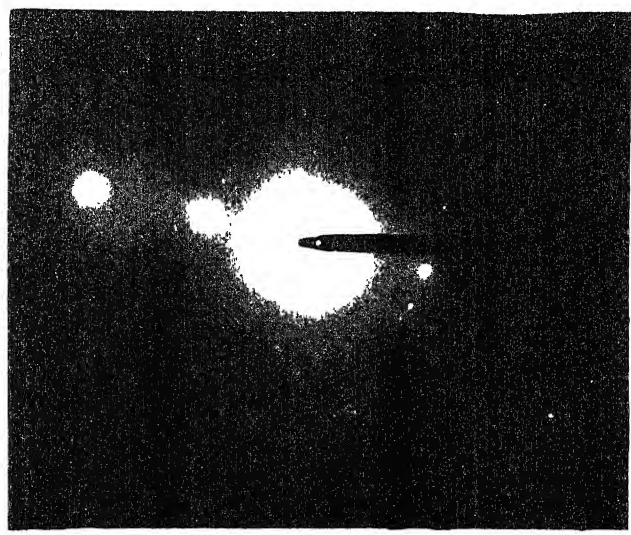
Fig. 58(b)   SAD of region 'A' of Fig. 58(a)
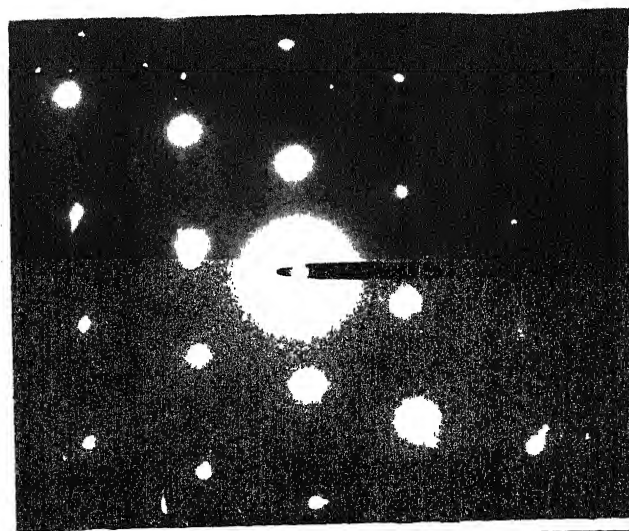
Fig. 58(c)   SAD of region 'B' of Fig. 58(a)
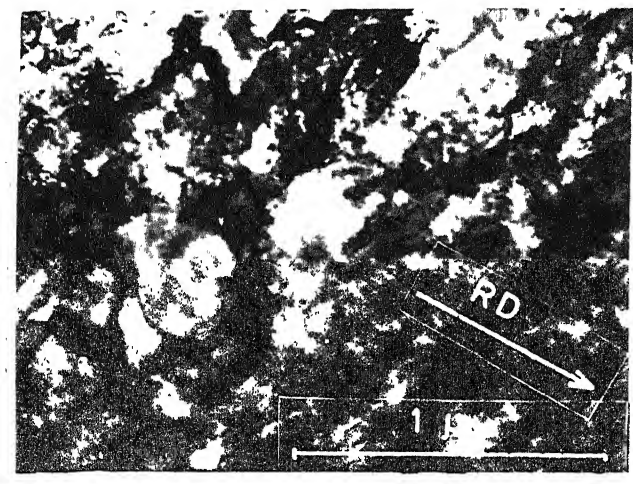
Fig. 59(a)   Alloy B
(annealed, 5 minutes)

Fig. 59(b)   SAD of Fig. 59(a)
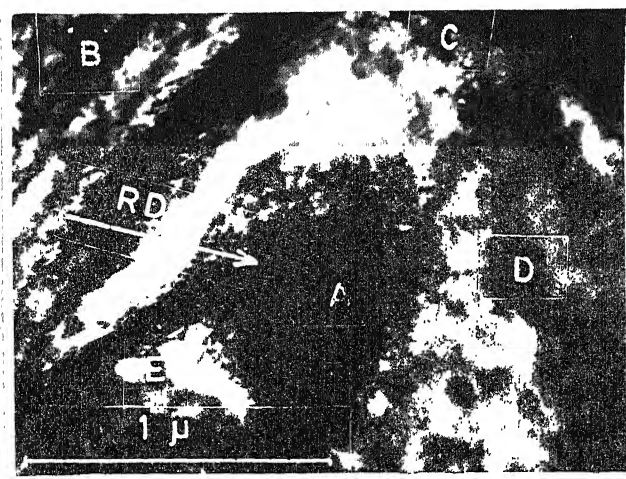
Fig. 60(a)   Alloy B
(annealed, 6½ minutes)
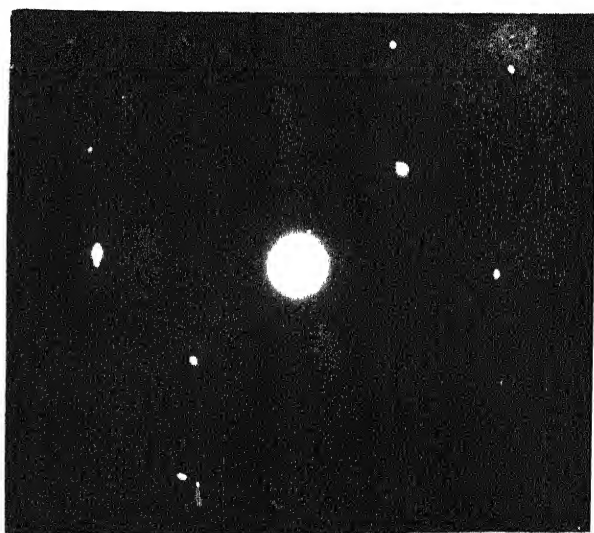
Fig. 60(b)   SAD of region 'A'
of Fig. 60(a)
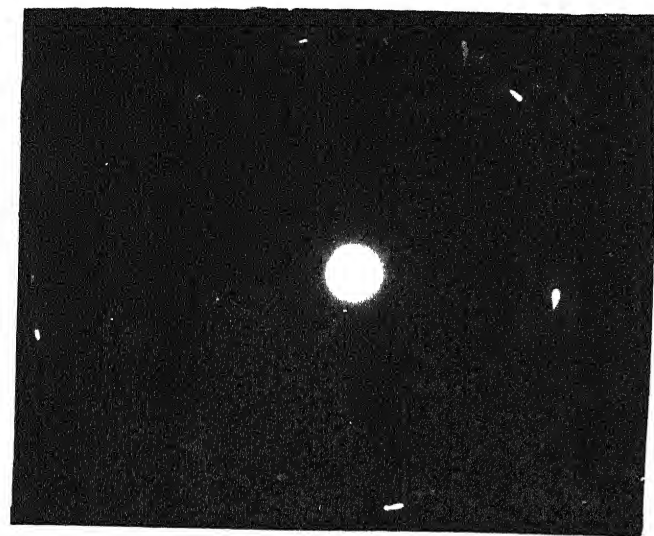
Fig. 60(c) SAD of region 'D'
of Fig. 60(a)
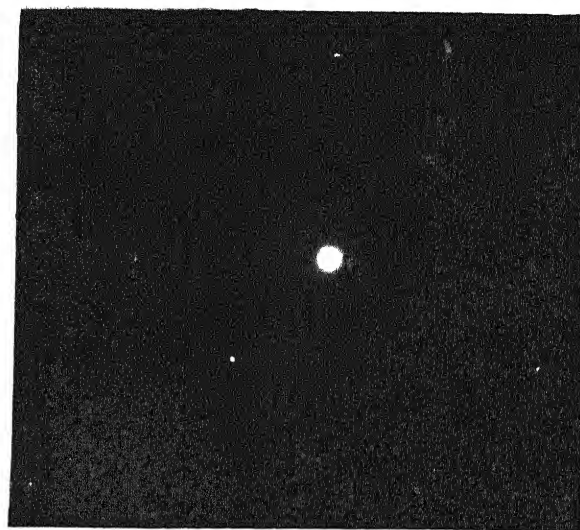
Fig. 60(d) SAD of region 'B'
of Fig. 60(a)
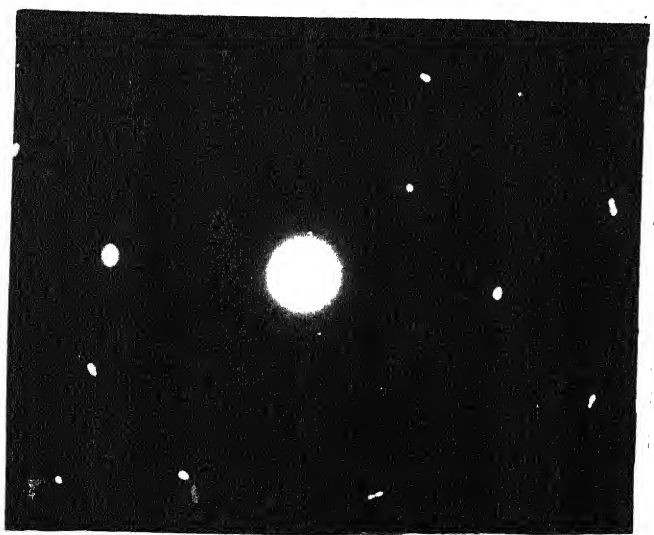
Fig. 60(e) SAD of region 'C'
of Fig. 60(a)
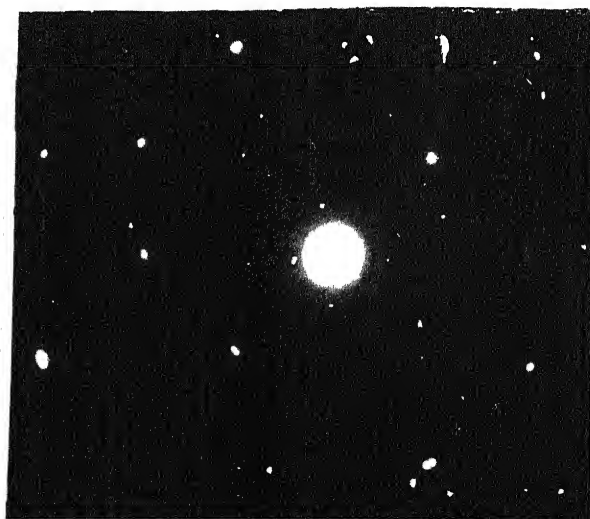
Fig. 60(f) SAD of region 'E'
of Fig. 60(a)
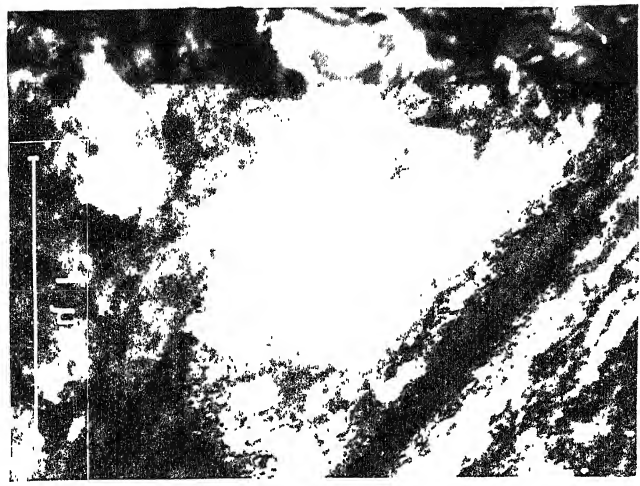
Fig. 61   Growth of central
         subgrain in Fig. 60(a)
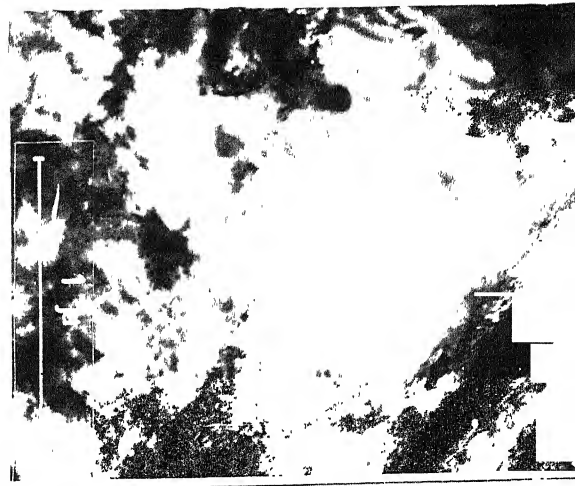
Fig. 62   Growth of central
         subgrain in Fig. 60(a)
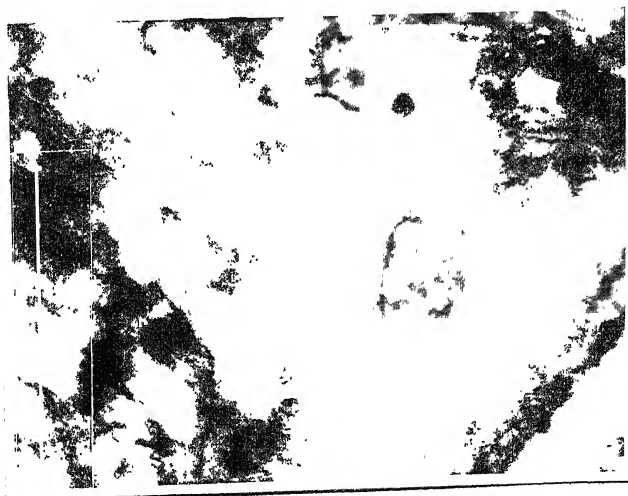
Fig. 63   Growth of central subgrain in Fig. 60(a)
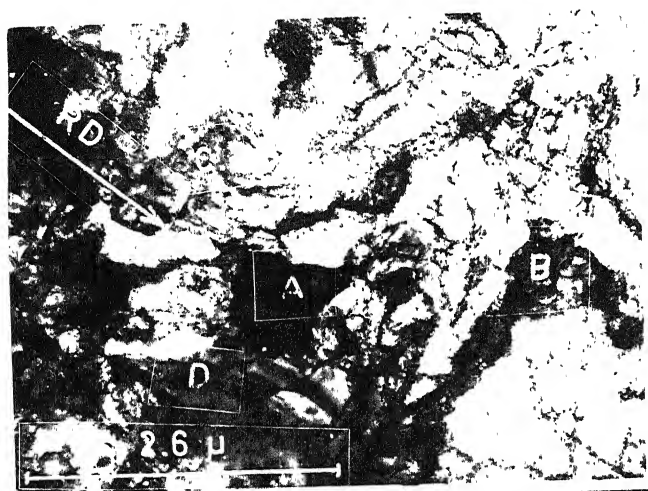
Fig. 64(a)   Alloy B
(annealed, 7 minutes)
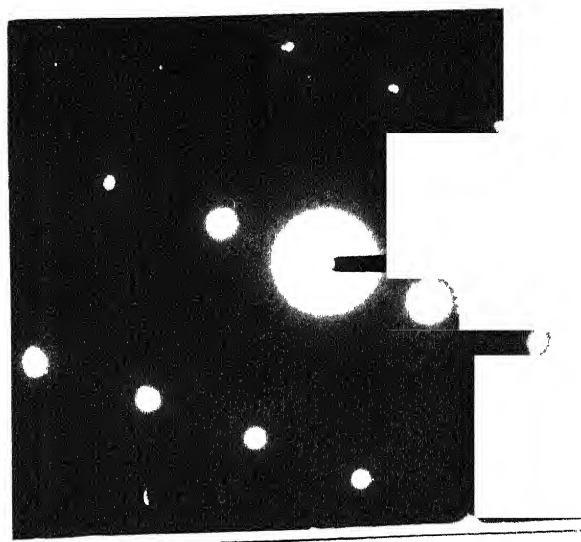
Fig. 64(b)   SAD of region 'B'
of Fig. 64(a)
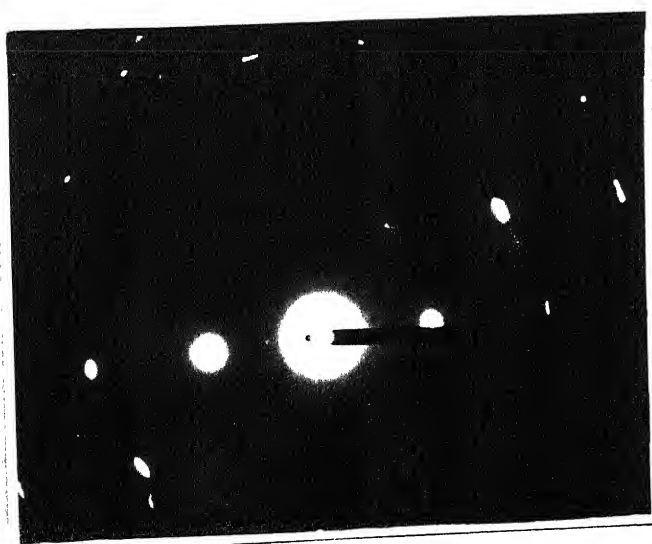
Fig. 64(c)   SAD of region 'C'
of Fig. 64(a)
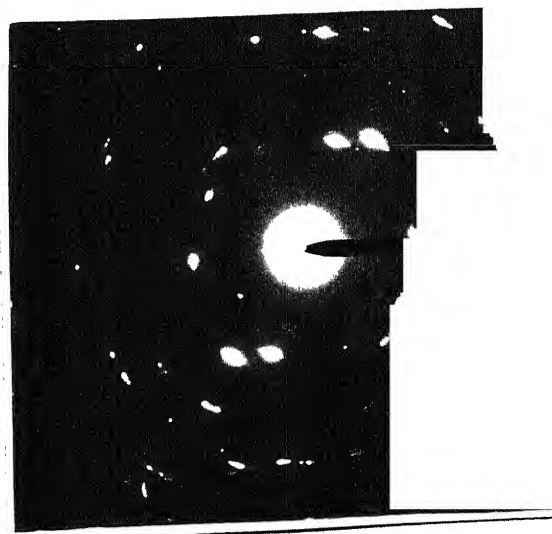
Fig. 64(d)   SAD of region 'A'
of Fig. 64(a)
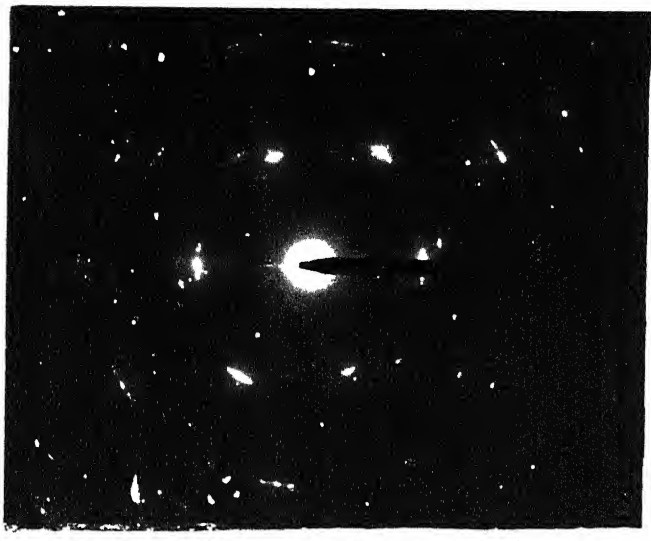
Fig. 64(e)   SAD of region 'D'
          of Fig. 64(a)
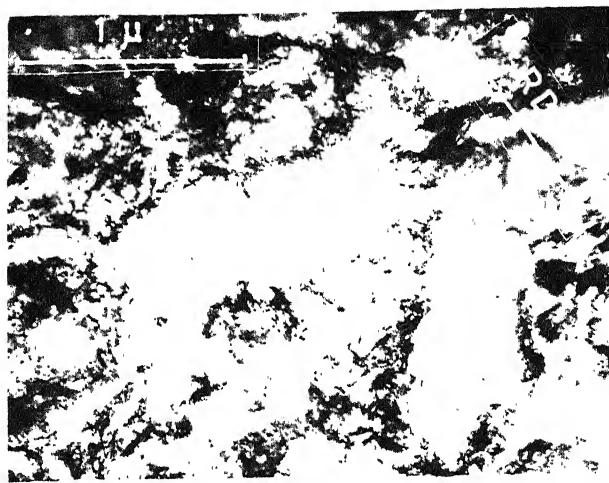
Fig. 65(a)   Alloy C
          (annealed, 5 minutes)
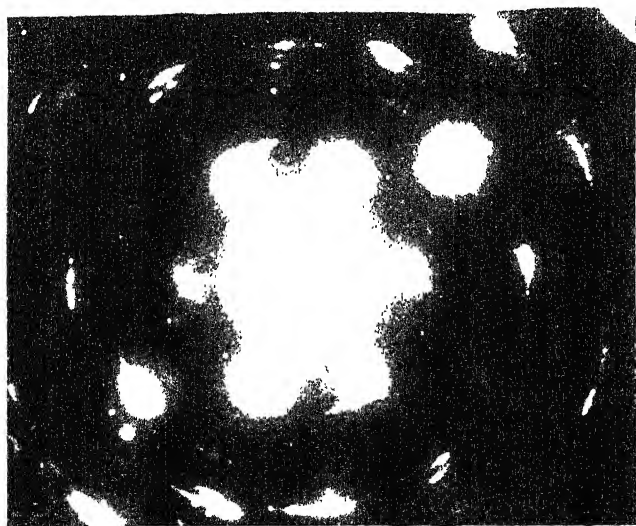
Fig. 65(b)   SAD of Fig. 65(a)

Fig. 66(a)   Alloy C
          (annealed, 6½ minutes)
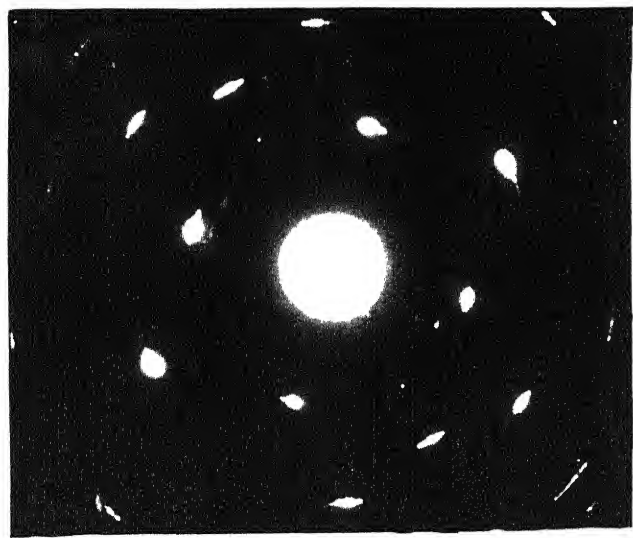
Fig. 66(b)   SAD of Fig. 66(a)
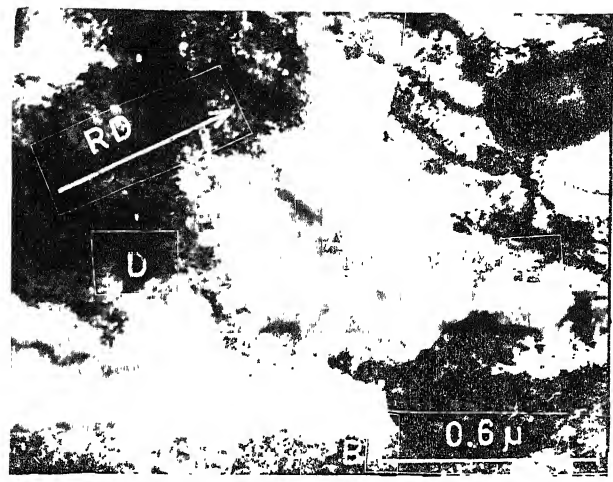
Fig. 67(a)   Alloy C
(annealed, 6½ minutes)
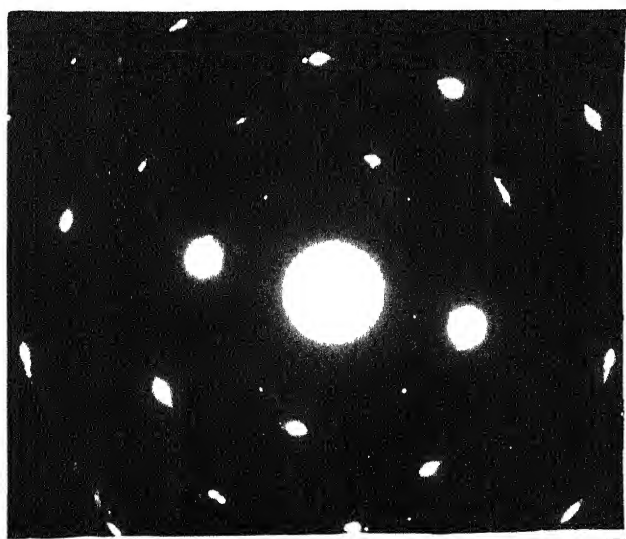
Fig. 67(b)   SAD of region 'A'
of Fig. 67(a)
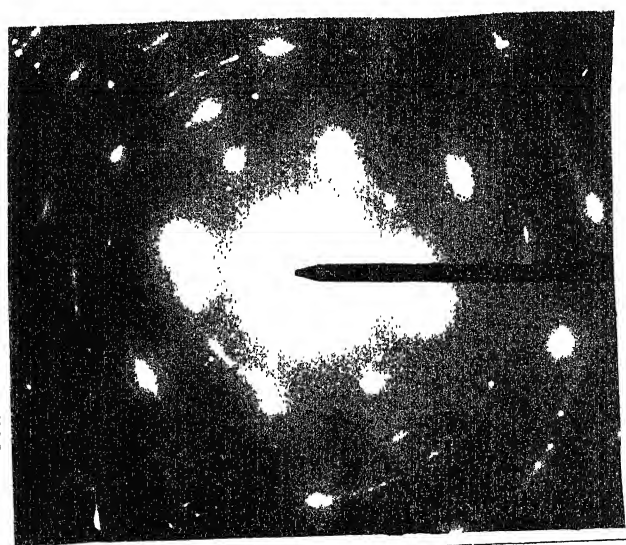
Fig. 67(c)   SAD of region 'D'
of Fig. 67(a)
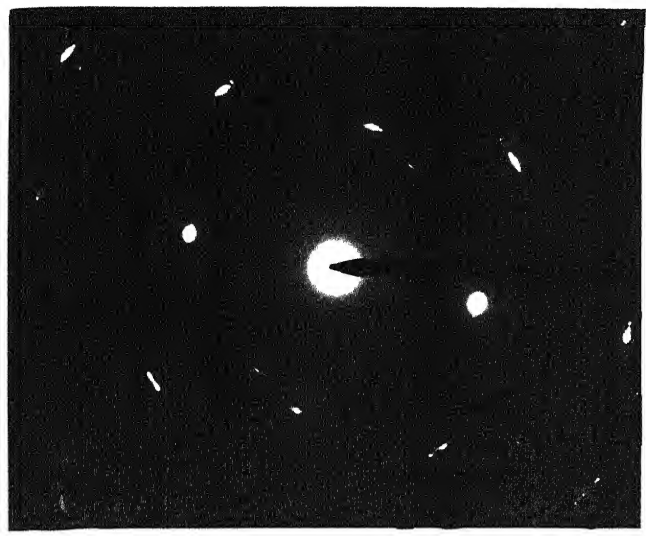
Fig. 67(d)   SAD of region 'E'
of Fig. 67(a)
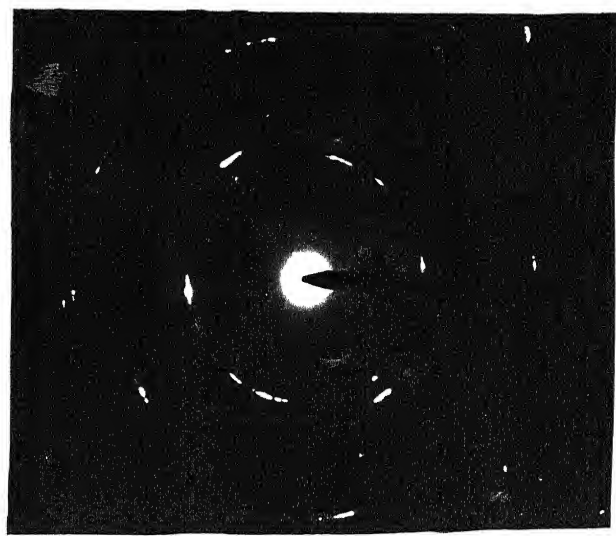
Fig. 67(e)   SAD of region 'B'
of Fig. 67(a)
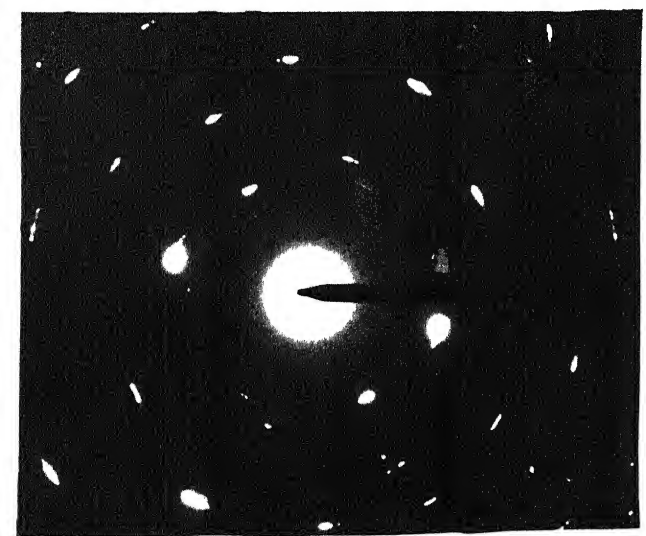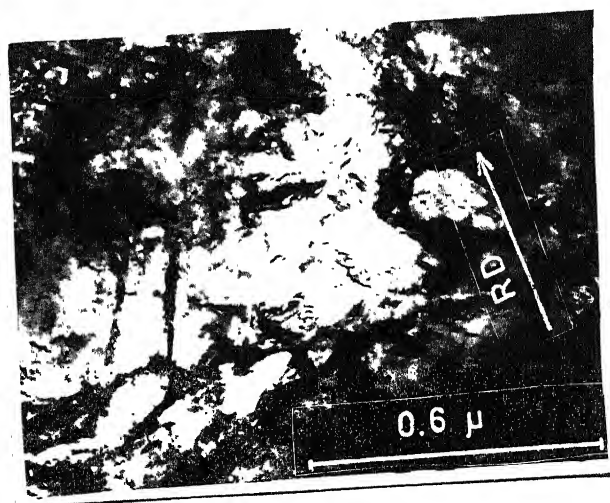

Fig. 67(f)   SAD of region 'C'
of Fig. 67(a)
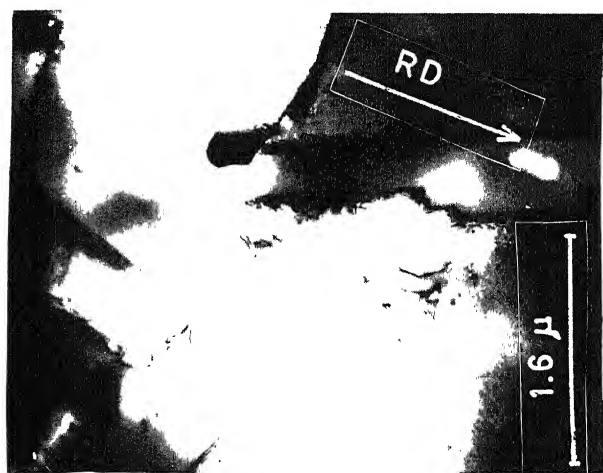
Fig. 68(a)   Alloy C
(annealed, 8 minutes)
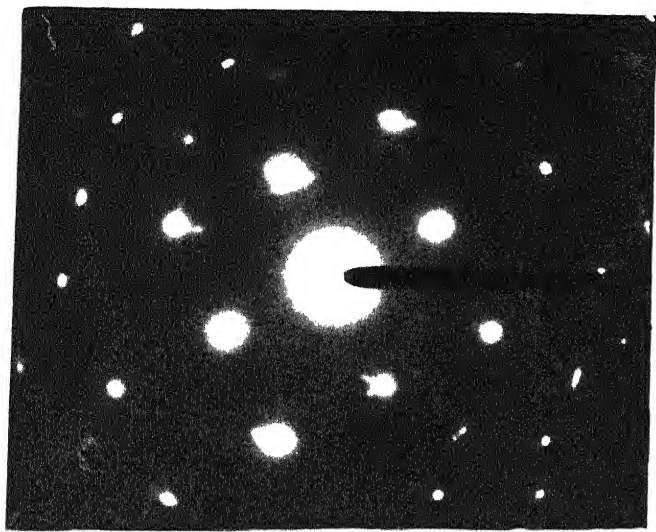
Fig. 70(b)   SAD of Fig. 70(a)
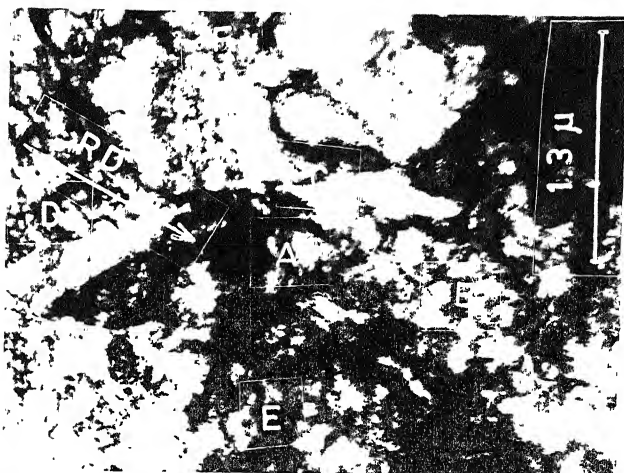
Fig. 71(a)   Alloy D
(annealed, 6 minutes)
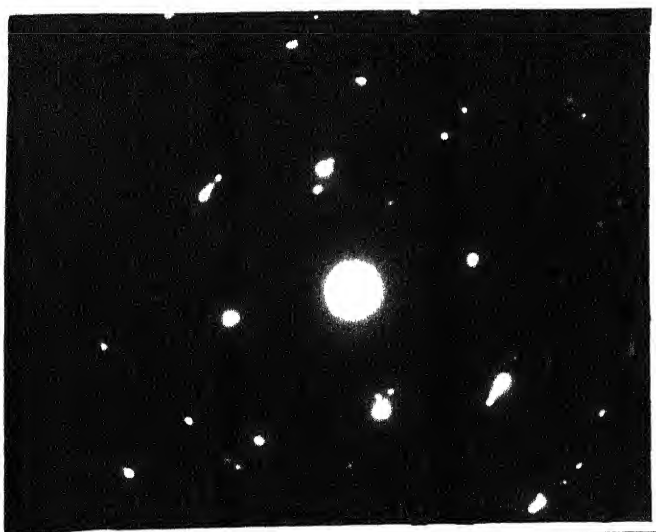
Fig. 71(b)   SAD of region 'A'
of Fig. 71(a)

Fig. 71(c)   SAD of region 'B'
of Fig. 71(a)
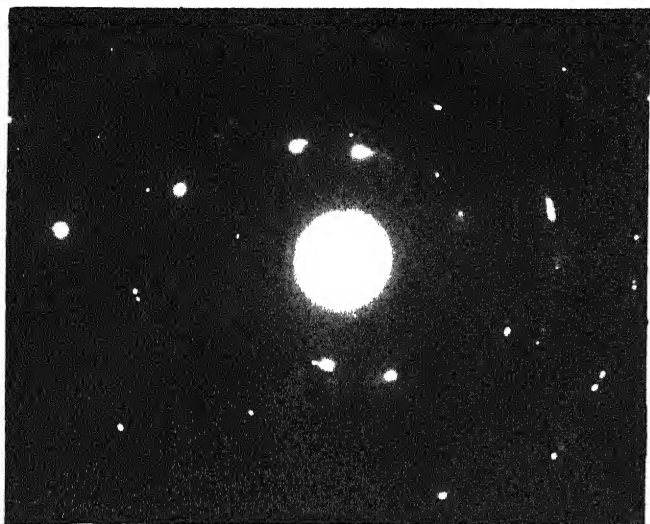
Fig. 71(d)   SAD of region 'C'
of Fig. 71(a)
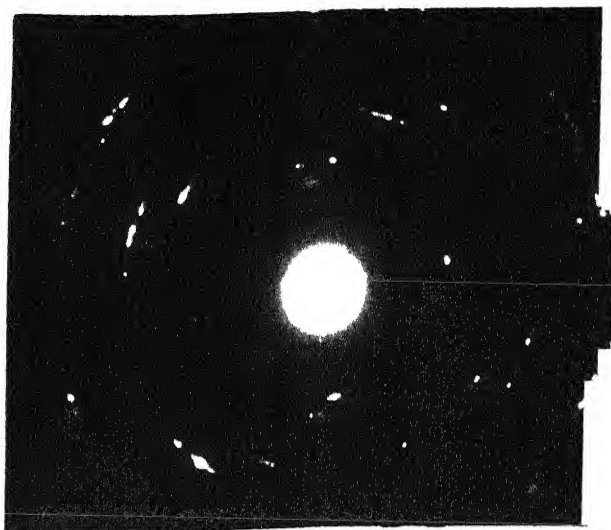
Fig. 71(e)   SAD of region 'D'
of Fig. 71(a)
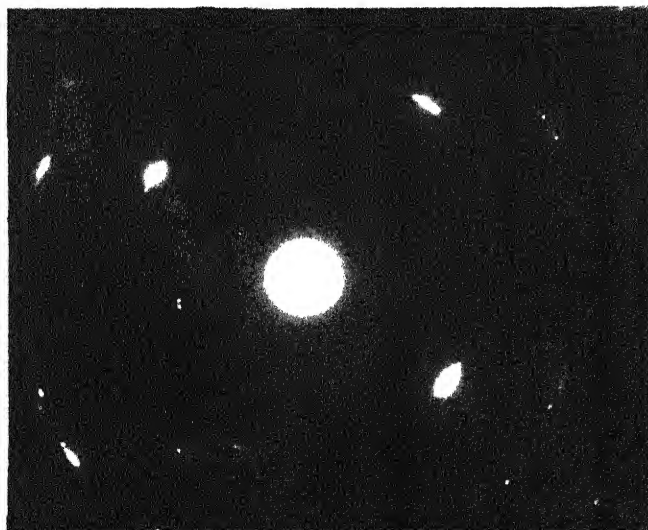
Fig. 71(f)   SAD of region 'E'
of Fig. 71(a)
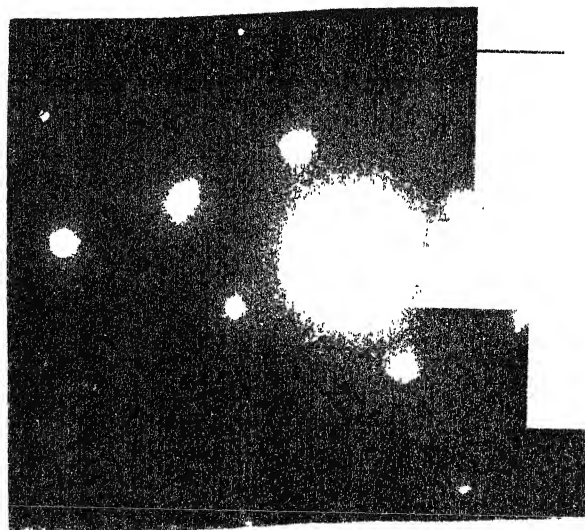
Fig. 71(g)   SAD of region 'F'
of Fig. 71(a)
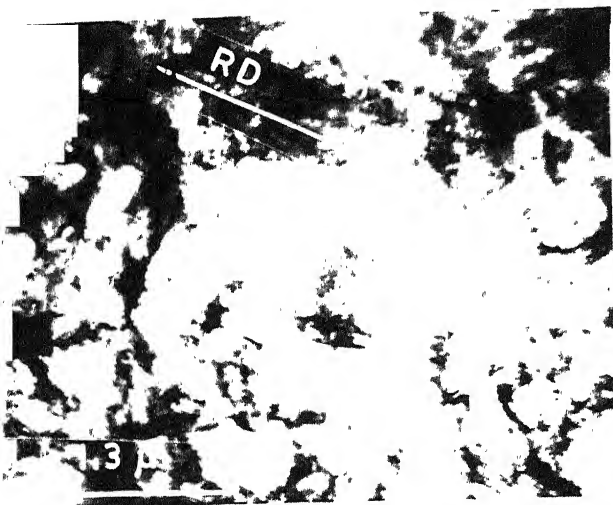
Fig. 72(a)   Alloy D
    (annealed, 6 minutes)
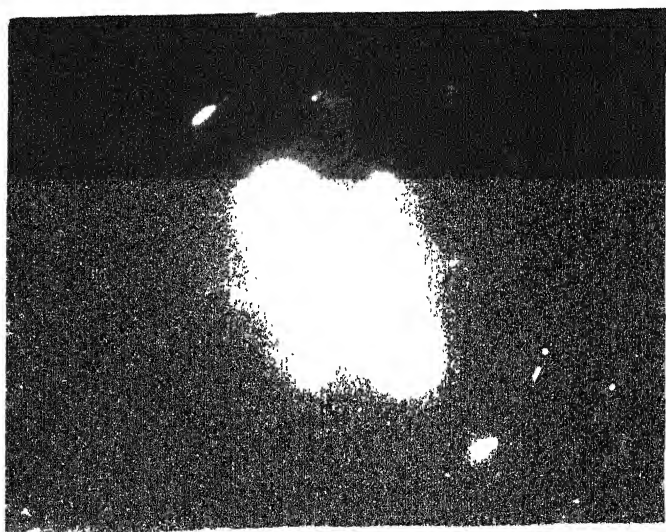
Fig. 72(b)   SAD of Fig. 72(a)
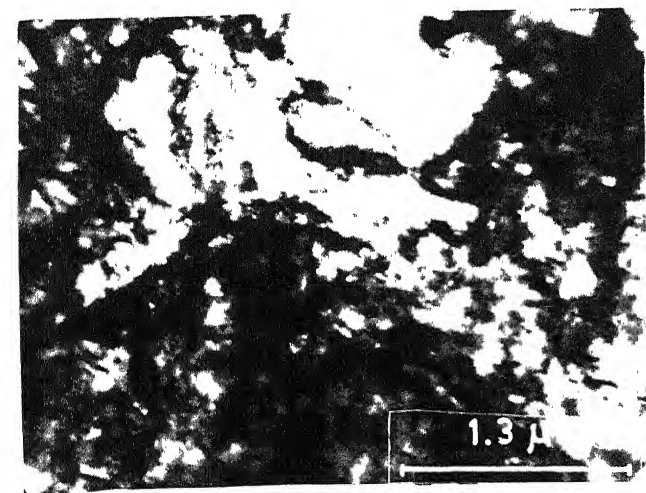
Fig. 73   Grain growth of sub-
    grain in Fig. 71(a)
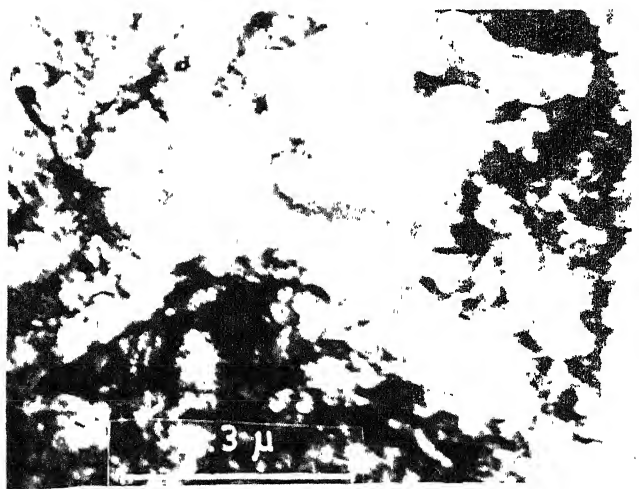
Fig. 74   Grain growth of sub-
    grain in Fig. 71(a)
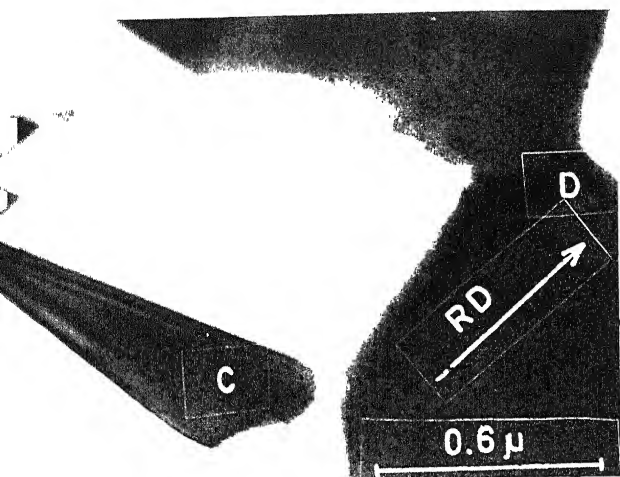
Fig. 75(a)   Alloy D
(annealed, 8 minutes)
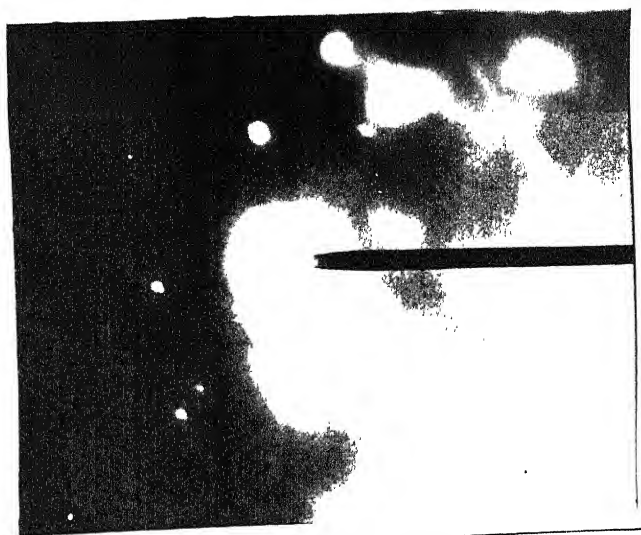
Fig. 75(b)   SAD of grain 'A'
of Fig. 75(a)
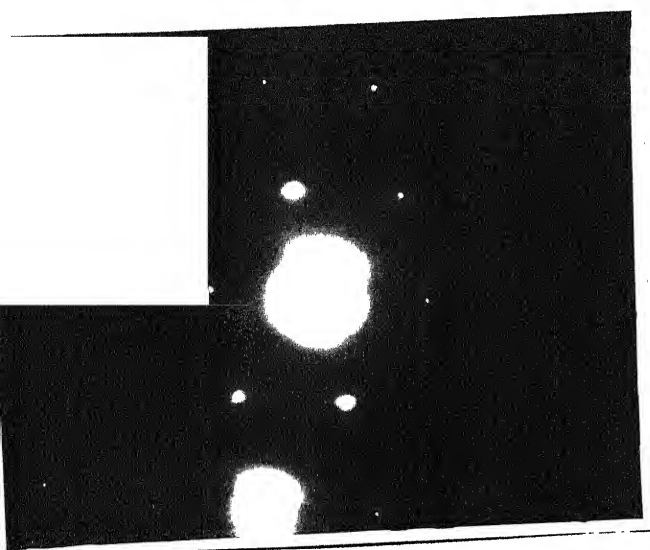
Fig. 75(c)   SAD of grain 'D'
of Fig. 75(a)

Fig. 76(a)   Alloy D
(annealed, 5 minutes)
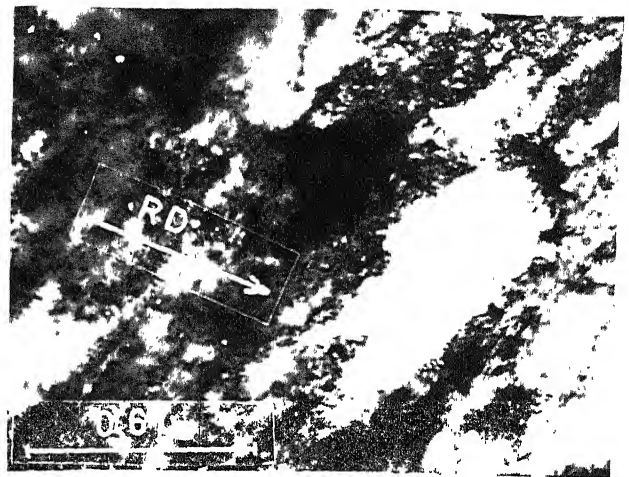
Fig. 76(b)   SAD of Fig. 76(a)
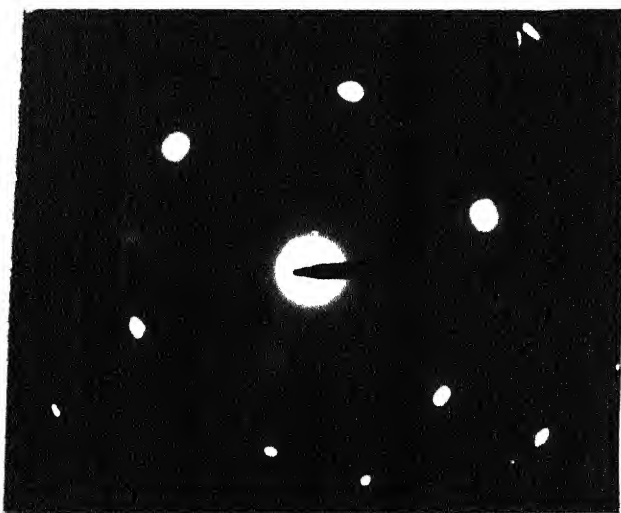

Fig. 77(a)   Alloy E
(annealed, 5 minutes)

Fig. 77.(b)   SAD of Fig. 77.(a)
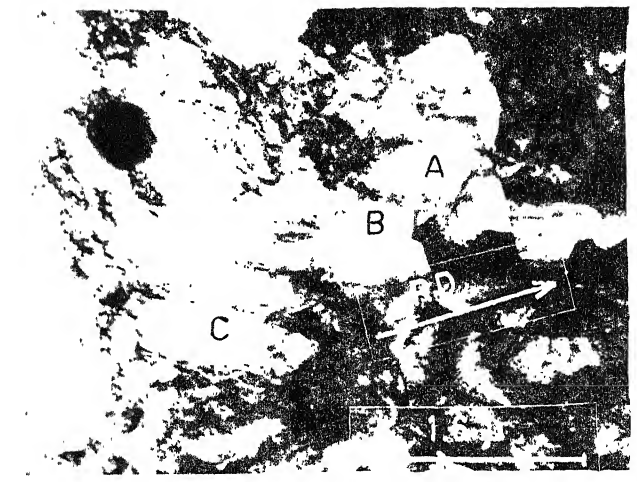

Fig. 78(a)   Alloy E
(annealed, 6½ minutes)
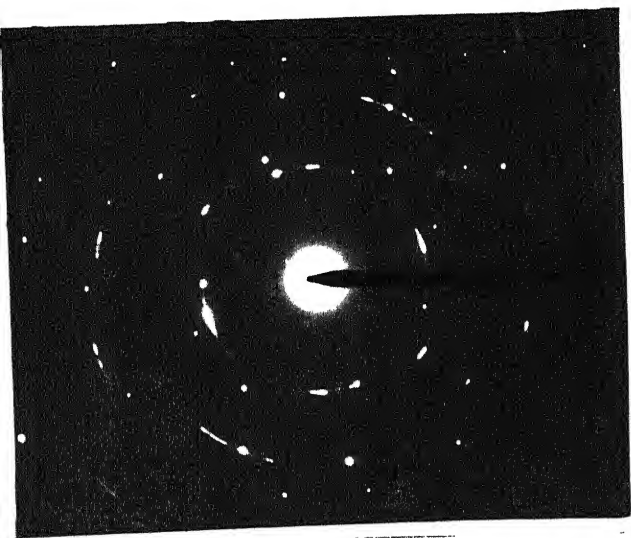
Fig. 78(b)   SAD of region 'A'
             of Fig. 78(a)
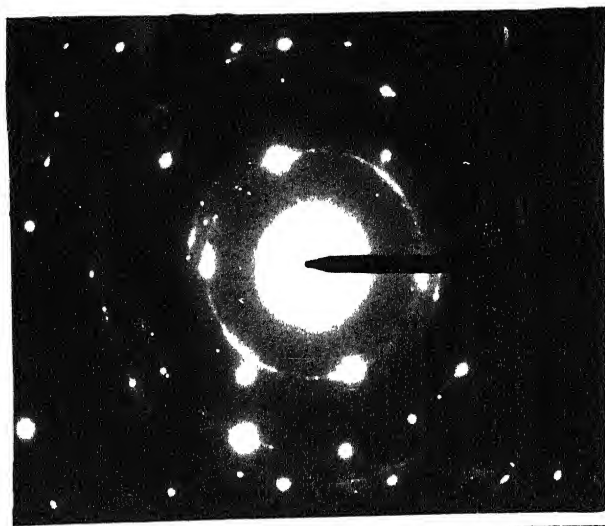

Fig. 78(c)   SAD of region 'B'
             of Fig. 78(a)
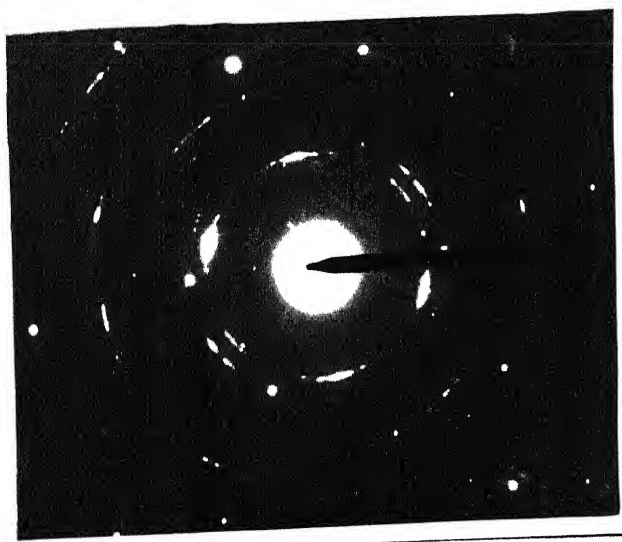

Fig. 78(d)   SAD of region 'C'
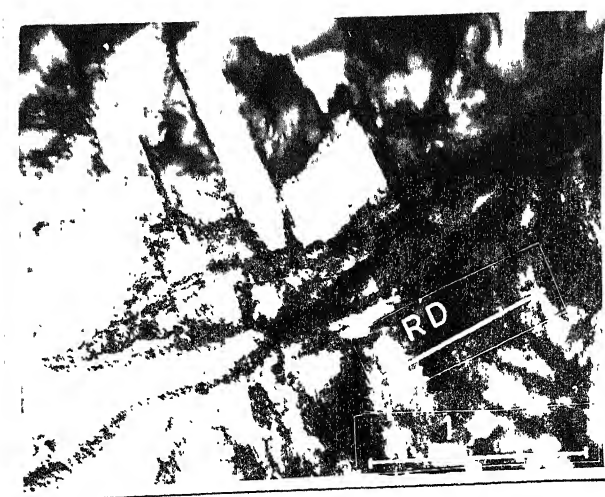   of Fig. 78(a)

Fig. 79(a)   Alloy E
             (annealed, 7 minutes)

Fig. 79(b)   SAD of Fig. 79(a)

Fig. 80(a)   Alloy E
(annealed, 7 minutes)

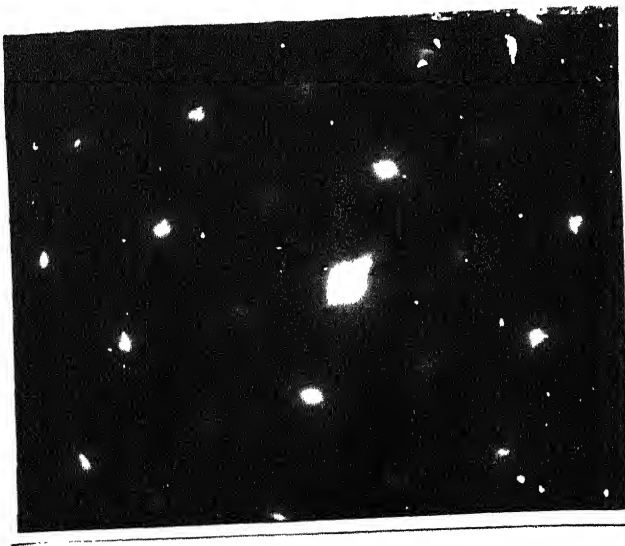Fig. 80(b)   SAD of region 'A'
of Fig. 80(a)

Fig. 80(c)   SAD of region 'B'
of Fig. 80(a)

Fig. 81(a)   Alloy E
(annealed, 8 minutes)

Fig. 81(b)   SAD of grain 'A'
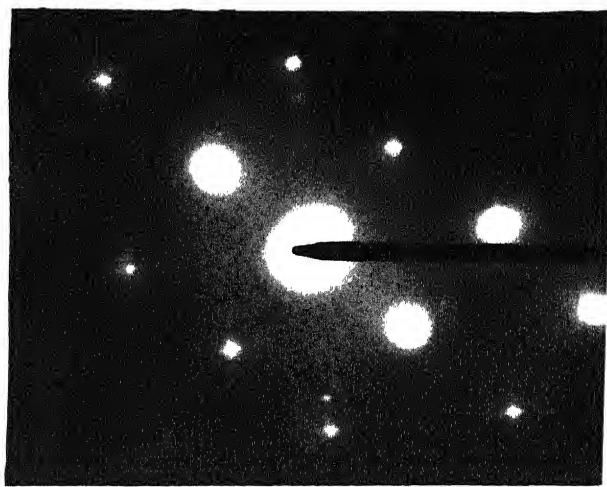of Fig. 81(a)

Fig. 81(c)   SAD of grain 'B'
of Fig. 81(a)
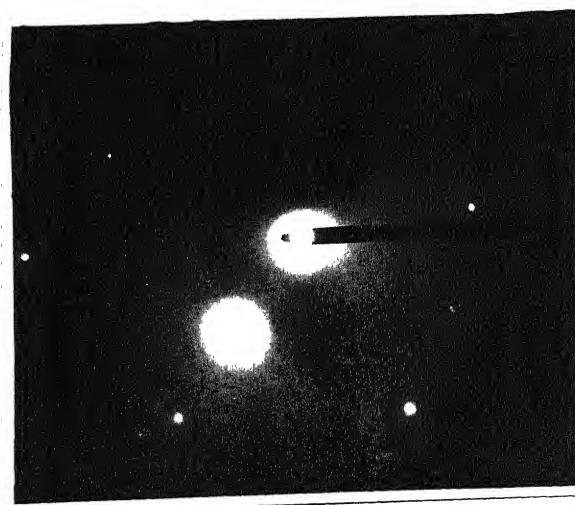
Fig. 81(d)   SAD of grain 'C'
of Fig. 81(a)
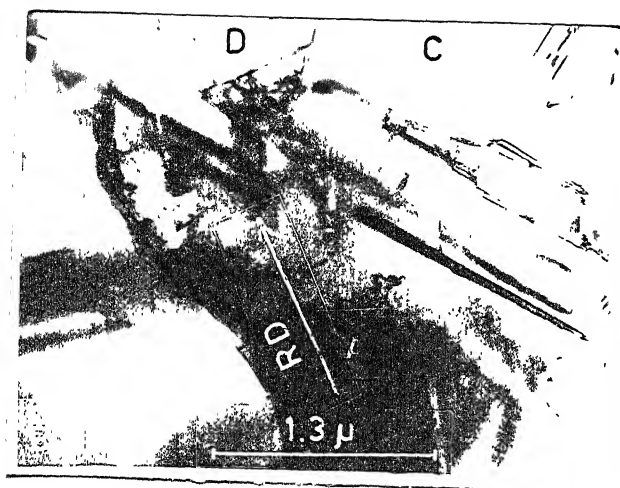
Fig. 82(a)   Alloy E
(annealed, 8 minutes)
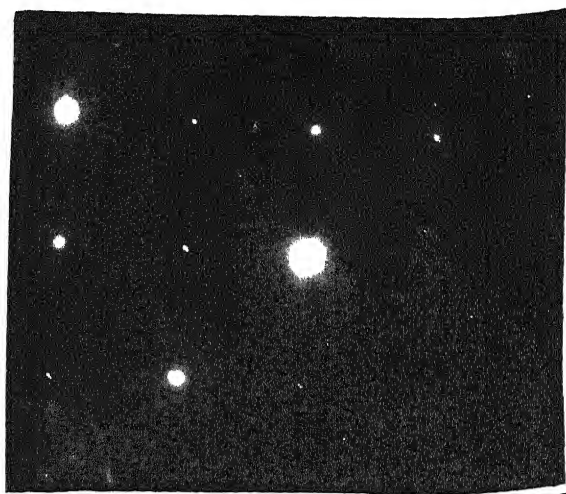
Fig. 82(b)   SAD of grain 'A'
of Fig. 82(a)
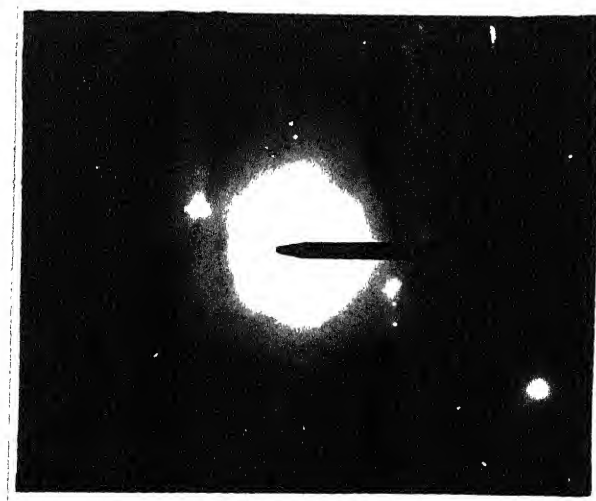
Fig. 82(c)   SAD of grain 'B'
of Fig. 82(a)
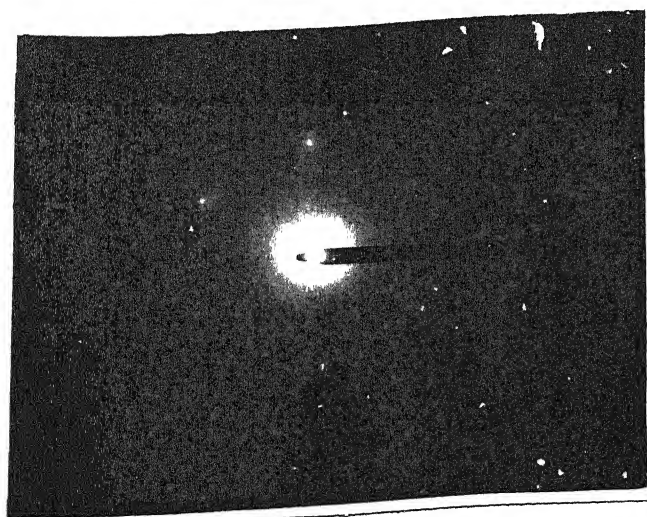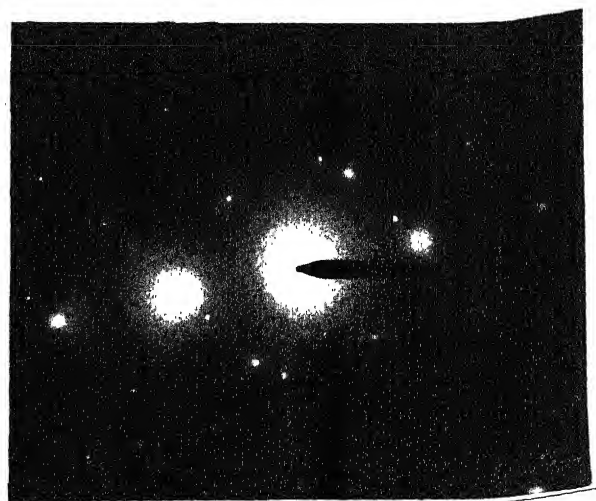

Fig. 82(d)   SAD of grain 'C'
of Fig. 82(a)

Fig. 82(e)   SAD of grain 'D' of Fig. 82(a)
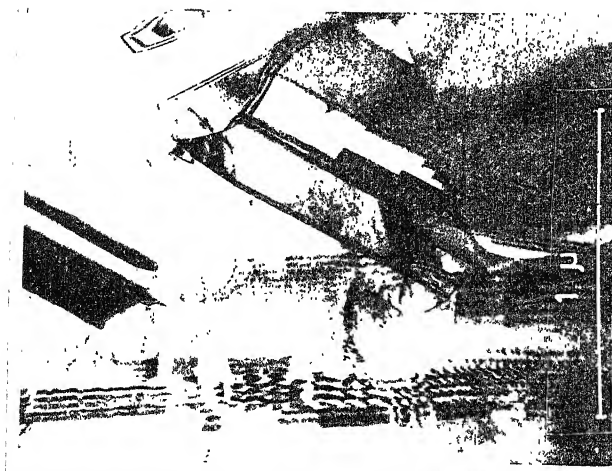
Fig. 83   Alloy E (annealed, 8 minutes)
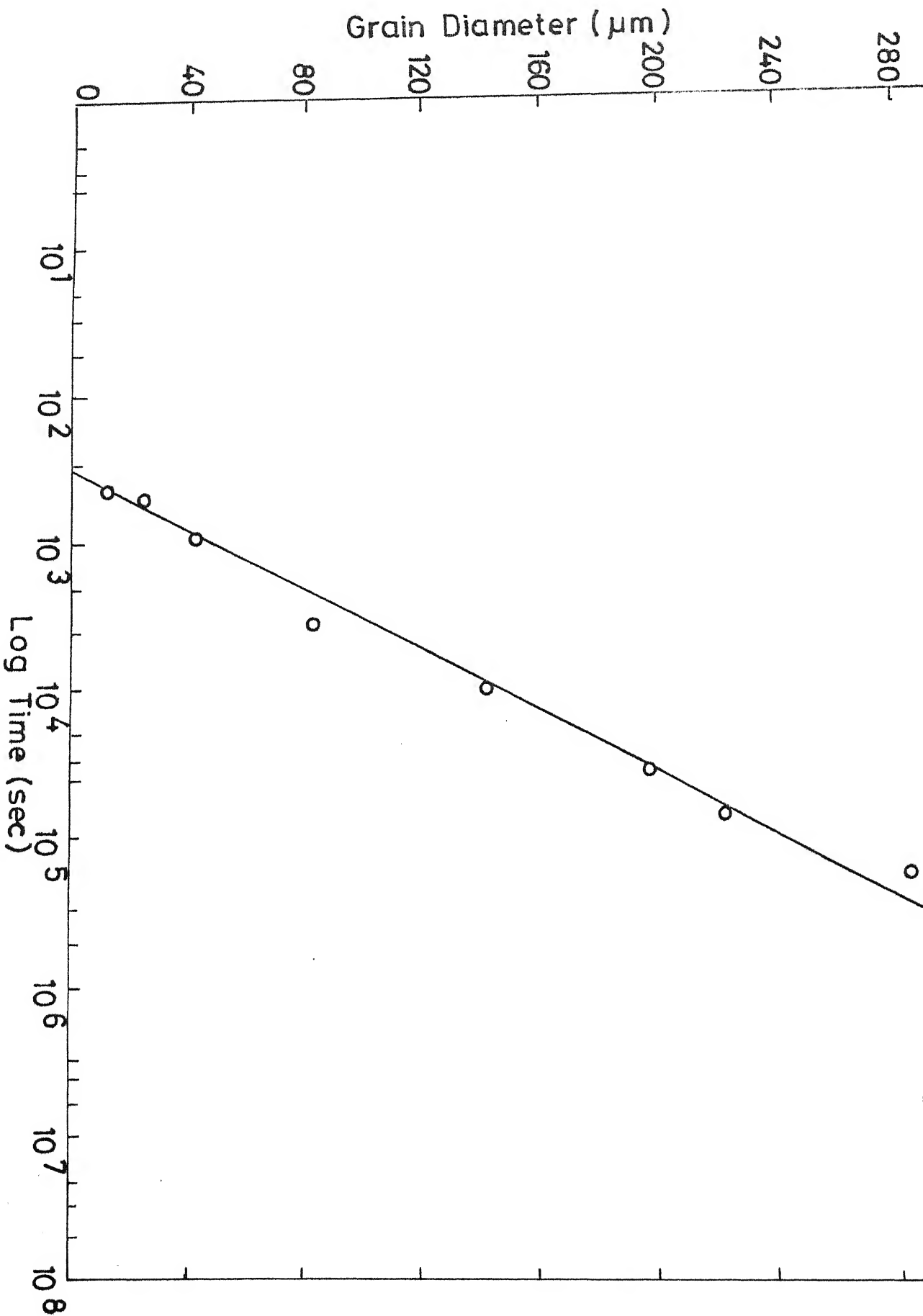
Fig. 84 Variation of Grain Dia(μm) with Log Time(sec) of Alloy A.

Fig. 85. Variation of Grain Dia (μm) with Log Time(sec) of Alloy B.

Fig. 88 Variation of Grain Dia.(μm) with Log Time (sec) of Alloy F
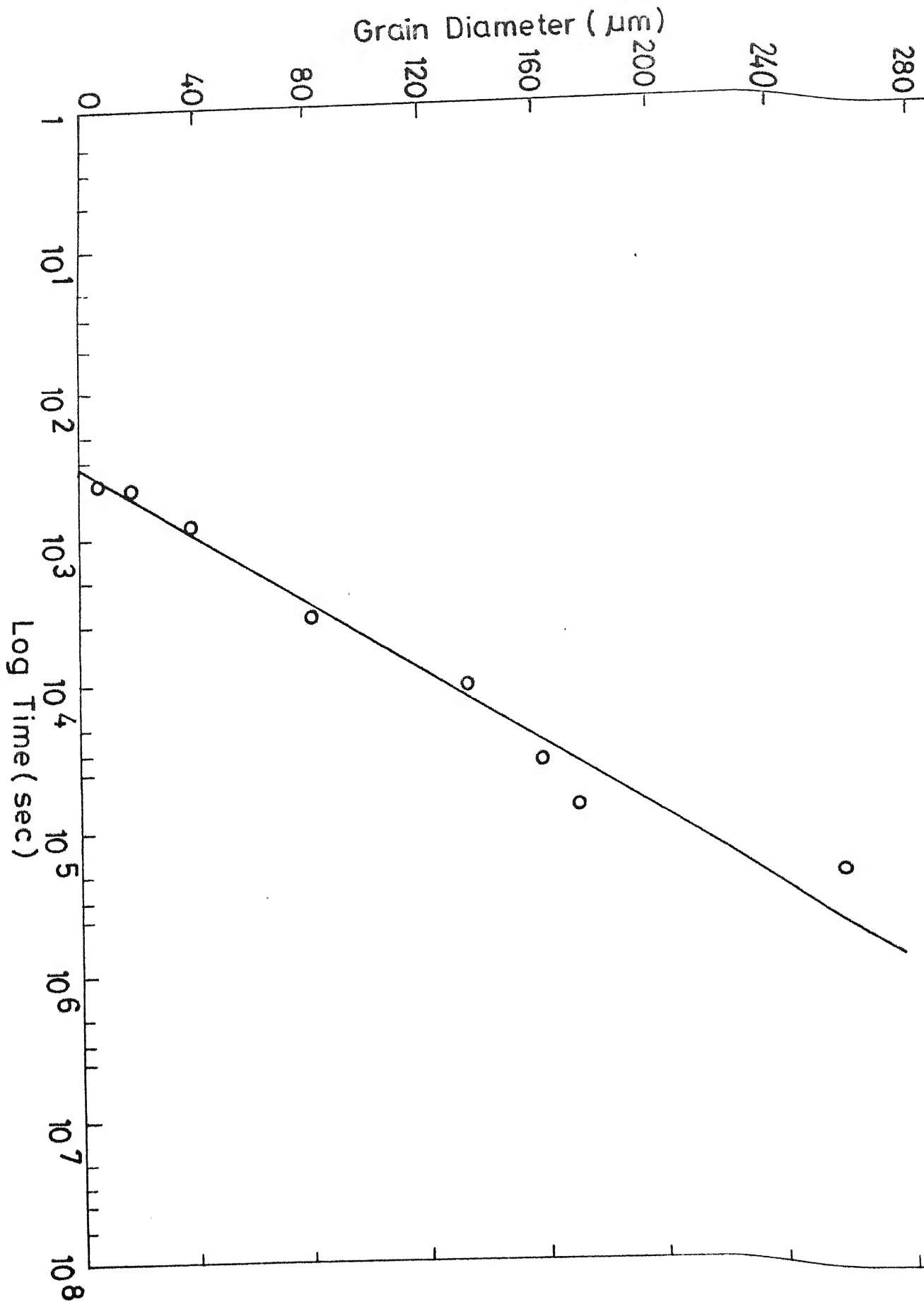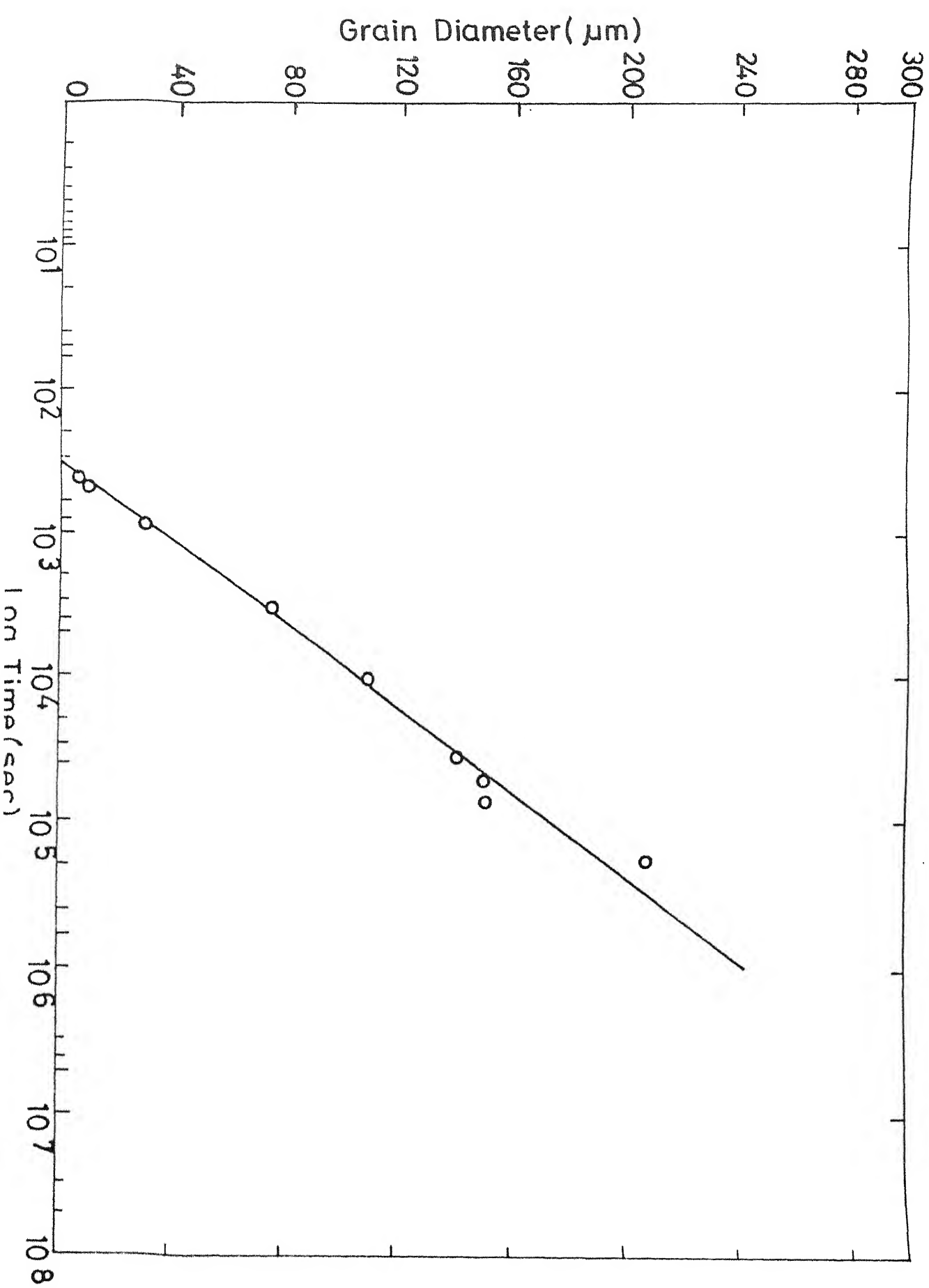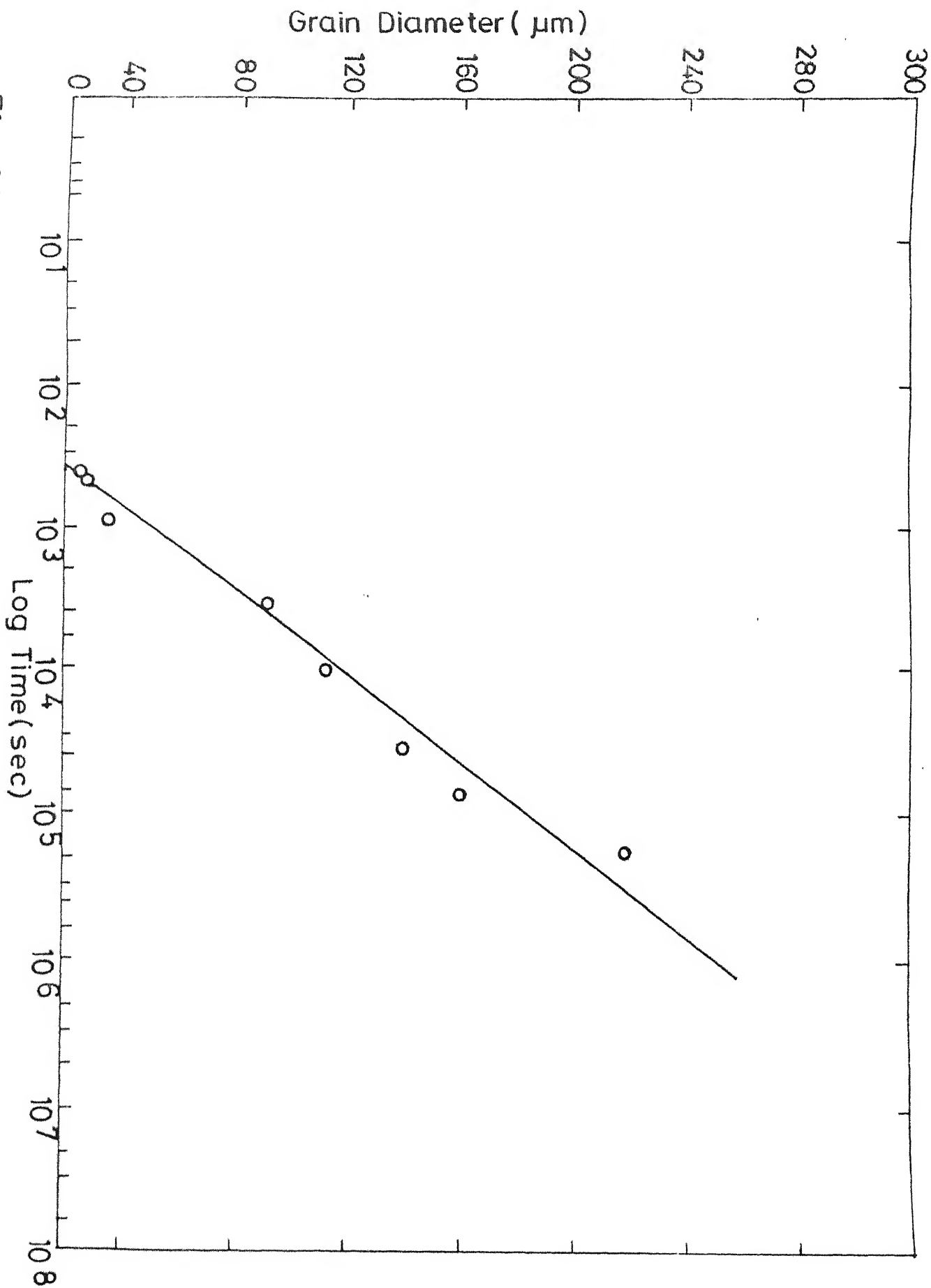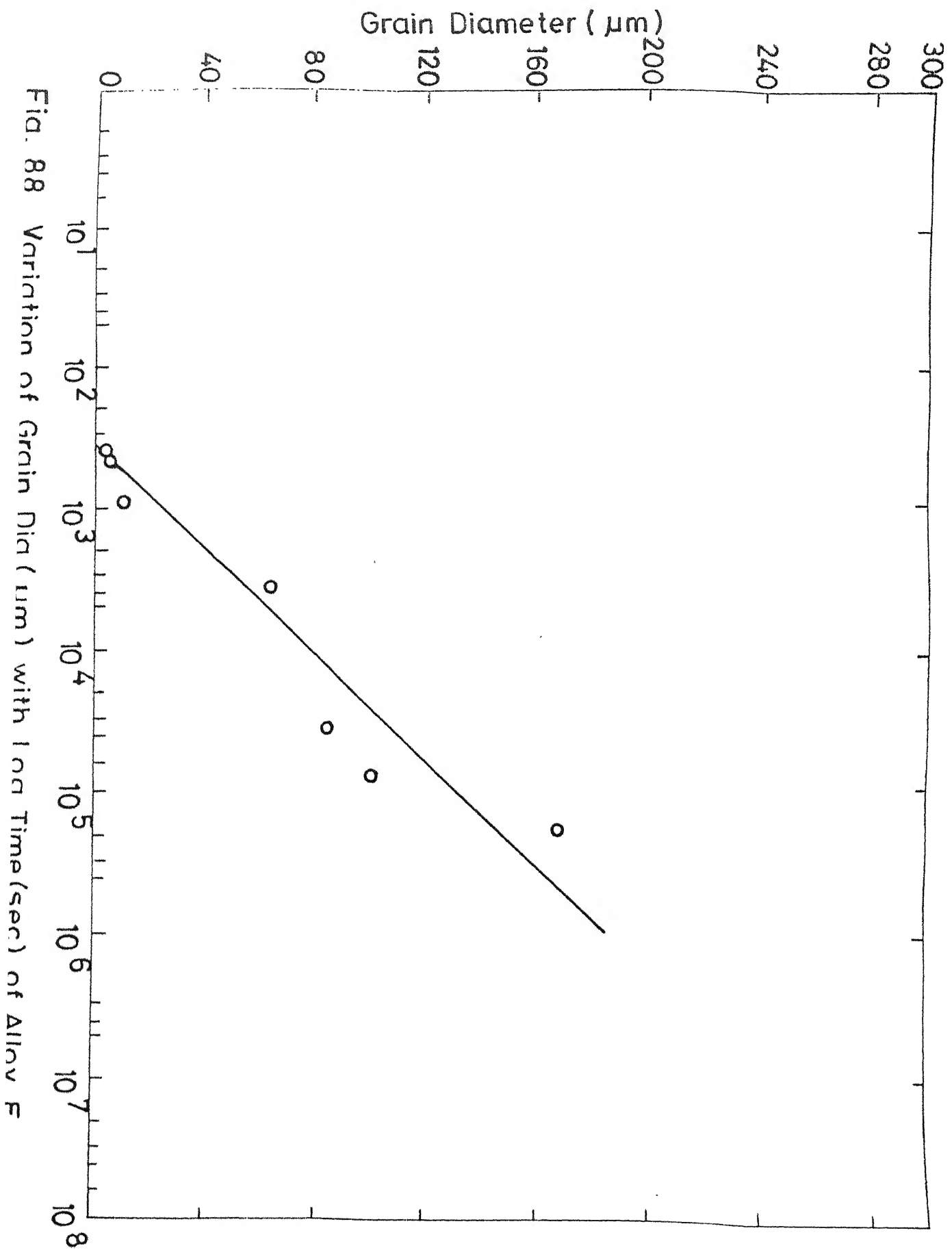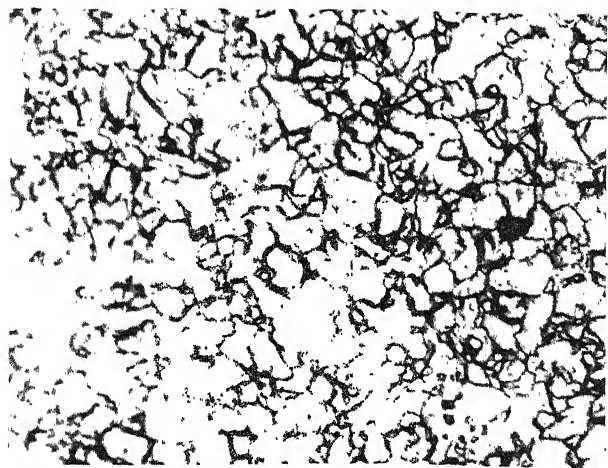
Fig. 89 Alloy A
(annealed, 15 minutes)
(Mag. 200X)
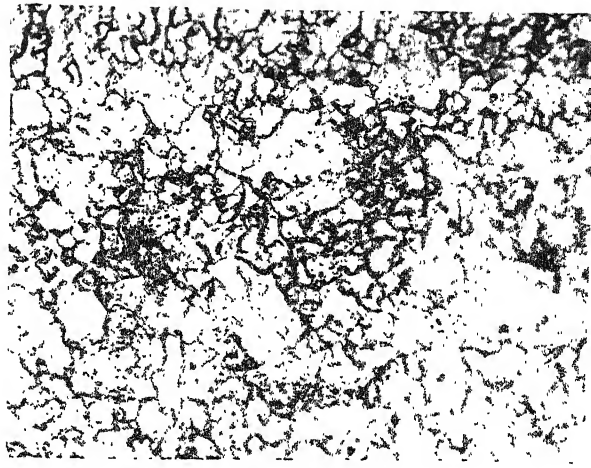
Fig. 90 Alloy B
(annealed, 15 minutes)
(Mag. 200X)
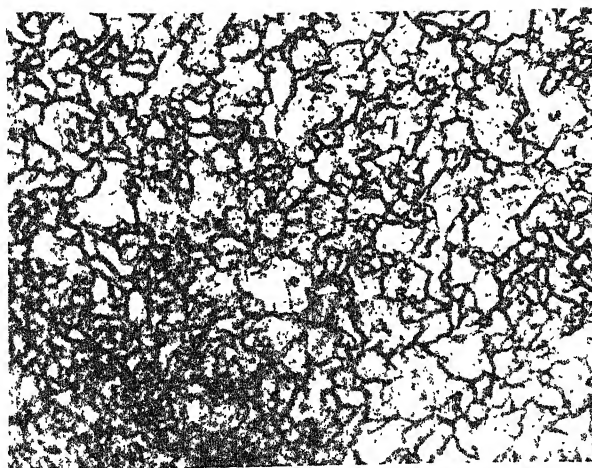
Fig. 91   Alloy C (annealed, 15 minutes)
(Mag. 200X)
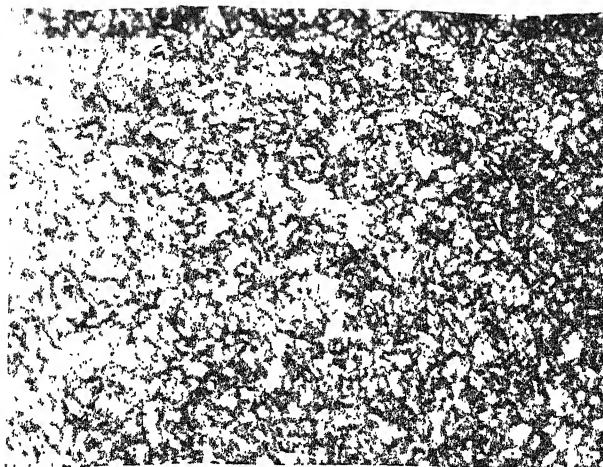
Fig. 92   Alloy D (annealed, 15 minutes)
           (Mag. 200X)
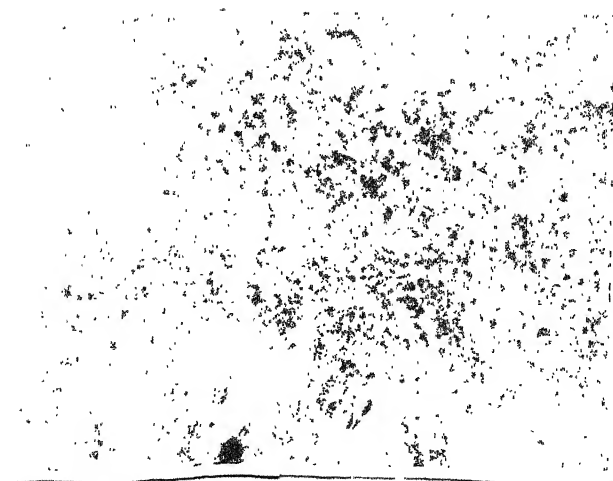
Fig. 93   Alloy E (annealed, 15 minutes)
           (Mag. 200X)

CHAPTER - 5

CONCLUSIONS

(1) Widely differing deformation textures have been found in the present series of alloys. While the deformation textures in alloys A, B and C have been found to be pure-metal type, that of alloy E is alloy-type. The deformation texture of alloy D has been found to lie somewhat in-between these two extremes.

(2) The recrystallisation textures of alloys A, B and C are rather similar showing mostly the cube-component. The recrystallisation texture of alloy E does not show any cube but a rather strong Goss component. The recrystallisatiom texture of alloy D has been found to be rather weak and more or less random.

(3) Addition of Co to Ni is found to decrease the average grain size of the recrystallised grains as well as their rate of growth.

(4) The differences in the deformation and recrystallisation textures in the present series of alloys has been attributed to the difference in stacking fault energies of the alloys as a function of cobalt content.

(5) The effect of Co-addition to Ni on the average recrystallised grain size as well as their rate of growth has been explained as due to a retardation effect on the effective grain-boundary migration rate.

REFERENCES

1. J.G. Byrne, 'Recovery Recrystallisation and Grain Growth', p. 1 (1965), The Macmillan Co., New York.

2. J.E. Bailey, Phil. Mag., $\underline{5}$, 833 (1960).

3. J.E. Bailey and P.B. Hirsch, Proc. Roy. Soc., $\underline{A267}$, 11 (1962).

4. W. Bollmann, J. Inst. Met., $\underline{87}$, 439 (1959).

5. S. Weissmann, T. Imura and N. Hosokawa, 'Recovery and Recrystallisation of Metals', Ed. L. Himmet, p. 241 (1963), New York (Interscience).

6. H. Hu, R.S. Cline and S.R. Goodman, 'Recrystallisation Grain Growth and Textures', p. 295 (1966), A.S.M., Metals Park, Ohio.

7. B.L. Averbach, M.B. Bener, M.F. Comerford and J.L. Leach, Acta Met., $\underline{4}$, 477 (1956).

8. D. Michell, Phil. Mag., $\underline{1}$, 584 (1956).

9. D. Michell and F.D. Haig, Phil. Mag., $\underline{2}$, 15 (1957).

10. F. Haessner, 'Recrystallisation of Metallic Materials', Ed. F. Haessner, p. 5, Dr. Reidorer-Verlag, GMBH, Stuttgart (1971).

11. L.M. Clarebrough, M.E. Hargreaves and M.H. Loretto, Acta Met., $\underline{6}$, 725 (1958).

12. L.M. Clarebrough, M.E. Hargreaves, D. Michell and G.W. West, Proc. Roy. Soc., $\underline{A215}$, 507 (1952).

13. L.M. Clarebrough, M.E. Hargreaves and G.W. West, Proc. Roy. Soc., $\underline{A232}$, 252 (1955).

14. L.M. Clarebrough, M.E. Hargreaves, G.W. West and A.K. Head, Proc. Roy. Soc., $\underline{A242}$, 160 (1957).

15. J.W. Henderson and J.S. Koehler, Phys. Rev., $\underline{104}$, 626 (1956).

16. J.G. Byrne, 'Recovery, Recrystallisation and Grain Growth', p. 37 (1965), The Macmillan Co., New York.

17. R. Drouard, J. Washburn and E.R. Parker, Trans. A.I.M.E., $\underline{197}$, 1226 (1953).

18. B.E. Warren and B.L. Averbach, J. Appl. Phys., 23, 497 (1952).

19. H. Hu, 'Recovery and Recrystallisation of Metals', Ed. L. Himmel, p. 311 (1963), New York (Interscience).

20. A.L. Tichener and M.B. Bever, 'Progress in Metal Physics', 7, 247 (1958).

21. T.V. Cherian, P. Pietrokowsky and J.E. Dorn, Trans. A.I.M.E., 185, 948 (1949).

22. A.S. Keh, 'Direct Observation of Imperfections in Crystals', New York (Interscience), (1962).

23. J.C.M. Li, 'Recrystallisation, Grain Growth and Textures', p. 45 (1966), A.S.M., Metals Park, Ohio.

24. P.B. Price, Phil. Mag., 5, 873 (1960).

25. C.N.J. Wagner, Acta Met., 5, 427 (1957).

26. E. Orowan, Communication to Congres de la Societe Francias de la Metallurgie d'Octobre (1947).

27. R.W. Cahn, J. Inst. Met., 76, 121 (1949).

28. R.W. Cahn, 'Progress in Metal Physics', 2, 151 (1950).

29. C.T. Wei and P.A. Beck, J. Appl. Phys., 27, 1508 (1956).

30. P.P. Sinha and P.A. Beck, J. Appl. Physics, 32, 1222 (1961).

31. P.P. Sinha and P.A. Beck, J. Appl. Phys., 33, 625 (1962).

32. W.R. Hibbard and C.G. Dunn, 'Creep and Recovery', A.S.M., Cleveland (1957).

33. C.G. Dunn and F.W. Daniels, Trans. A.I.M.E., 191, 147 (1951).

34. J.J. Gilman, Acta Met., 3, 277 (1955).

35. J.C.M. Li, Acta Met., 8, 563 (1960).

36. N.A. Bryshko, V.V. Gubernatorov, B.K. Sokolov, I.V. Gervaseva and V.N. Gundyrev, Dokl. Akad. Nauk. SSSR, 255 (6), 1367-1369.

37. H. Hu, Trans. A.I.M.E., 224, 75 (1962).

38. H. Hu and A. Szirmae, Trans. A.I.M.E., 221, 839 (1961).

39. D.W. Bainbridge, C.H. Li and E.H. Edwards, Acta Met., 2, 322 (1954).

40. M. Fujita, J. Phys. Soc. (Japan), 16, 397 (1961).

41. J.C.M. Li, J. Appl. Phys., 33, 2958 (1962).

42. W.T. Read, 'Dislocations in Crystals', (1953), New York (McGraw-Hill).

43. C.G. Dunn and F. Lionetti, Trans. A.I.M.E., 185, 125 (1949).

44. C.G. Dunn, F.W. Daniels and M.J. Bolton, Trans. A.I.M.E., 188, 1245 (1950).

45. K.T. Aust and B. Chalmers, Proc. Roy. Soc., A201, 210 (1950).

46. K.T. Aust and B. Chalmers, Proc. Roy. Soc., A204, 359 (1950).

47. N.A. Gjostein and F.N. Rhines, Acta Met., 7, 319 (1959).

48. Y. Taneda, Japan J. Appl. Phys., 4(1), 16 (1965).

49. R.C. Koo and H.G. Sell, 'Recrystallisation, Grain Growth and Textures', A.S.M., Detroit (1965).

50. J.H. Walter, 'Recovery and Recrystallisation of Metals', Ed. L. Himmel, p. 264 (1962), Interscience.

51. C.J.E. Smith and I.L. Dillamore, Metal Sci. J., 4, 161 (1970).

52. J.E. Burke and D. Turnbull, 'Progress in Metal Physics', 3, 220 (1952).

53. P.A. Beck, J. Appl. Phys., 20, 633 (1948).

54. R.W. Cahn, Proc. Phys. Soc., 63A, 323 (1950).

55. A.H. Cottrell, 'Progress in Metal Physics', 4, 255 (1953).

56. R.W. Cahn, 'Recrystallisation of Metallic Materials', Ed. F. Haessner, p. 43 (1971), Dr. Riedorer-Verlag, GMBH, Stuttgart.

57. W.G. Burgers, 'Rekristallisation, Verformter Zustand und Erholung', (1941), Akademische Verlagsgesellschaft, Leipzig.

58. J.L. Walter and G.F. Koch, Acta Met., 11, 923 (1963).

59. L.C. Michels and B.G. Ricketts, Trans. A.I.M.E., 239, 1841 (1967).

60. F. Granzer and G. Haase, Z. Phys., 162, 504, 517 (1961).

61. P.K. Marsden, J. Mater. Sci., 6 (1971).

62. R.D. Dohertey, 'Metal Odlew', 5(2), 179-196 (1979).

63. H. Hu, 'Electron Microscopy and Strength of Crystals', p. 564 (1963), London and New York (Interscience).

64. H. Hu, 'Textures in Research and Practice', (Proc. of International Symposium at Clansthal-Zellerfeld), Ed. J. Grewen and G. Wassermann, p. 200, Springer-Verlag (1968).

65. P.A. Beck and P.R. Sperry, J. Appl. Phys., 21, 150 (1950).

66. B.B. Rath and H. Hu, Trans. A.I.M.E., 236, 1193 (1966).

67. S. Kohara, M.N. Parthasarathi and P.A. Beck, Trans. A.I.M.E., 212, 875 (1958).

68. K.T. Aust and J.W. Rutter, Trans. A.I.M.E., 215, 119 (1959).

69. K.T. Aust and J.W. Rutter, Trans. A.I.M.E., 215, 820 (1959).

70. J.W. Rutter and K.T. Aust, Trans. A.I.M.E., 218, 682 (1960).

71. C. Frois and O. Dimitrov, Compt. Rend., 252, 1465 (1961).

72. K.T. Aust, G. Ferran and O.G. Cizeron, Compt. Rend., 257, 3595 (1963).

73. M.L. Kronberg and F.H. Wilson, Trans. A.I.M.E., 185, 501 (1949).

74. G.H. Bishop and B. Chalmers, Scripta Met., 2, 133 (1968).

75. J.W. Cahn, Acta Met., 10, 789 (1962).

76. R.K. Ray, Ph.D. Thesis, March, 1973, Univ. of Birmingham.

77. V. Yu. Novikov, Poverkhn. Fiz., Khim. Mekh. 1982, 5, 47-49.

78. B.F. Decker, E.T. Asp and D. Harker, J. Appl. Phys., 19, 388 (1948).

79. L.G. Schultz, J. Appl. Phys., 20, 1030 (1949).

80. C.S. Barrett, 'The Structure of Metals', 2nd edn., 1952, New York (McGraw-Hill).

81. G.B. Harris, Phil. Mag., 43, 113 (1952).

82. H.J. Burge, Zeit. Fur Metallkde., 56, 378 (1965).

83. R.O. Williams, Trans. A.I.M.E., 242, 105 (1968).

84. R.O. Williams, J. Appl. Phys., 39, 4329 (1968).

85. H.J. Bunge and F. Haessner, J. Appl. Phys., 39, 5503 (1968).

86. R.J. Roe, J. Appl. Phys., 36, 2024 (1965).

87. N. Hansen, T. Leffers and J.K. Kjems, Acta. Met., Vol. 29, pp. 1523-1533 (1981).

88. C.S. Barrett and F.W. Steadman, Trans. A.I.M.E., 147, 57 (1942).

89. Y.C. Lin and W.R. Hibbard, Jr., Trans. A.I.M.E., 197, 673 (1953).

90. W.R. Hibbard, Jr. and W.R. Tully, Trans. A.I.M.E., 221, 336 (1961).

91. M. Hatherly, Thesis, School of Metallurgy, The University of New South Wales, Sydney, Australia (1962).

92. C.A. Verbraak, Acta Met., 6, 580 (1958).

93. W.G. Burgers and P.C. Louwerse, Z. Physik, 67, 605 (1931).

94. R.H. Brick, Trans. A.I.M.E., 137, 193 (1940).

95. H. Ahlborn, J. Grewen and G. Wassermann, Z. Metallkunde, 55, 598 (1964).

96. H.C. Vacher, J. Research NBS, 26, 385 (1941).

97. R.M. Brick and M.A. Williamson, Trans. A.I.M.E., 143, 84 (1941).

98. M.N. Parthasarathi and P.A. Beck, Trans. A.I.M.E., 221, 831 (1961).

99. C.H. Samans, Trans. A.I.M.E., 111, 119 (1934).

100. H. Hu and P.A. Beck, J. Metals, 2, 1214 (1950).

101. H. Hu, P.R. Sperry and P.A. Beck, Trans. A.I.M.E., 194, 76 (1952).

102. R.E. Smallman, J. Inst. Met., 84, 10 (1955-56).

103. F. Haessner, Z. Metallkunde, <u>53</u>, 403 (1962).

104. F. Haessner, Z. Metallkunde, <u>54</u>, 79 (1963).

105. M. Hatherly, J. Austr. Inst. Met., <u>8</u>, 140 (1963).

106. K. Detert, P. Dorsch and H. Migge, Z. Metallkunde, <u>54</u>, 263 (1963).

107. R.H. Richman and Y.C. Lin, Trans. A.I.M.E., <u>221</u>, 720 (1961).

108. Y.C. Lin and R.H. Richman, Trans. A.I.M.E., <u>218</u>, 688 (1960).

109. R.E. Smallman, J. Inst. Met., <u>83</u>, 408 (1954-55).

110. E.R.W. Jones and E.A. Fell, Acta Met., <u>5</u>, 689 (1957).

111. I.L. Dillamore and W.T. Roberts, Acta Met., <u>12</u>, 281 (1964).

112. K. Lucke, H. Perlwitz and W. Pitsch, Phys. Stat. Sol., <u>7</u>, 733 (1964).

113. F. Haessner, U. Jakubowski and M. Wilkens, Phys. Stat. Sol., <u>7</u>, 701 (1964).

114. C.A. Clark and P.B. Mee, Z. Metallkunde, <u>53</u>, 756 (1962).

115. F. Haessner, Z. Metallkunde, <u>53</u>, 403 (1962).

116. I.L. Dillamore, R.E. Smallman and W.T. Roberts, Phil. Mag., <u>9</u>, 517 (1964).

117. H. Muller, Osterr Akad Wiss Math-naturw. KI Sitz ber, <u>7</u>, 117 (1958).

118. R.E. Smallman and D. Green, Acta Met., <u>12</u>, 145 (1964).

119. K. Lucke, 7th Colloque de Metallurgie, Eeronissage, Restauration, Recristallisation, Paris, p. 1-16 (1963).

120. H. Hu and R.S. Cline, J. Appl. Phys., <u>32</u>, 760 (1961).

121. H. Hu, R.S. Cline and S.R. Goodman, J. Appl. Phys., <u>32</u>, 1392 (1961).

122. H. Hu and S.R. Goodman, Trans. A.I.M.E., <u>227</u>, 627 (1963).

123. S.R. Goodman and H. Hu, Trans. A.I.M.E., <u>230</u>, 1413 (1964).

124. F.A. Underwood, 'Textures in Metal Sheet', London (Macdonald), (1961).

125. I.L. Dillamore and W.T. Roberts, Met. Rev., 10, 271 (1965).

126. F. Haessner, 'Recrystallisation, Grain Growth and Textures', p. 386 (1966), A.S.M., Metals Park, Ohio.

127. F. Haessner, Z. Metallkunde, 54, 98 (1963).

128. T. Richards and S.F. Pugh, J. Inst. Met., 88, 399 (1959-60).

129. Y.C. Liu, Trans. A.I.M.E., 230, 656 (1964).

130. G. Schock and A. Seeger, 'Defects in Crystalline Solids', The Physical Society, London, p. 340 (1955).

131. H. Wolf, Z. Naturforsch, 15a, 180 (1960).

132. F.B. Hirsch, Phil. Mag., 7, 67 (1963).

133. G. Wassermann, Z. Metallk., 54, 61 (1963).

134. P.R. Thronton and T.E. Mitchell, Phil. Mag., 7, 371 (1962).

135. Y.C. Liu, Trans. A.I.M.E., 209, 836 (1957).

136. C.A. Verbraak, Z. Metallk., 51, 646 (1960).

137. C.A. Verbraak, Acta Met., 8, 65 (1960).

138. Y.C. Liu and W.R. Hibbard, Trans. A.I.M.E., 203, 381 (1955).

139. P.A. Beck and H. Hu, J. Metals, 4, 83 (1952).

140. E. Hirosawa and H. Okawa, Sumito Light Metal Tech. Rep., 1, (3), 37 (1960).

141. T. Kamijo and K. Yamamoto, Nippon Kinzoku Gakkai-Si, 25, 220 (1961).

142. W. Gruhl and J. Gumper, Metall., 8, 830 (1954).

143. E. Schmid and H. Thomas, Z. Physik, 130, 293 (1951).

144. T. Kamijo and K. Yamamoto, Nippon Kinzoku Gakkai-Si, 25, 151 (1961).

145. W. Bunk, K. Lucke and G. Masing, Z. Metallkunde, 45, 584 (1954).

146. K. Lucke, Z. Metallkunde, 45, 86 (1954).

147. L.C. Tai, S.Y. Cheng and R.P. Liu, Acta Met. Sinica, 4, 52 (1959).

148. J. Grewen, A. Segmullar and G. Wassermann, Arch. Eisenhuttenwesen, _29_, 119 (1958).

149. E. Schmid and H. Thomas, Z. Metallkunde, _41_, 45 (1950).

150. M.F. Littmann, Trans. A.I.M.E., _206_, 593 (1956).

151. W.E. Seymour and D. Harker, Trans. A.I.M.E., _188_, 1001 (1950).

152. C.S. Barrett, Trans. A.I.M.E., _137_, 128 (1940).

153. P.A. Beck and H. Hu, Trans. A.I.M.E., _185_, 627 (1949).

154. N.K. Chen and C.H. Mathewson, Trans. A.I.M.E., _194_, 501 (1952).

155. R. Maddin, C.H. Mathewson and W.R. Hibbard, Jr., Trans. A.I.M.E., _185_, 655 (1949).

156. W.G. Bergers and J.C.M. Basart, Z. Physik, _51_, 545 (1928).

157. A. Laloeuf and C. Crussard, Rev. de. Met., _48_, 462 (1951).

158. P.A. Beck and H. Hu, 'Recrystallisation, Grain Growth and Textures', p. 393 (1966), A.S.M., Metals Park, Ohio.

159. P.A. Beck, Trans. A.I.M.E., _203_, 1270 (1955).

160. Y.C. Liu and W.R. Hibbard, Jr., Trans. A.I.M.E., _203_, 1249 (1955).

161. W.G. Burgers, Y.H. Liu and T.J. Tiedema, Proc. Kon. Ned. Acad. V Wet., _54_, 459 (1951).

162. W.G. Burgers, Proc. Ninth Solvay Conference, Brussels (1951).

163. B.F. Decker and D. Harker, J. Appl. Phys., _22_, 900 (1951).

164. H. Stadelmaier and B.F. Brown, Z. Metallkunde, _47_, 1 (1956).

165. E. Schmid and H. Thomas, Z. Metallkunde, _41_, 45 (1950).

166. A. Merlini and P.A. Beck, Acta Met., _1_, 598 (1953).

167. W.G. Burgers and C.A. Verbraak, Acta Met., _5_, 765 (1957).

168. P.R. Rowlands, J. Inst. Metals, _83_, 455 (1954-55).

169. T. Richards, 'X-ray Diffraction by Polycrystalline Materials', Ed. H.S. Peiser, H.P. Rooksby and A.J.C. Wilson, p. 298 (1955), London (Inst. Physics).

170. C.A. Verbraak, Proc. K. Akad. Wetensch, 60, 8, 393 (1957).

171. C.A. Verbraak, Thesis, Delft (1959).

172. P.A. Beck, Trans. A.I.M.E., 191, 475 (1951).

173. G. Ibe and K. Lucke, paper presented at meeting of Deutsche Gesellschaft fur Metallkunde in London (1964).

174. G. Ibe, Doctoral thesis, Univ. Aachen (1964).

175. I.L. Dillamore, Trans. A.I.M.E., 233, 702 (1965).

176. P.A. Beck, P.R. Sperry and H. Hu, J. Appl. Phys., 21, 420 (1950).

177. J.E. Burke, Trans. A.I.M.E., 194, 263 (1952).

178. S. Kohara, M.N. Parthasarathi and P.A. Beck, J. Appl. Phys., 29, 1125 (1958).

179. G. Czjzek and F. Haessner, Z. Metallkunde, 51, 567 (1960).

180. J.J. Becker, Trans. A.I.M.E., 191, 115 (1951).

181. P.A. Beck, Trans. A.I.M.E., 191, 474 (1951).

182. W.G. Burgers and T.J. Tiedema, Proc. Kon. Ned. Akad. V Wet., 53, 1525 (1950).

183. C.G. Dunn, Cold Working of Metals, A.S.M., p. 113 (1940).

184. P.A. Beck, Advances in Physics, 3, 245 (1954).

185. P.A. Beck, Acta Met., 1, 230 (1953).

186. H.P. Stuwe, Z. Metallkunde, 52, 34 (1961).

187. P.C.J. Gallagher, Met. Trans., 1, p. 2429 (1970).

188. R.K. Ray, Trans. I.I.M., 38, No. 3, 187 (1985).

R.D.↑

⊙	{100} ⟨001⟩
▲	{110} ⟨001⟩
●	{110} ⟨112⟩
X	{110} ⟨113⟩
■	{112} ⟨111⟩
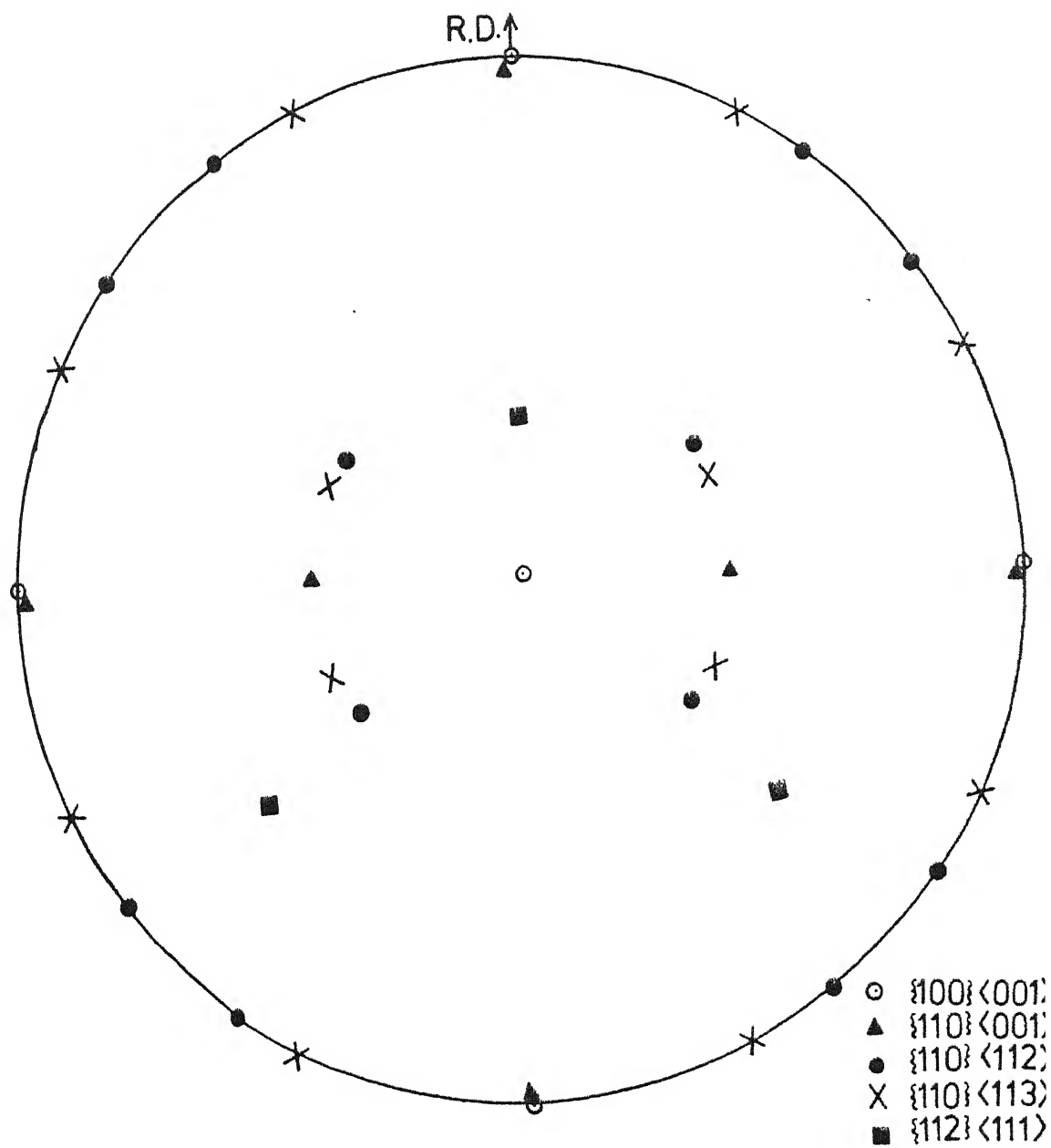
Ideal Orientations in a {200} Pole Figure.